NACA

RESEARCH MEMORANDUM

ALTITUDE-WIND-TUNNEL INVESTIGATION OF A 4000-POUND-THRUST AXIAL-FLOW TURBOJET ENGINE

I - PERFORMANCE AND WINDMILLING DRAG CHARACTERISTICS

By William A. Fleming

Flight Propulsion Research Laboratory
Cleveland, Ohio

NATIONAL ADVISORY COMMITTEE
FOR AERONAUTICS

WASHINGTON

August 3, 1948

NATIONAL ADVISORY COMMITTEE FOR AERONAUTICS

RESEARCH MEMORANDUM

ALTITUDE-WIND-TUNNEL INVESTIGATION OF A 4000-POUND-THRUST AXIAL-FLOW TURBOJET ENGINE

I - PERFORMANCE AND WINDMILLING DRAG CHARACTERISTICS

By William A. Fleming

SUMMARY

The results of altitude-wind-tunnel tests conducted to determine the performance of an axial-flow-type 4000-pound-thrust turbojet engine for a range of pressure altitudes from 5000 to 40,000 feet and ram pressure ratios from 1.02 to 1.86 are presented and the experimental and analytical methods employed are discussed. By means of suitable generalizing factors applied to the measured performance data, curves were obtained from which the engine performance at any altitude for a given ram pressure ratio can be estimated. The data presented include the windmilling drag characteristics of the turbojet engine for the ranges of altitudes and ram pressure ratios covered by the performance data.

The efficiency of the engine increased rapidly with airspeed. With a true airspeed of 500 miles per hour at 40,000 feet the specific fuel consumption based on net thrust horsepower was 0.94, and at 645 miles per hour the specific fuel consumption was 0.73. It was found that the windmilling drag of the engine is high and the inlet should be closed when the engine is inoperative in flight. In the range of low engine speeds, the combustion efficiency decreased rapidly as the altitude was increased, which resulted in high specific fuel consumptions. The results show that an accurate calculation of the jet thrust of the engine can be made from measurements of the temperatures and pressures obtained from a survey across the jet at the nozzle exit.

INTRODUCTION

An investigation has been conducted in the NACA Cleveland altitude wind tunnel to determine the operational and performance characteristics of an axial-flow-type turbojet engine with a

4000-pound-thrust rating at a range of pressure altitudes from 5000 to 40,000 feet and ram pressure ratios from 1.02 to 1.86, with tunnel temperatures from 60° to -50° F. The tunnel temperatures were held at approximately NACA standard values for each altitude condition. The results of performance tests on the engine with the standard low-flow compressor and a tail-pipe nozzle of $16\frac{3}{4}$-inch diameter are presented. The engine performance data presented comprise standard characteristic curves such as thrust, horsepower, fuel consumption, specific fuel consumption, and air flow plotted against engine speed and true airspeed. The effect of combustion on performance characteristics of the engine is briefly analyzed.

The engine was tested with two inlet configurations. For the static tests the engine combustion air was taken from the tunnel test section in a normal manner; for the ram tests air was introduced into the engine through a duct at pressures corresponding to ram pressures for various flight speeds at the tunnel pressure altitude. Extensive instrumentation was installed on the engine in order to obtain detailed information on the individual components of the engine as well as the over-all engine performance.

Characteristic performance data are presented in order to show the effect of altitude and airspeed, assuming 100-percent ram recovery, on engine performance and windmilling drag. The applicability of methods used to generalize the data in order to estimate performance at various altitudes from performance data determined at any altitude has been investigated.

SYMBOLS

The following symbols are used in the calculations:

A	cross-sectional area, square feet
B	thrust-scale reading, pounds
C_D	external drag coefficient of installation
c_p	specific heat of gas at constant pressure, Btu per pound per °R
D_w	windmilling drag, pounds

F_j	jet thrust, pounds
F_n	net thrust, pounds
g	acceleration of gravity, feet per second per second
H	total pressure, pounds per square foot absolute
H_1/p_0	ram pressure ratio
h	heating value of fuel, Btu per pound
J	mechanical equivalent of heat, foot-pounds per Btu
M	Mach number
m	mass rate of flow, slugs per second
N	engine speed, rpm
p	static pressure, pounds per square foot absolute
p_0	test-section static pressure, pounds per square foot absolute
q	equivalent free-stream dynamic pressure obtained with closed duct, pounds per square foot
q_0	test-section free-stream dynamic pressure, pounds per square foot
R	gas constant
S	wing-section area, square feet
T	total temperature, $^\circ R$
T_i	indicated temperature, $^\circ R$
t	static temperature, $^\circ R$
thp	net thrust horsepower
V	velocity, feet per second
V_0	test-section velocity, feet per second
v	effective true airspeed, miles per hour

W	weight rate of flow, pounds per second
W_f	fuel consumption, pounds per hour
W_f/F_j	specific fuel consumption based on jet thrust, pounds per hour per pound thrust
W_f/thp	specific fuel consumption based on net thrust horsepower, pounds per thrust horsepower-hour (same as corrected value)
w_f	fuel consumption, pounds per second
γ	ratio of specific heats for gases
δ	ratio of absolute total pressure at compressor inlet to absolute static pressure of NACA standard atmospheric conditions at sea level
η_b	combustion efficiency, percent
θ	ratio of absolute total temperature at compressor inlet to absolute static temperature of NACA standard atmospheric conditions at sea level
ρ	mass density of gas, slugs per cubic foot

Subscripts:

a	air
b	combustion
br	bearing cooling air
c	compressor
f	fuel
g	exhaust gas
j	jet
n	net
0	tunnel test-section free-air stream
t	turbine

X	closed inlet duct at slip joint, station X
1	cowl inlet
2	compressor inlet
4	compressor outlet
5	turbine inlet
8	tail-pipe nozzle

The following engine parameters are corrected to NACA standard atmospheric conditions at sea level:

F_j/δ	corrected jet thrust, pounds
F_n/δ	corrected net thrust, pounds
$N/\sqrt{\theta}$	corrected engine speed, rpm
$thp/(\delta\sqrt{\theta})$	corrected net thrust horsepower
$v/\sqrt{\theta}$	corrected effective true airspeed, miles per hour
$(W_a\sqrt{\theta})/\delta$	corrected air flow, pounds per second
$W_f/\delta(\sqrt{\theta})$	corrected fuel consumption, pounds per hour
$W_f/(F_j\sqrt{\theta})$	corrected specific fuel consumption based on jet thrust, pounds per hour per pound thrust
$w_f/(W_a\theta)$	corrected fuel-air ratio

WIND-TUNNEL INSTALLATION AND TEST PROCEUDRE

Description of Engine

The J35 engine used for the investigation has a sea-level rating of 4000-pounds static thrust at an engine speed of 7600 rpm. At this rating the air flow is approximately 75 pounds per second and the fuel consumption 4400 pounds per hour. The over-all length of the engine is about 14 feet; the maximum diameter, 36 inches; and the total weight, 2300 pounds. The compressor has 11 axial-flow stages and provides a pressure ratio of approximately 4 at rated engine speed. There are eight individual combustion chambers on

the engine, which are joined by small interconnecting tubes for cross ignition. A single-stage turbine is used to drive the compressor. The tail-pipe nozzle used in these runs is $16\frac{3}{4}$ inches in diameter.

Installation and Test Procedure

The engine was supported on a 7-foot-chord airfoil installed in the 20-foot-diameter test section of the wind tunnel (See fig. 1.) The cowling extended back only as far as the rear of the compressor; therefore, the burners and the tail pipe were cooled by the movement of the air in the test section. Air was supplied to the engine by two methods: For the static tests a wooden cowl was attached to the engine inlet and air was supplied from the tunnel test section in a normal manner; for the ram tests inlet pressures corresponding to flight at high speed were obtained by introducing dry refrigerated air from the tunnel make-up air system throttled from approximately sea-level pressure to the desired pressure at the engine inlet while maintaining the wind-tunnel pressure and temperature corresponding to the test altitude. The make-up duct was connected to the engine intake by means of a slip joint located 40 feet upstream of the engine. (See fig. 2, station X.) The slip joint permitted engine-thrust and installation-drag measurements to be made with the tunnel scales. An orifice for measuring the air flow is shown in the ram-pipe installation, but the results obtained were not sufficiently accurate to be used. For both the static and the ram tests the velocity in the tunnel test section varied from 40 to 100 feet per second, as induced by the ejector effect of the jet and by the tunnel-exhauster scoop located immediately downstream of the test section.

The engine was extensively instrumented as shown in figure 3. Temperature and pressure measurements of the air and gases were taken at eight stations in the engine (fig. 4). Thrust was measured by the balance scales and was also calculated from pressure and temperature measurements obtained with the tail-pipe-nozzle rake. (See fig. 5.) In order to determine the external drag of the installation to correct the scale thrust measurements, power-off drag tests were conducted with the engine inlet so covered that the external drag coefficient of the installation could be determined.

METHODS OF CALCULATION

Thrust

The thrust was determined by two methods: (1) measurement directly on the balance scales and (2) calculation from temperature

and pressure measurements obtained with the tail-rake survey (fig. 5) located at the tail-pipe-nozzle exit. For the static tests, when the inlet of the engine was open to the tunnel, the jet thrust was determined from the balance-scale measurement by adding the external drag of the installation and the rate of momentum of the engine intake air at free-stream velocity to the thrust reading to give

$$F_j = B + C_D q_0 S + m_a V_0 \tag{1}$$

When the closed duct was attached to the inlet of the engine to obtain high ram pressure conditions, the forces on the installation were combined in the equation

$$F_j = B + C_D q_0 S + m_a V_X + A_X (p_X - p_0) \tag{2}$$

The momentum and pressure terms in equation (2) replace the momentum term in equation (1).

Calculation of the jet thrust from temperature and pressure measurements obtained with the tail-rake survey was accomplished by the use of an equation derived from the basic formula for jet thrust

$$F_j = m_g V_j \tag{3}$$

which is the ultimate rate of momentum of the gases in the jet. The jet thrust may then be expressed as

$$F_j = m_g V_8 + A_8 (p_8 - p_0)$$

which is

$$F_j = \rho_8 A_8 V_8^2 + A_8 (p_8 - p_0) \tag{4}$$

When Bernoulli's compressible-flow equation for velocity is applied, the velocity of the jet at the nozzle exit is

$$V_8^2 = 2Jgc_p t_8 \left[(H_8/p_8)^{\frac{\gamma-1}{\gamma}} - 1 \right] \tag{5}$$

By substitution of the relation

$$Jc_p = R \frac{\gamma}{\gamma - 1}$$

into equation (5), the tail-pipe-nozzle velocity may be expressed as

$$V_8^2 = \frac{2\gamma}{\gamma - 1} gRt_8 \left[(H_8/p_8)^{\frac{\gamma-1}{\gamma}} - 1 \right] \tag{6}$$

The relation

$$gRt_8 = \frac{p_8 gRt_8}{p_8} = \frac{p_8}{\rho_8}$$

may then be substituted into equation (6), which gives

$$V_8^2 = \frac{2\gamma}{\gamma - 1} \frac{H_8}{\rho_8} \left[\left(\frac{H_8}{p_8} \right)^{\frac{\gamma-1}{\gamma}} - 1 \right] \tag{7}$$

By substitution of equation (7) into equation (4), the final expression for jet thrust becomes

$$F_j = \frac{2\gamma}{\gamma - 1} p_8 A_8 (H_8/p_8)^{\frac{\gamma-1}{\gamma}} - 1 + A_8 (p_8 - p_0) \tag{8}$$

At all altitudes and ram pressure ratios the ratio of measured jet thrust to calculated jet thrust was constant at a value of 0.985 (figs. 6 and 7), with the measured thrust obtained from either equation (1) or equation (2) and the calculated thrust obtained from equation (8).

When the initial free-stream momentum of the inlet air is subtracted from the jet thrust, the following equation for net thrust is obtained

$$F_n = F_j - m_a V \tag{9}$$

It is the net thrust that acts on an airplane to propel it through the air.

The net thrust horsepower may then be determined from the product of the true airspeed in feet per second and the net thrust in the relation

$$thp = \frac{F_n V}{550} \tag{10}$$

Air Flow

The air flow to the engine was determined by two methods: (1) calculation from temperatures and pressures obtained by the tail-rake survey at station 8 and (2) calculation from temperatures and pressures obtained by the cowl-inlet survey at station 1. The air flow determined from the tail-rake survey, which is used to determine the performance, is found by first calculating the gas flow out of the tail pipe by the equation

$$W_g = \rho_8 A_8 V_8 g \tag{11}$$

which, when combined with equation (5), gives

$$W_g = \frac{p_8 A_8}{R} \sqrt{\frac{2Jgc_p}{t_8}\left[\left(\frac{H_8}{p_8}\right)^{\frac{\gamma-1}{\gamma}} - 1\right]} \tag{12}$$

The air flow is then found by subtracting the fuel flow w_f and adding the bearing cooling-air flow W_{br} to the gas flow, which gives

$$W_a = W_g - w_f + W_{br} \tag{13}$$

The bearing cooling-air flow varies from 0.25 to 0.75 percent of the total air flow.

In order to determine the air flow from the cowl-inlet survey, a weighted average, corresponding to the annular area covered by each total-pressure tube, of the square root of the total pressure minus the static pressure was used. The total inlet area in the plane of survey including the cross-sectional area of the guide vanes was used and the cowl-inlet velocity was multiplied by the calculated factor 0.963 to correct for the interference effect of the guide vanes on the air stream. Assuming that the flow at the cowl inlet is incompressible, the resultant equation for air flow is

$$W = 0.963\ \rho_1 A_1 g \sqrt{\frac{2\ (H_1 - p_1)}{\rho_1}} \tag{14}$$

Temperatures

In equation (8), the jet thrust is dependent on temperature only to the extent of determining the value of the ratio of specific

heats. Calibration of the type of thermocouple used in the tail-rake survey, neglecting radiation effect, showed that the thermocouple measures the static temperature plus approximately 85 percent of the adiabatic temperature rise due to the impact of the air on the thermocouple. The static temperature used to determine the ratio of specific heats is then

$$t_8 = \frac{T_{i,8}}{1 + 0.85\left[(H_8/p_8)^{\frac{\gamma-1}{\gamma}} - 1\right]} \tag{15}$$

Equivalent Airspeeds

Inasmuch as all the calculations are based on 100-percent ram efficiency, the equivalent velocity corresponding to the ram pressure ratio is used to determine the initial momentum term in equation (9). The equivalent airspeed is given by the equation

$$V = \sqrt{2Jgc_pT_{i,1}\left[1 - \left(\frac{p_0}{H_1}\right)^{\frac{\gamma-1}{\gamma}}\right]} \tag{16}$$

Because the adiabatic temperature rise due to the cowl-inlet velocity, (station 1) was low, the equivalent free-stream total temperature can be assumed equal to the cowl-inlet indicated temperature. The use of this assumption caused an error in the airspeed of less than 1 percent.

Combustion Efficiency

The combustion efficiency is obtained from the fundamental relation

$$\eta_b = \frac{\text{heat out}}{\text{heat in}} = \frac{W_g c_{p,b}(T_5 - T_4)}{w_f h} \tag{17}$$

where the value of the specific heat $c_{p,b}$ is the average of the specific heats for the entering air and the products of combustion. The lower heating value of the kerosene used as fuel for the runs is 18,600 Btu per pound of fuel. The value of the turbine-inlet total temperature T_5 can be determined from the relation that the work done by the turbine equals the work done on the compressor plus the mechanical losses. Because the mechanical losses are negligible

and the mass air flow through the compressor may be assumed to be equal to the mass gas flow through the turbine, the turbine-inlet total temperature may be expressed as

$$T_5 = T_8 + \frac{c_{p,c}}{c_{p,t}} (T_4 - T_2) \qquad (18)$$

where the values of the specific heats $c_{p,c}$ and $c_{p,t}$ are the average values through the compressor and the turbine, respectively. The tail-rake total temperature was assumed equal to the turbine-outlet total temperature and, because more accurate temperature measurements can be made at the tail rake, this value was used.

RESULTS AND DISCUSSION

Altitude and Ram Effects on Performance

Engine performance. - A comparison of the performance of the engine at pressure altitudes of 10,000, 20,000, 30,000, and 40,000 feet at a ram pressure ratio of approximately 1.2 (figs. 8 to 11) shows that the reduced density of the air and consequently the reduced weight air flow through the engine at altitude (fig. 12) caused the jet thrust, the net thrust, the net thrust horsepower, and the fuel consumption to decrease.

The air flow measured by the tail-rake survey at station 8 (fig. 12(a)) is approximately 10 percent lower than the air flow measured by the cowl-inlet survey at station 1 (fig. 12(b)). Values of the air flow measured by the tail-rake survey gave reasonable and consistent component efficiencies and heat balances in all cases; whereas the air flow calculated by the cowl-inlet survey gave burner efficiencies of more than 100 percent in many cases and inconsistent thrust values and heat balances.

In the range of high engine speeds at a constant ram pressure ratio for all altitudes, the specific fuel consumption based on jet thrust fell on a single curve, but in the range of low engine speeds the specific fuel consumption increased as the altitude became higher. (See fig. 13.) The increased specific fuel consumption in the low-speed range at high altitude is attributed to lower component efficiencies.

The specific fuel consumption based on the net thrust horsepower (fig. 14) was almost constant for all altitudes at high engine speeds and a given ram pressure ratio. At low engine speeds, however, the specific fuel consumption decreased with increasing altitude, except at 40,000 feet where the specific fuel consumption was

higher than at 30,000 feet. As the altitude was increased from sea level and the ambient temperature correspondingly decreased, the compressor pressure ratio at constant engine speed was increased. The improvement in cycle efficiency accompanying the increased pressure ratio resulted in lower specific fuel consumption as the altitude increased to 30,000 feet. Between 30,000 and 40,000 feet the decrease in component efficiencies was greater than the gain obtained from the increased cycle efficiency and the specific fuel consumption increased.

The fuel-air ratio increased with altitude throughout the entire range of engine speeds. (See fig. 15.)

From performance data obtained at 40,000 feet and ram pressure ratios of 1.02, 1.20, 1.41, 1.62, and 1.86,(figs. 16 to 19), the jet thrust, the net thrust horsepower, and the fuel consumption are seen to increase with ram pressure ratio. As the ram pressure ratio was increased, the weight air flow through the engine became greater throughout the entire range of engine speeds (fig. 20) and the overall pressure ratio between the free stream and the compressor outlet became greater, which resulted in the increase in jet thrust with airspeed. Again the air flow measured with the tail-rake survey (fig. 20(a)) is approximately 10 percent lower than the air flow measured with the cowl-inlet survey (fig. 20(b)).

The net thrust at maximum engine speed decreased with airspeed up to approximately 250 miles per hour and increased above that value. (See figs. 21 and 22.) At low airspeeds the ram pressure ratio increased slowly with airspeed according to the relation

$$\frac{H_1}{p_0} = 1 + \frac{\frac{1}{2}\rho_0 V^2\left(1 + \frac{M^2}{4} + \frac{M^4}{40}\right)}{p_0} \qquad (19)$$

and the jet thrust was therefore not appreciably affected by changes in airspeed, but the term $m_a V$ required to obtain the net thrust according to equation (9) is directly proportional to airspeed. The result is that at low airspeeds the rate of change of $m_a V$ with airspeed is greater than the corresponding rate of change in jet thrust. The net thrust therefore decreased with increased airspeed. At the higher airspeeds the last term of equation (19), which involves the square of the airspeed, becomes appreciable. The rate of change of jet thrust with airspeed then exceeds the corresponding rate of change of $m_a V$ resulting in an increase in net thrust with airspeed.

The specific fuel consumption based on jet thrust and on net thrust horsepower decreased rapidly as the airspeed became higher. (See figs. 23 to 25.) At 500 miles per hour the specific fuel consumption based on net thrust horsepower with the engine operating above 7000 rpm was approximately 0.94 and at 645 miles per hour, approximately 0.73. The rapidly decreasing specific fuel consumption indicated that above a true airspeed of 500 miles per hour the engine became quite efficient. With increased ram pressure ratios, the fuel-air ratio decreased slightly at the high engine speeds and markedly decreased at the low. (See fig. 26.) The decrease of fuel-air ratio as the ram pressure ratio increased is attributed in part to the fact that the compression ratio across the compressor increased without appreciable change in expansion ratio across the turbine. The cycle efficiency was improved by this change of compression ratio relative to the expansion ratio and less fuel was required to maintain a constant engine speed.

Data on component efficiencies, which were obtained in the test program but are not presented in this paper, show that combustion efficiency changes more rapidly with altitude than any other component efficiency. The combustion efficiency determined with equation (17) at altitudes of 10,000, 20,000, 30,000, and 40,000 feet are shown in figure 27. With an increase in ram pressure ratio the combustion efficiency markedly increased, as shown by the data obtained at 40,000 feet. (See fig. 28.)

Generalized performance. - From an analysis of jet-engine performance data, several reduction parameters have been developed for generalizing experimental performance data taken at any altitude in order that these data may serve to estimate jet-engine performance at all altitudes. (See reference 1.)

The application of the reduction factors θ and δ to the engine-performance parameters give the following generalized parameters: corrected engine speed $N/\sqrt{\theta}$; corrected jet thrust F_j/δ; corrected net thrust F/δ; corrected net thrust horsepower $thp/(\delta\sqrt{\theta})$; corrected air flow $(W_a\sqrt{\theta})/\delta$; corrected fuel consumption, $W_f/(\delta\sqrt{\theta})$; corrected specific fuel consumption based on jet thrust $W_f/(F_j\sqrt{\theta})$; corrected specific fuel consumption based on net thrust W_f/thp; and corrected fuel-air ratio $w_f/(W_a\theta)$.

Application of four reduction factors is shown in figures 29 to 32, in which corrected jet thrust, corrected net thrust, corrected net thrust horsepower, and corrected air flow are plotted against corrected engine speed for a ram pressure ratio of approximately 1.2. The data obtained at all altitudes determine a single curve for each performance parameter, which indicates that such generalized curves can be used with a high degree of reliability for predicting these engine per formance characteristics.

The fuel consumptions measured at 10,000, 20,000, 30,000, and 40,000 feet with a ram pressure ratio of approximately 1.2 were reduced to a single curve by the generalization factors for only the upper range of engine speeds. (See fig. 33.) In the lower range of engine speeds, the corrected fuel consumption was higher at the high altitudes owing to the variation of the component efficiencies of the engine, mainly the combustion efficiency. In order to accurately generalize the fuel consumption throughout the entire range of engine speeds, the reduction factors should include a term that takes into account the variation of combustion efficiency with engine speed and altitude. Such a term was not used with the data in this paper.

The corrected specific fuel consumption based on jet thrust (fig. 34) has the same characteristics as the fuel-flow curve in that at high engine speeds the corrected specific fuel consumption falls on a single curve for each altitude and in the low engine-speed range the corrected specific fuel consumption increases with altitude. The specific fuel consumption based on net thrust horsepower (fig. 35) did not change with altitude throughout the entire range of engine speeds, except at 40,000 feet where the specific fuel consumption at low engine speeds increased because of low component efficiencies.

Inasmuch as the corrected air flow remains unchanged with altitude and the corrected fuel flow is constant for all altitudes in the upper range of engine speeds but increased with altitude in the lower range of engine speeds, the corrected fuel-air ratio (fig. 36) remains unchanged with altitude at high engine speeds but increased with altitude in the low-speed range.

An increase in ram pressure ratio resulted in a corresponding increase in corrected jet thrust (fig. 37), a decrease in corrected net thrust as low ram ratios and little change in high ram ratios (fig. 38), an increase in corrected net thrust horsepower (figs. 39 and 40), and a decrease in corrected fuel consumption (fig. 41). The variation of these generalized factors gives corrected specific fuel consumption based on jet thrust (fig. 42) and a specific fuel consumption based on net thrust horsepower (figs. 43 and 44) that decrease rapidly with increased airspeeds. From these data and from the generalized data presented for several altitudes, it is apparent that runs at several ram pressure ratios give generalized data that fall on a family of curves and data must be obtained at each ram pressure ratio in order to determine the family of generalized curves representative of the performance at all airspeeds.

The air flow obtained by the tail-rake and cowl-inlet surveys are shown in generalized form in figures 45(a) and 45(b), respectively. Two distinct curves were obtained for each method. The upper curve represents the data obtained from the ram tests and the lower curve the data obtained from the static tests, which were made at a ram pressure ratio of 1.02. The low values of air flow obtained in the static tests were attributed to a thick boundary layer at the compressor inlet, which was caused by breaking away of the air from the inner surface of the cowling as a result of operation at inlet velocity ratios V_1/V_0 between 2.5 and 4.0. Such flow characteristics could be expected with ground operation of the engine before take-off. The upper air-flow curve represents runs made with the duct on the inlet, which caused very little turbulence or boundary layer at the compressor inlet. With the exception of the static air-flow curves, figure 45 indicates that the generalization factors correct the air flow to a single curve at high engine speeds for all ram pressure ratios. Because the idling speed of the engine is very high at high airspeeds, it is impossible to predict whether the correction will also apply in the lower range of engine speeds; however, from data not herein presented, a family of diverging curves showing an increase in air flow with airspeed is expected in the low range of engine speeds.

The corrected fuel-air ratio is slightly lower at high ram pressure ratios in the upper range of engine speeds and as the engine speed is reduced the curves become more divergent. (See fig. 46.) Again the data give a family of curves covering the range of ram pressure ratios.

The method of generalization of data does not permit estimation of performance parameters involving the fuel flow at low engine speeds because the effects of varying combustion efficiency are not properly accounted for; nor can the method of generalization of data be used for estimating the effects of ram pressure on performance.

Windmilling Drag

Very little information has been published on the drag values obtained when an engine is inoperative during flight and is allowed to windmill. The magnitude of the windmilling drag is equal to the rate of change of momentum of the air decelerated by passing through the engine. Relative to the airplane, the rate of change of momentum of the mass of air per second m_a flowing through the engine, as calculated from the results of the wind-tunnel investigation, is

$$D_w = m_a (V - V) \qquad (20)$$

The windmilling drag was also measured on the wind-tunnel balance scales and was determined from the relation

$$D_w = m_a V - \left[B + m_a V_X + C_D q_0 S + A_X (p_X - p_0)\right] \qquad (21)$$

Agreement between the results calculated with these two equations was very close. The windmilling drag determined from equation (21) is presented herein.

Altitude was found to have no effect on engine windmilling speed, but the windmilling speed varied almost linearly with true airspeed. (See fig. 47.) The windmilling drag (fig. 48) increased rapidly with airspeed and decreased with increasing altitude. If the windmilling drag of the engine is divided by the net thrust at rated engine speed for each altitude and airspeed (fig. 49), the values lie on a common curve for all altitudes. At a true airspeed of 500 miles per hour, at any altitude approximately 15 percent of the net thrust of one engine operating at rated speed is required to pull a windmilling engine through the air and at 650 miles per hour the windmilling drag equals 25 percent of the maximum net thrust of one engine. The inlet to the engine should, therefore, be closed when the engine is inoperative during flight. Dividing the windmilling drag of the engine by the equivalent free-stream dynamic pressure (fig. 50) resulted in a dimensional coefficient that lies on a single curve.

The corrected air flow when the engine is windmilling was found to be approximately 25 percent greater than the flow when the engine is operating at a given corrected engine speed. (See fig. 51.) The lower air flow through the engine when it is operating results from greater losses through the combustion chambers and turbine nozzles due to the high gas velocity produced to burning.

When the engine is windmilling, the pressure rises through the first stages of the compressor and the remaining stages act as a turbine. A pressure survey through the windmilling engine at 40,000 feet and a true airspeed of 575 miles per hour is shown in figure 52.

SUMMARY OF RESULTS

From an investigation of the performance and the windmilling drag characteristics of an axial-flow-type 4000-pound-thrust turbojet engine at pressure altitudes from 5000 to 40,000 feet and ram pressure ratios from 1.02 to 1.86, and from the application of the performance generalization factors, the following results were observed:

1. The efficiency of the turbojet engine rapidly improved with an increase in airspeed and above a true airspeed of 500 miles per hour at a pressure altitude of 40,000 feet the specific fuel consumption based on net thrust horsepower is 0.94 and at 645 miles per hour is 0.73.

2. Thrust, horsepower, and air-flow data at a given ram pressure ratio can be generalized with the use of reduction factors so that the data obtained at any altitude can be used to estimate the performance at any other altitude. In order to generalize accurately performance parameters involving the fuel consumption throughout the entire range of engine speeds, the reduction factors should include a term that takes into account the variation of combustion efficiency with engine speed and altitude.

3. The specific fuel consumption of the engine in the upper range of engine speeds at a given ram pressure ratio remained unchanged with variations in altitude, but in the low engine-speed range the specific fuel consumption was higher at high altitudes owing to poor combustion efficiency.

4. Windmilling drag values of 15 percent of the maximum net thrust at 500 miles per hour and 25 percent of the maximum net thrust at 650 miles per hour were obtained in the windmilling drag tests. These results indicate that closing the inlet to the engine when the engine is inoperative during flight is desirable.

5. An accurate calculation of the jet thrust of the engine can be made from measurements of temperatures and pressures obtained from a survey across the jet at the nozzle exit.

Flight Propulsion Research Laboratory
National Advisory Committee for Aeronautics,
Cleveland, Ohio.

REFERENCE

1. Sanders, Newell D.: Performance Parameters for Jet-Propulsion Engines. NACA TN No. 1106, 1946.

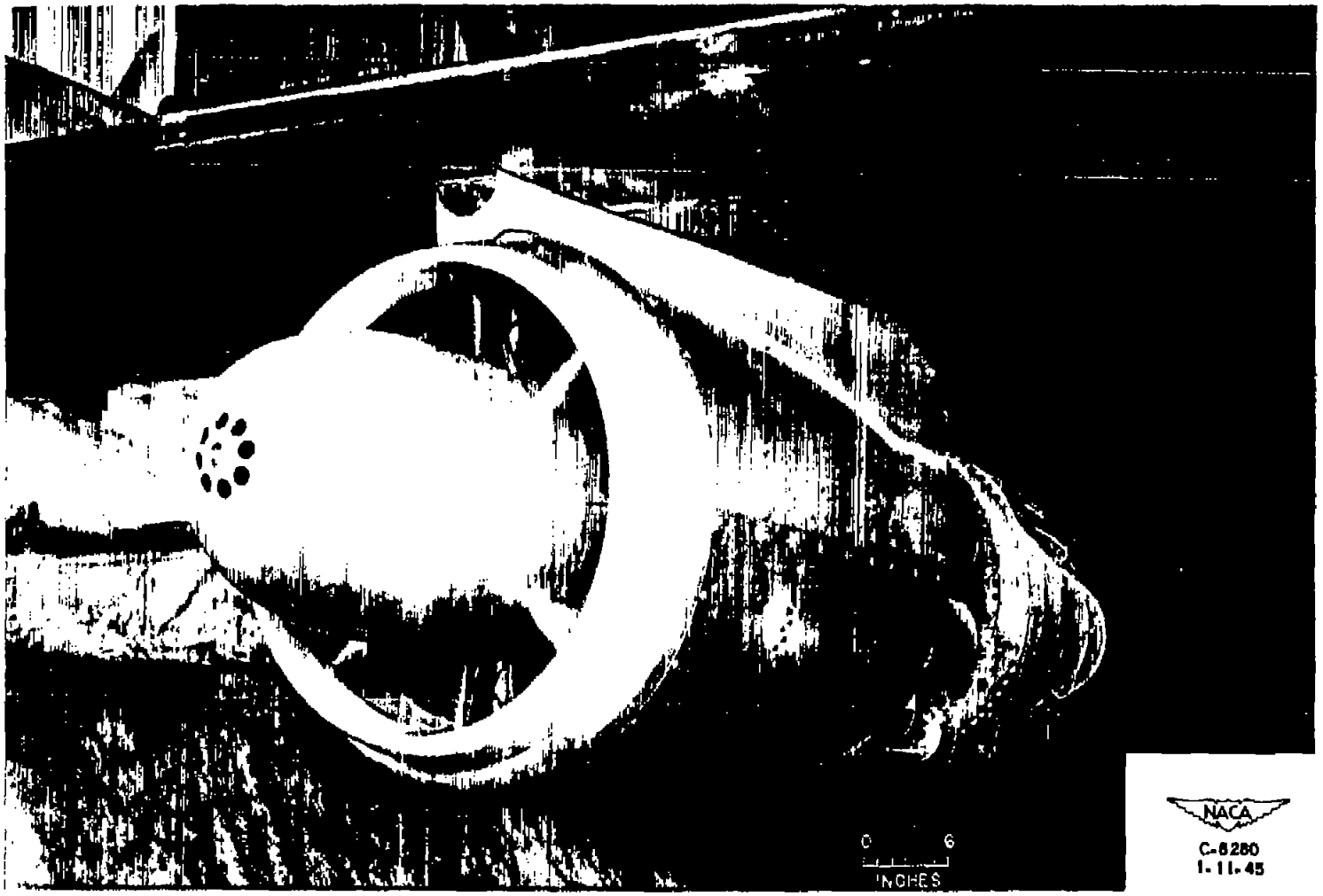

(a) Left-side view with cowling.

Figure 1. - Installation of 4000-pound-thrust axial-flow-turbojet engine in altitude wind tunnel.

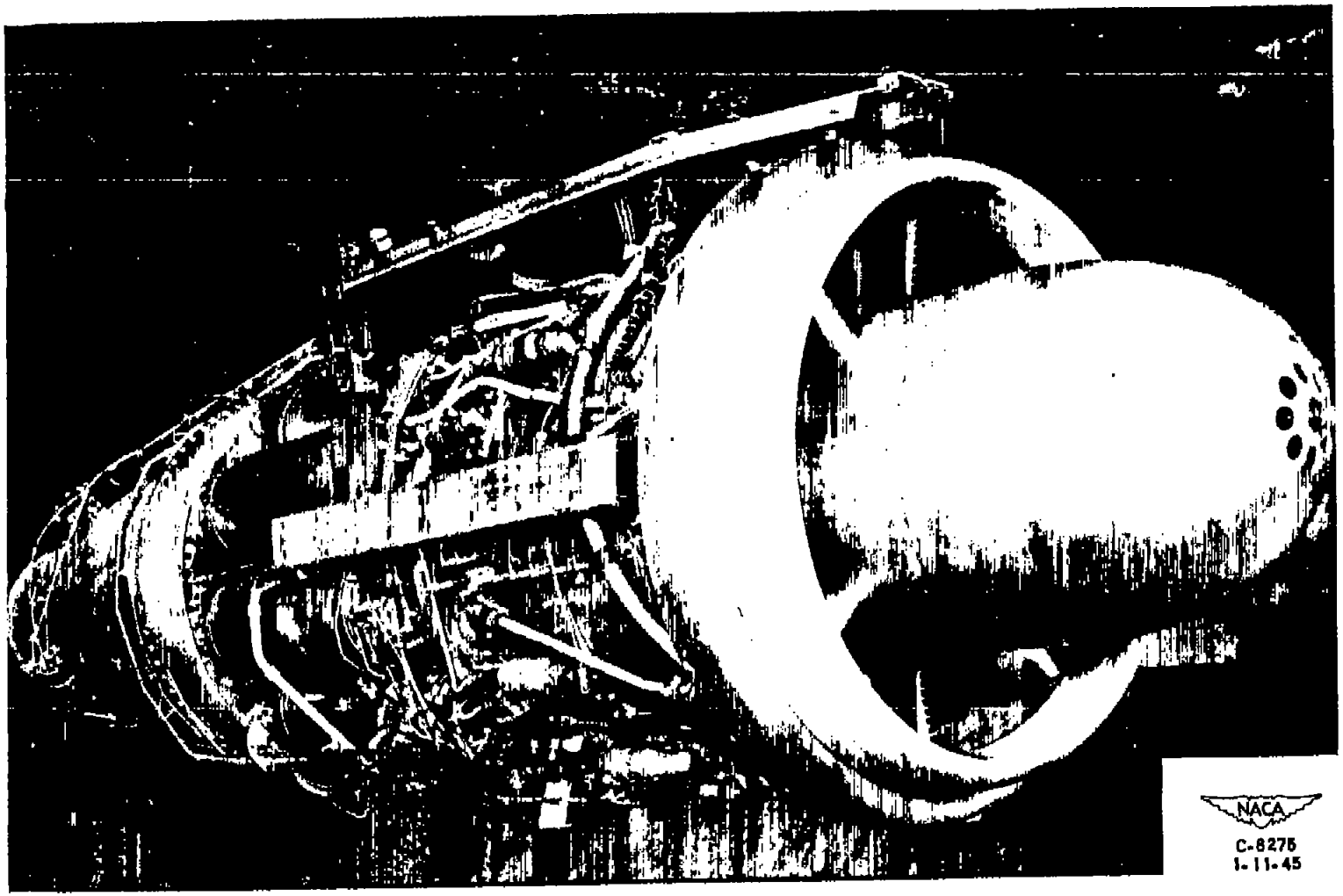

(b) Right-side view without cowling.

Figure 1. - Concluded.

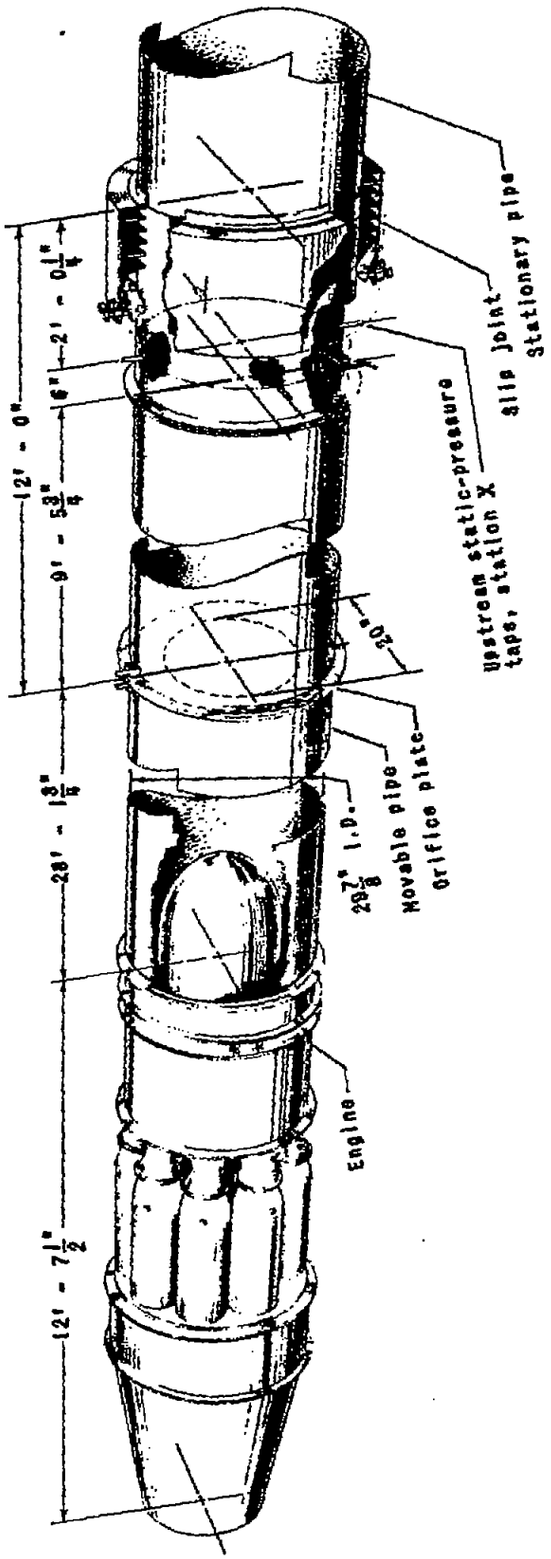

Figure 2. - Installation of closed dust from tunnel make-up air system to engine inlet for supplying air at ram pressures.

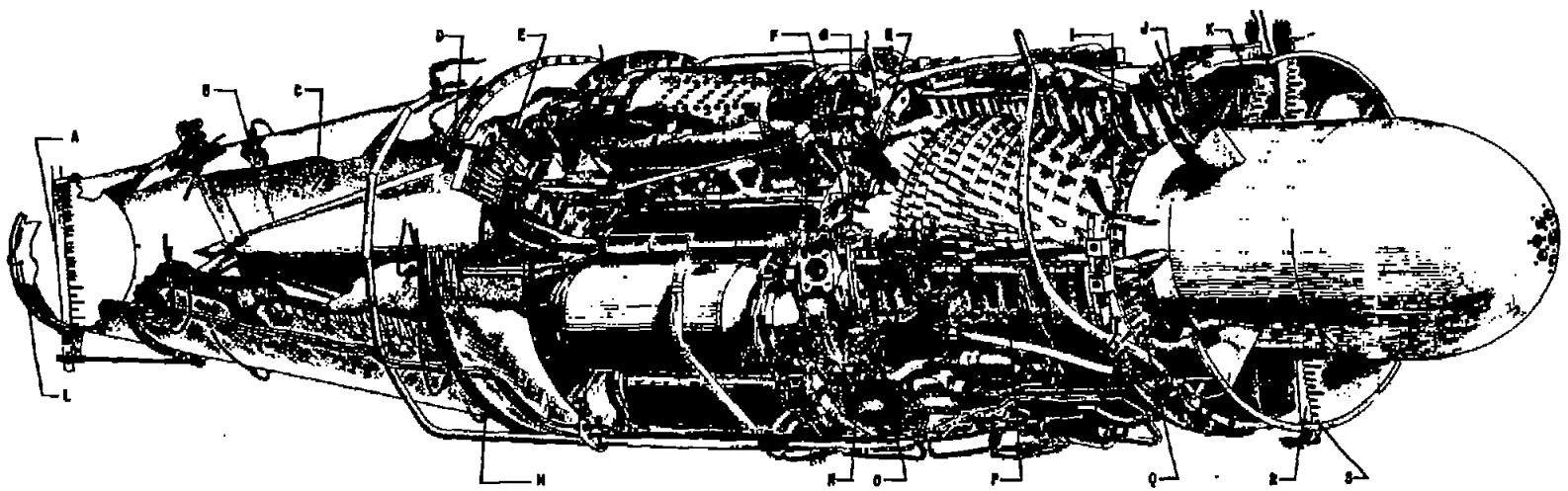

A Tail-pipe-discharge total and static-pressure and temperature survey (NACA)
B Tail-pipe total-pressure tube
C Tail-pipe thermocouple
D Turbine-outlet thermocouple
E Turbine-inlet total-pressure tube
F Compressor-outlet total-pressure tube
G Compressor-outlet static-pressure wall orifice (NACA)
H Compressor-outlet total-pressure and temperature survey (NACA)
I Compressor-inlet static-pressure wall orifice
J Compressor-inlet thermocouple
K Compressor-inlet total- and static-pressure survey (NACA)
L Tail-pipe-discharge static-pressure wall orifice (NACA)
M Turbine-outlet static-pressure wall orifice
N Compressor-outlet thermocouple
O Compressor-outlet static-pressure survey (NACA)
P Compressor-interstage static-pressure wall orifices
Q Compressor-inlet total-pressure tube
R Cowl-inlet total- and static-pressure and temperature survey (NACA)
S Cowl-inlet static-pressure wall orifice (NACA)

(NACA) Instrumentation installed by NACA for altitude-wind-tunnel tests. All other instrumentation standard.

Figure 3. - Instrumentation of 4000-pound-thrust axial-flow-turbojet engine for altitude-wind-tunnel investigation.

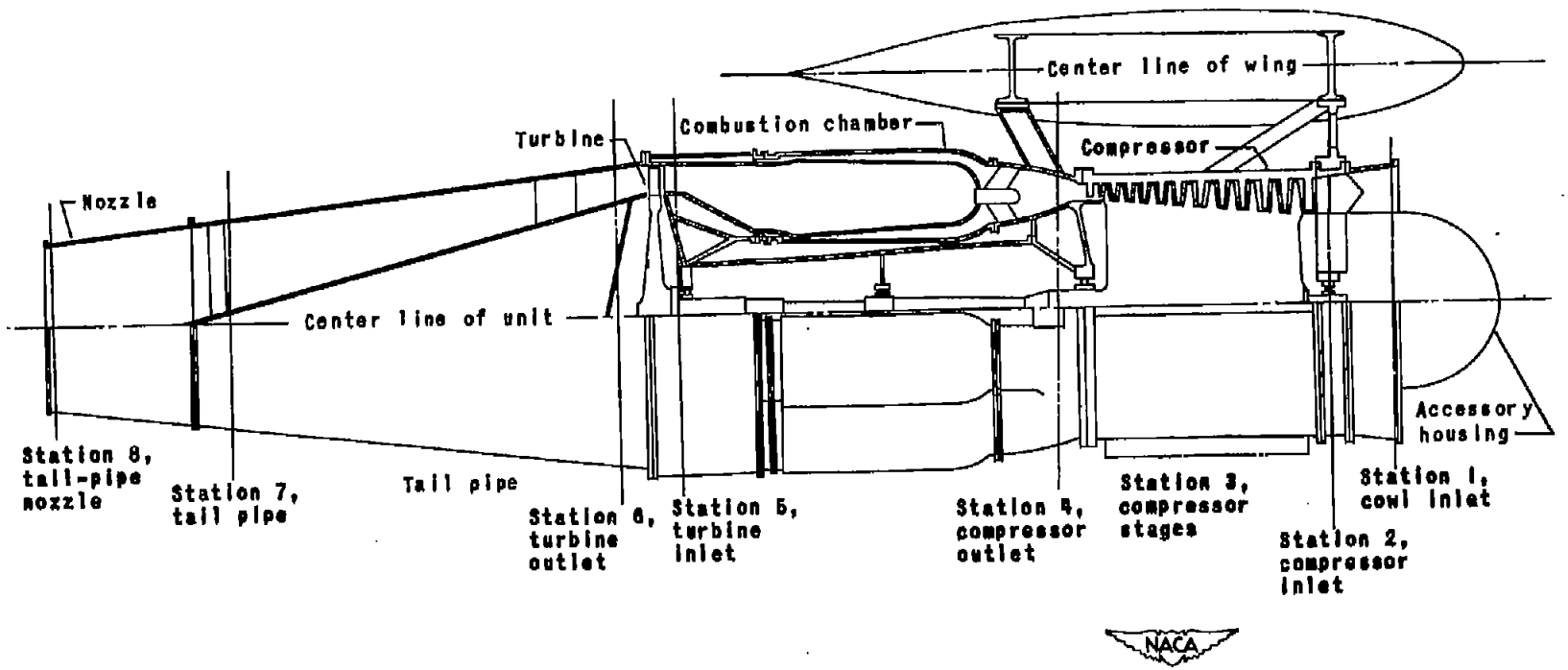

Figure 4. - Side view of 4000-pound-thrust axial flow turbojet installation showing measuring stations.

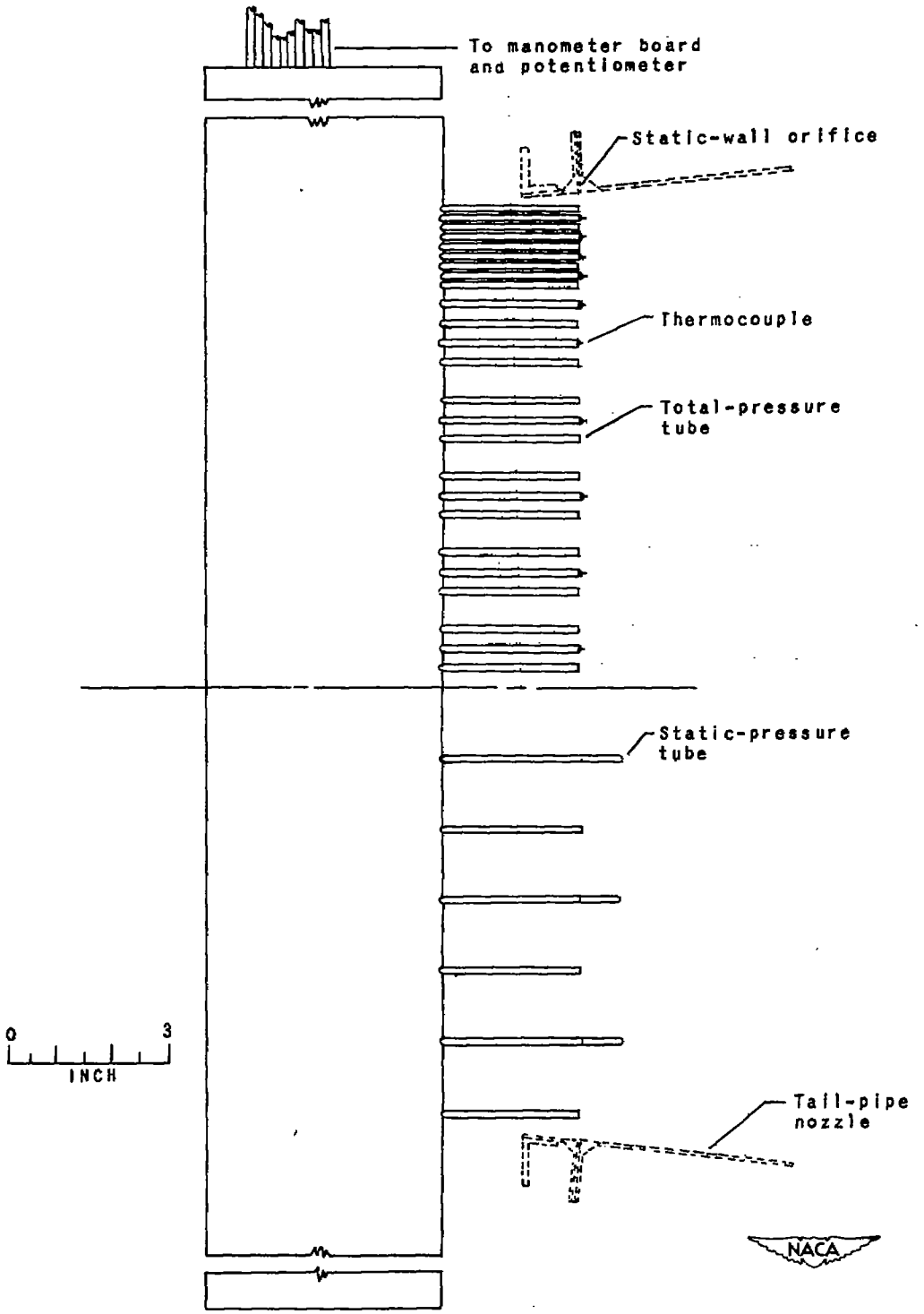

Figure 5. - Details of total- and static-pressure-tube and thermocouple installation at nozzle outlet.

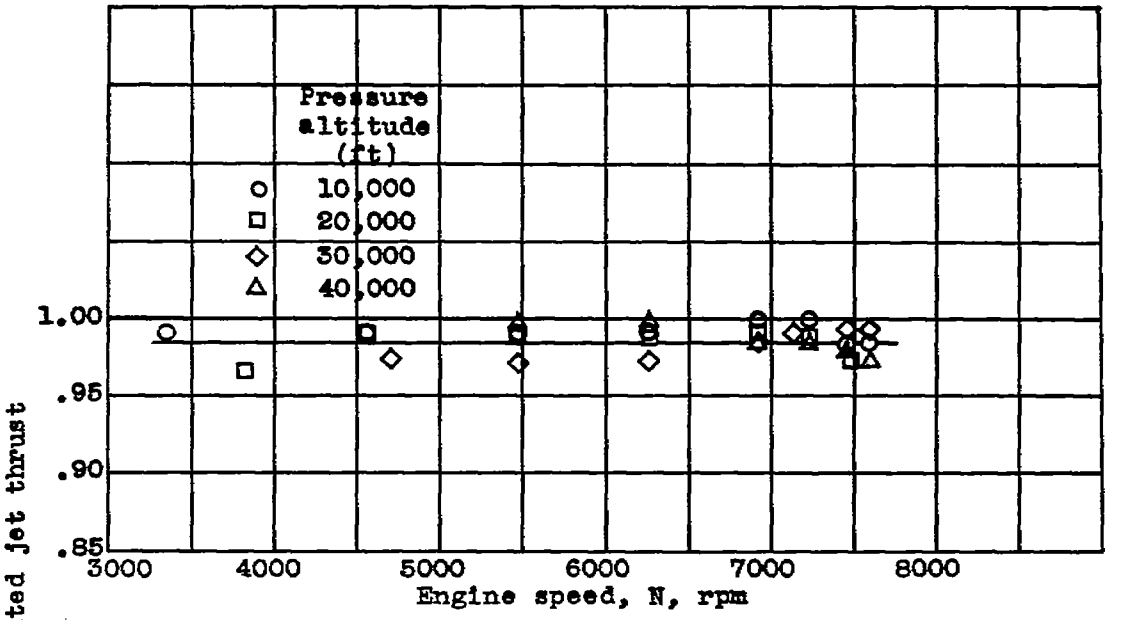

Figure 6.- Ratio of measured jet thrust to calculated jet thrust for various engine speeds and altitudes at a ram pressure ratio of 1.2.

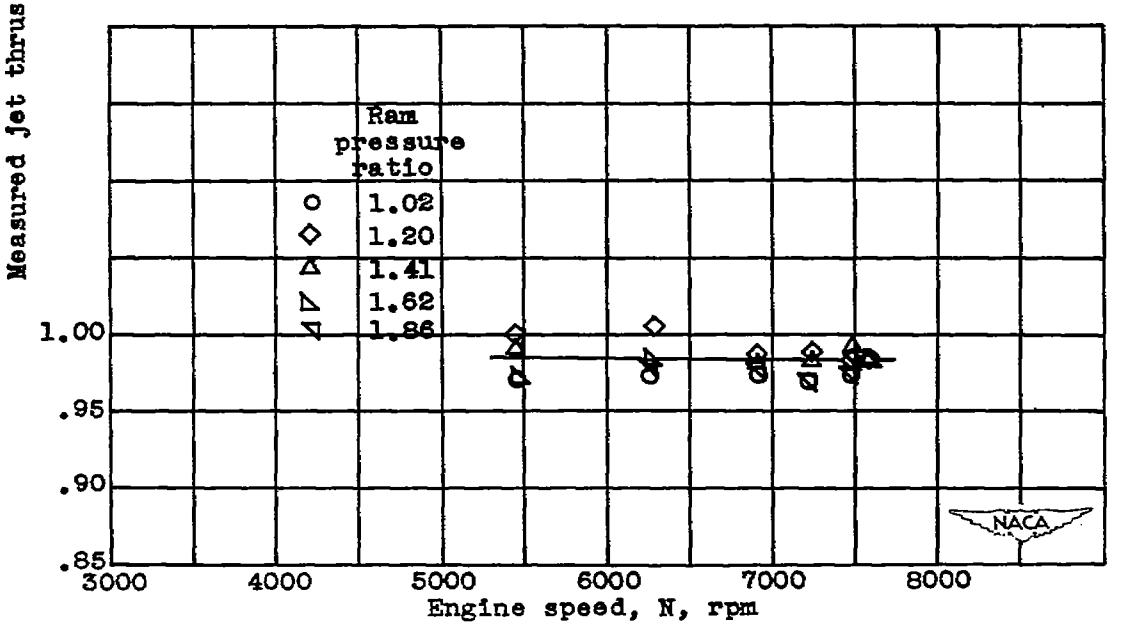

Figure 7.- Ratio of measured jet thrust to calculated jet thrust for various engine speeds and ram pressure ratios at an altitude of 40,000 feet.

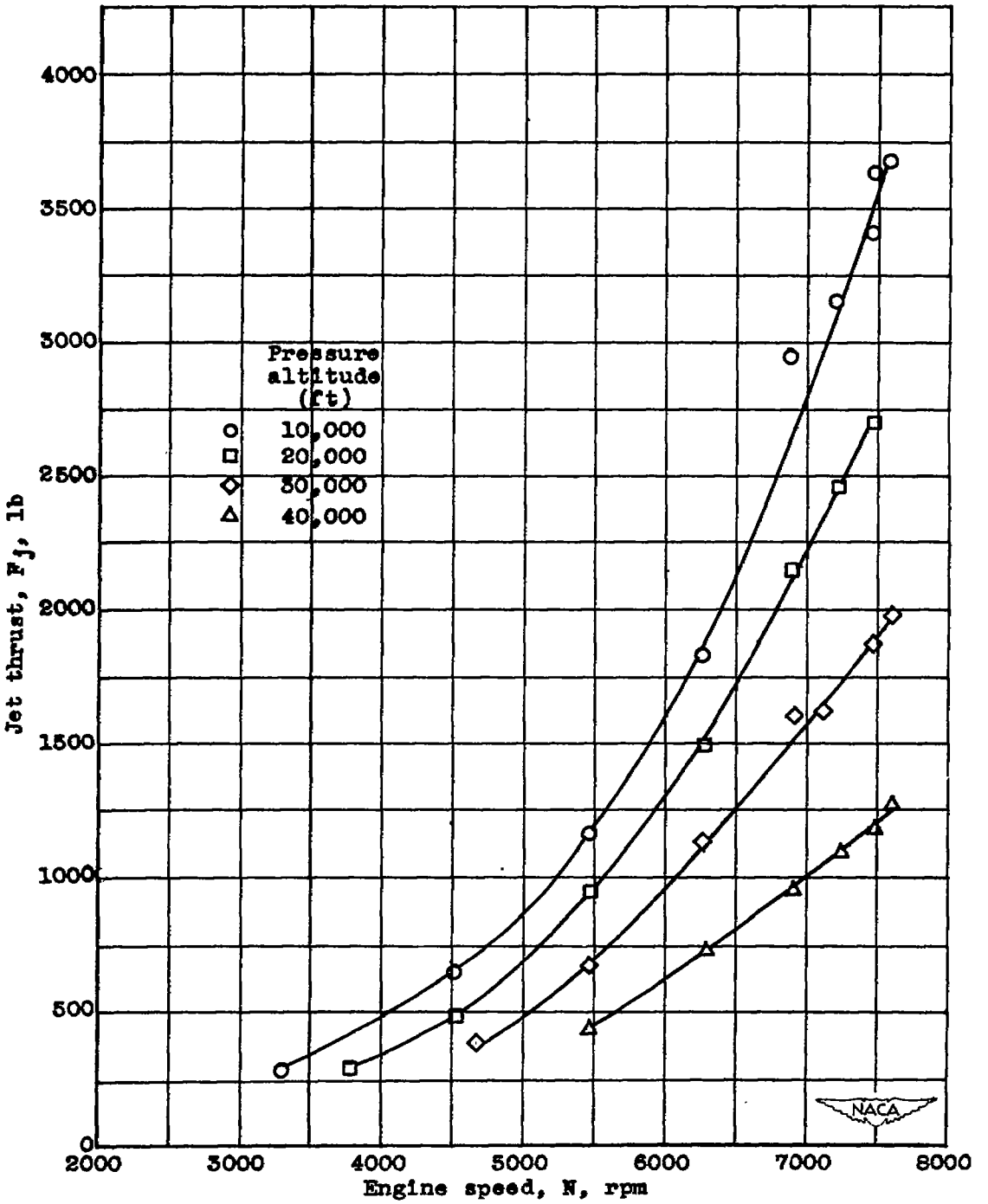

Figure 8.- Effect of engine speed and altitude on jet thrust at a ram pressure ratio of approximately 1.2.

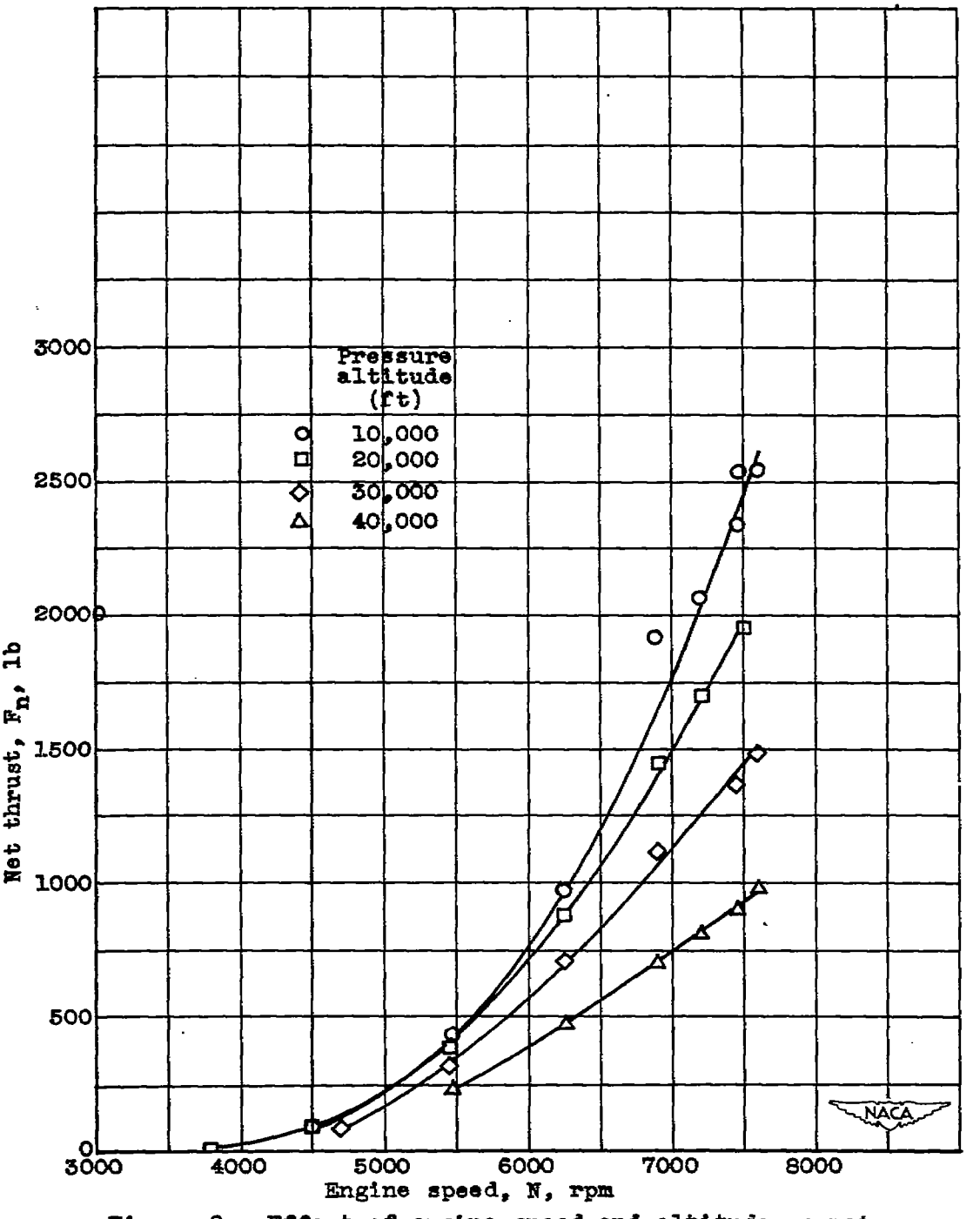

Figure 9.- Effect of engine speed and altitude on net thrust at a ram pressure ratio of approximately 1.2.

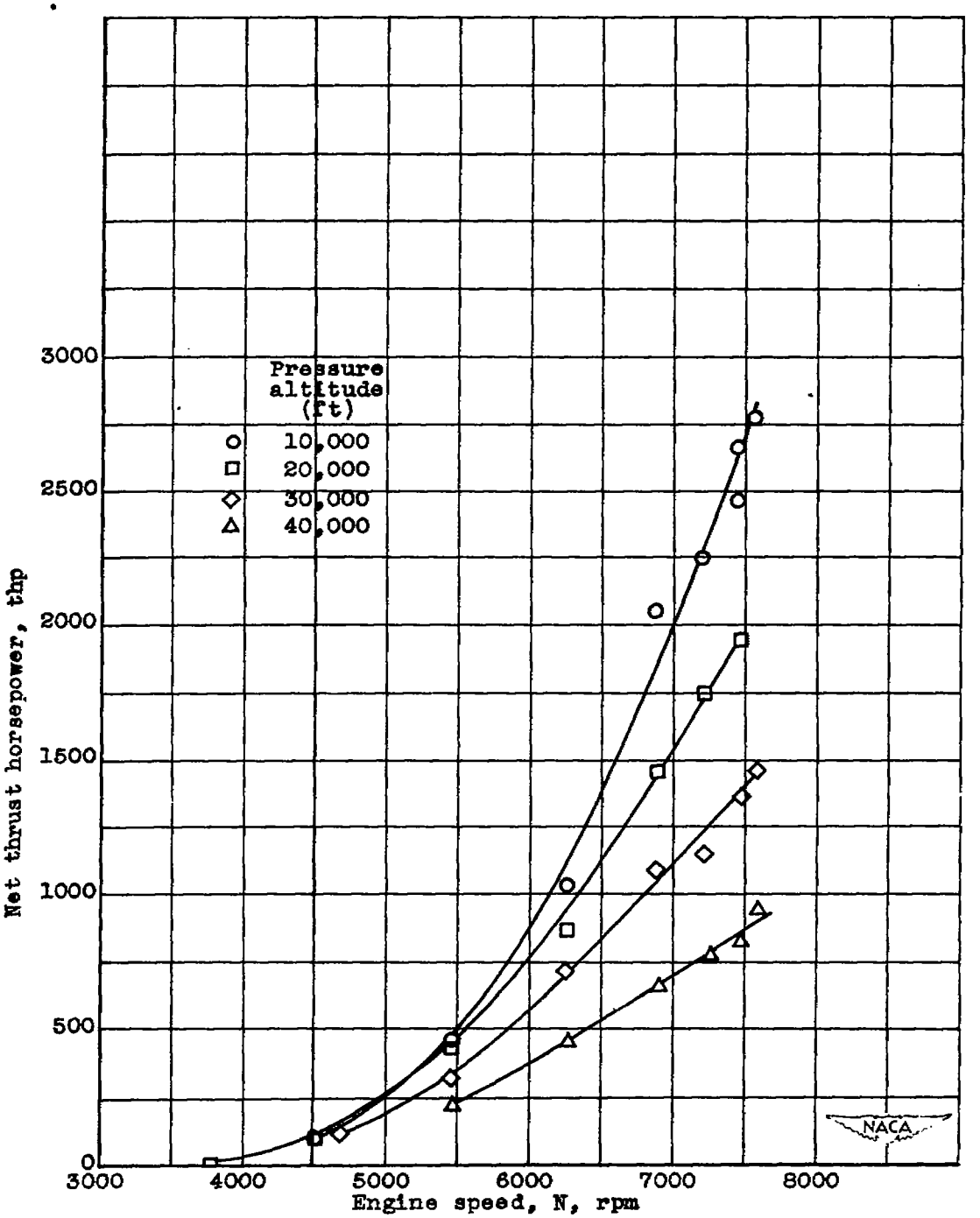

Figure 10.- Effect of engine speed and altitude on net thrust horsepower at a ram pressure ratio of approximately 1.2.

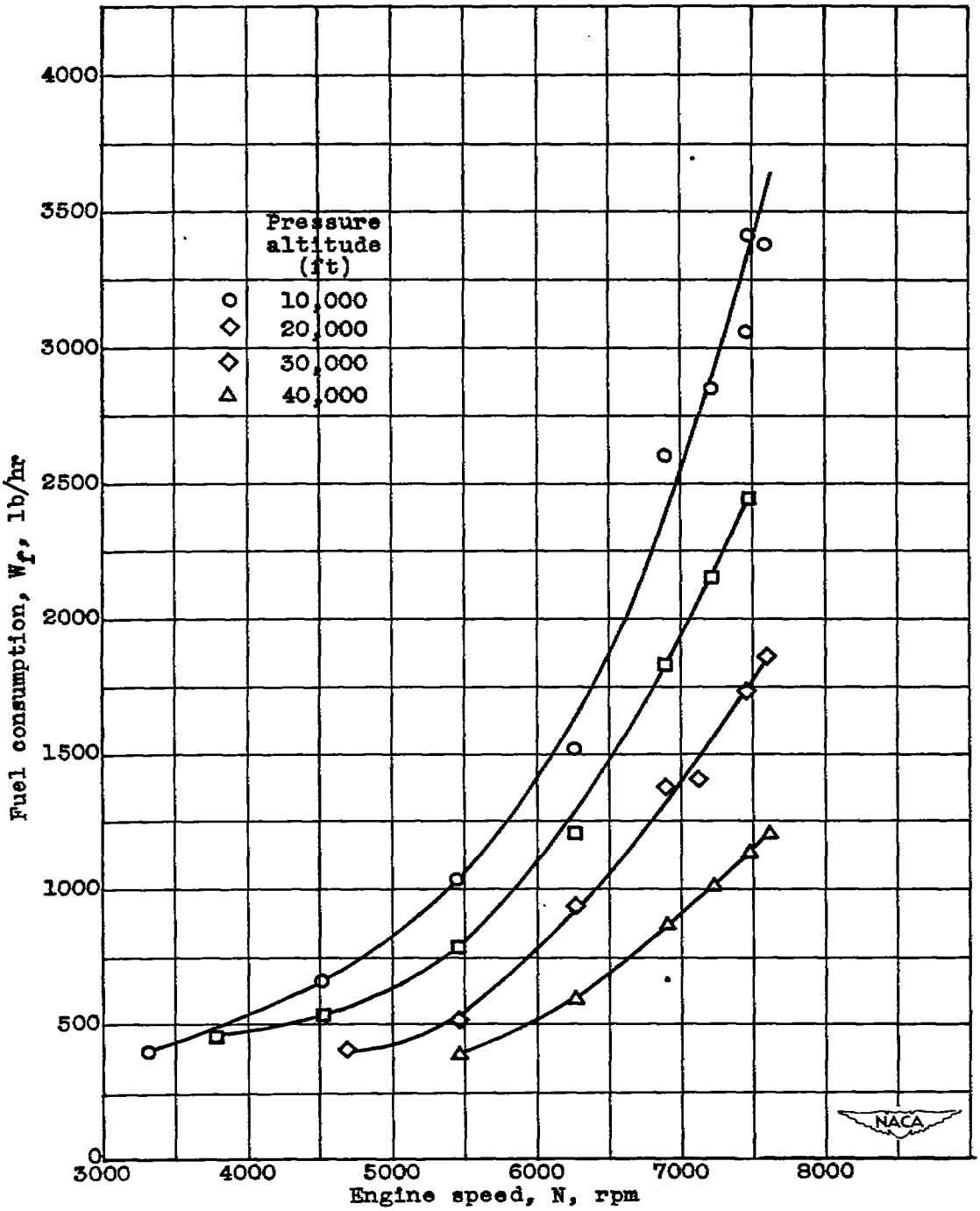

Figure 11.- Effect of engine speed and altitude on fuel consumption at a ram pressure ratio of approximately 1.2.

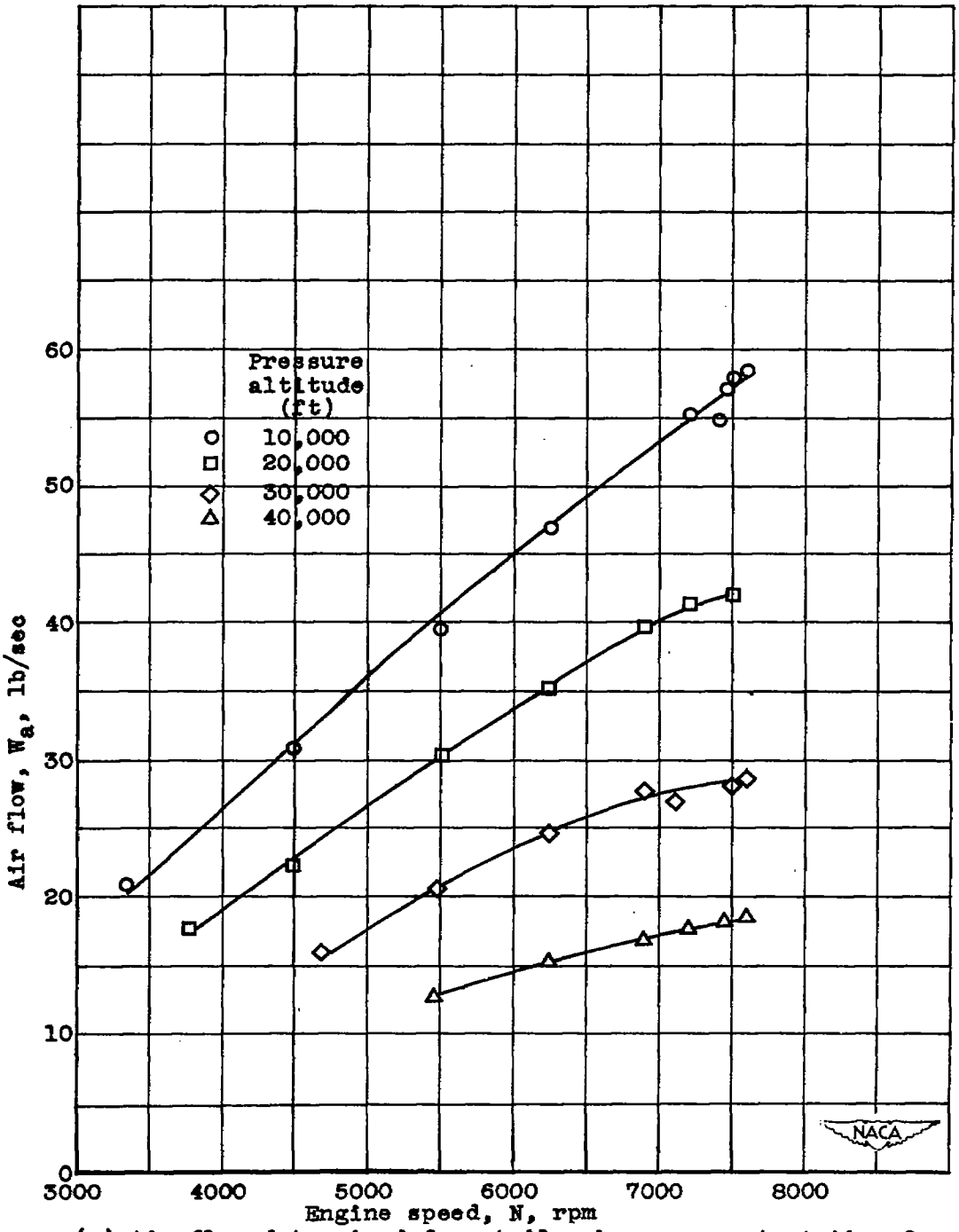

(a) Air flow determined from tail-rake survey at station 8.

Figure 12.- Effect of engine speed and altitude on air flow at a ram pressure ratio of approximately 1.2.

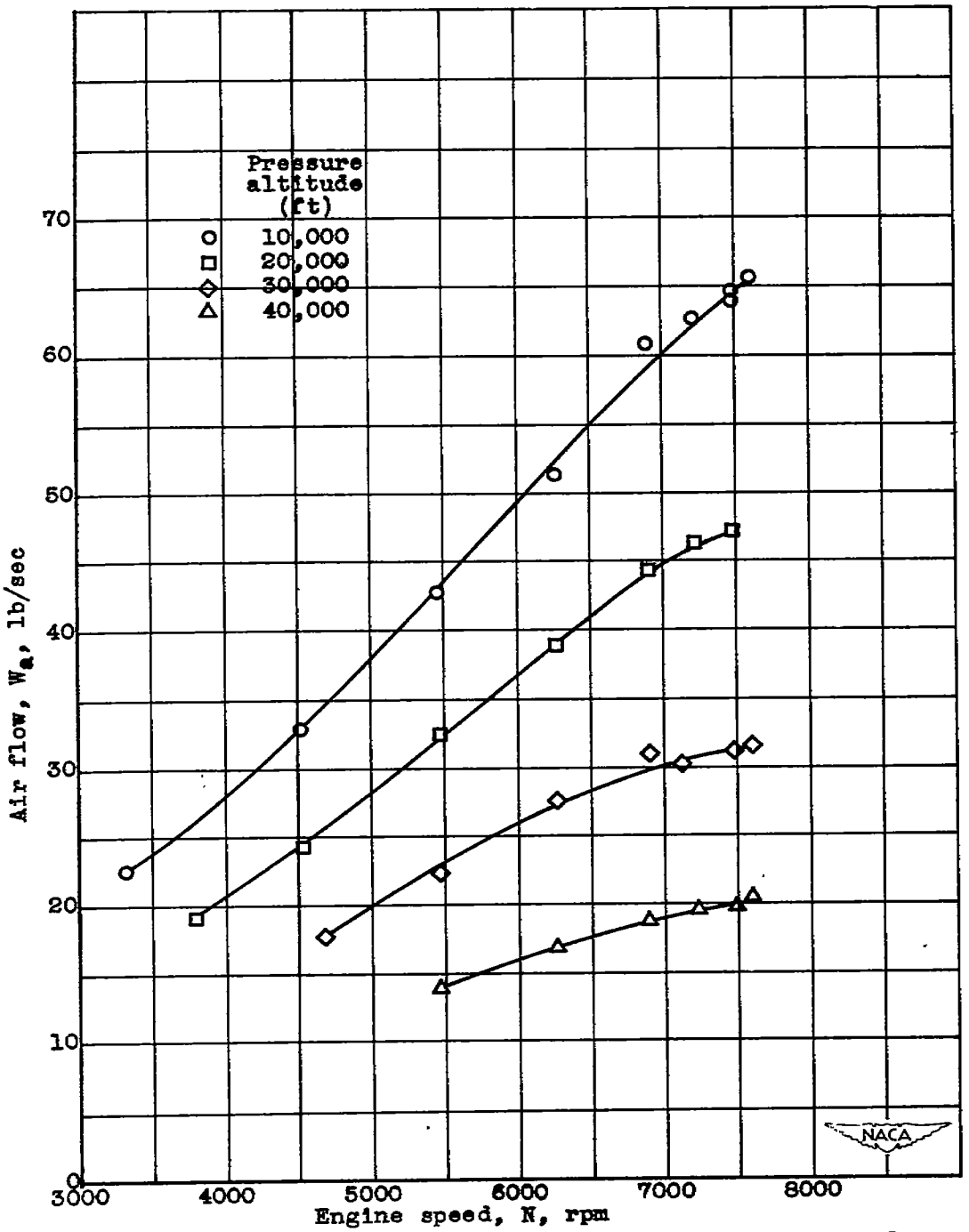

(b) Air flow determined from cowl-inlet survey at station 1.

Figure 12.- Concluded.

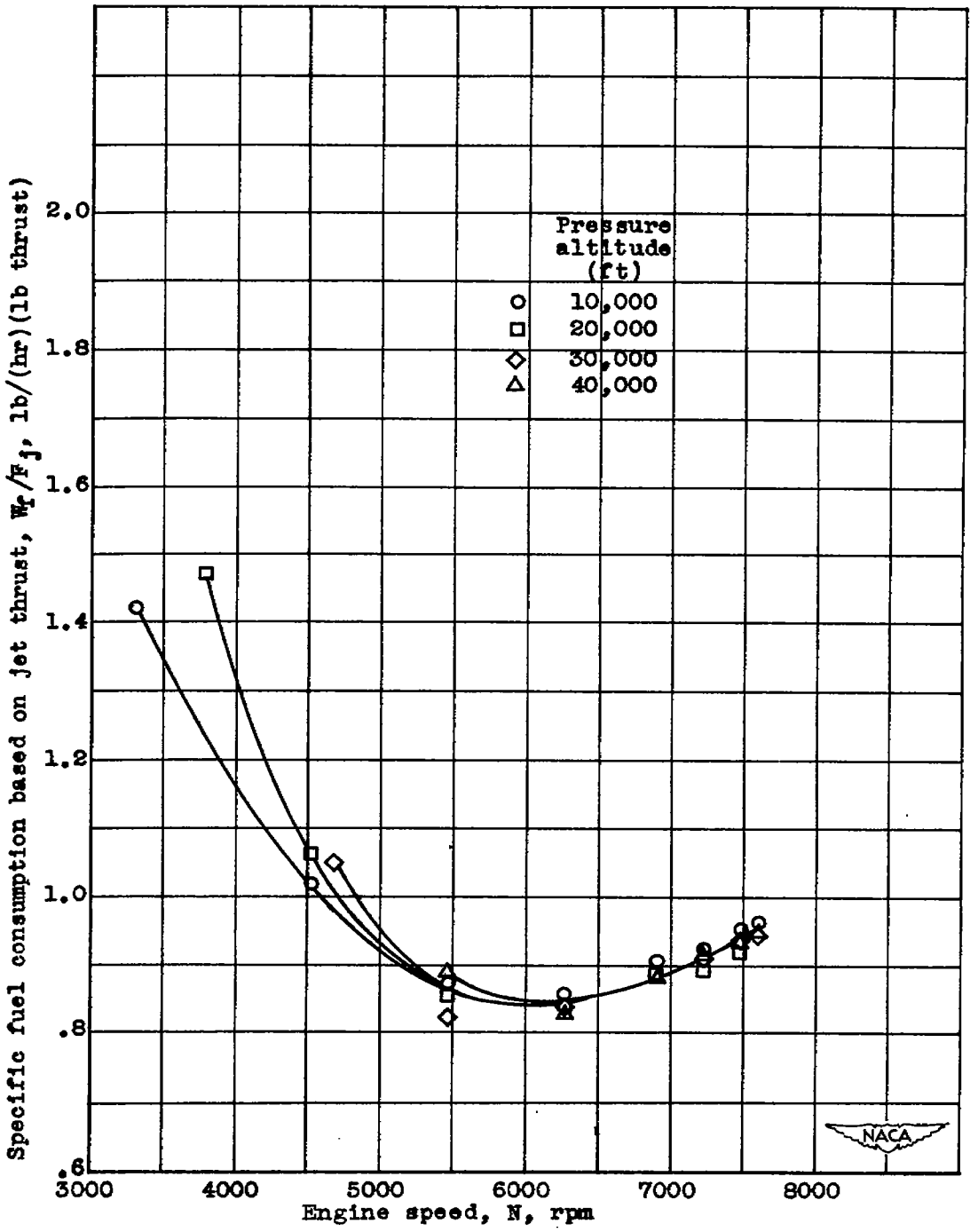

Figure 13.- Variation of specific fuel consumption based on jet thrust with engine speed and pressure altitude at a ram pressure ratio of approximately 1.2.

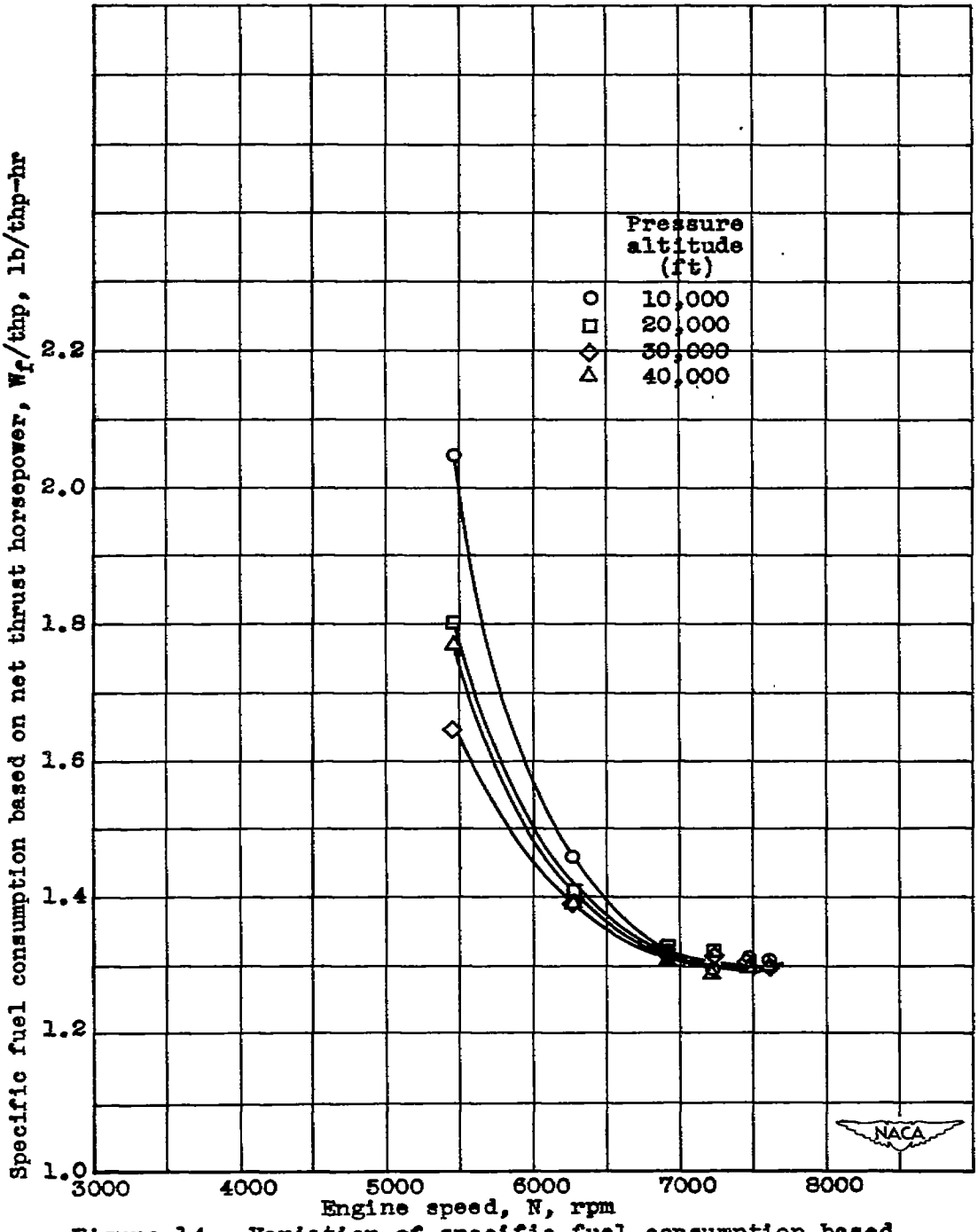

Figure 14.- Variation of specific fuel consumption based on net thrust horsepower with engine speed and pressure altitude at a ram pressure ratio of approximately 1.2.

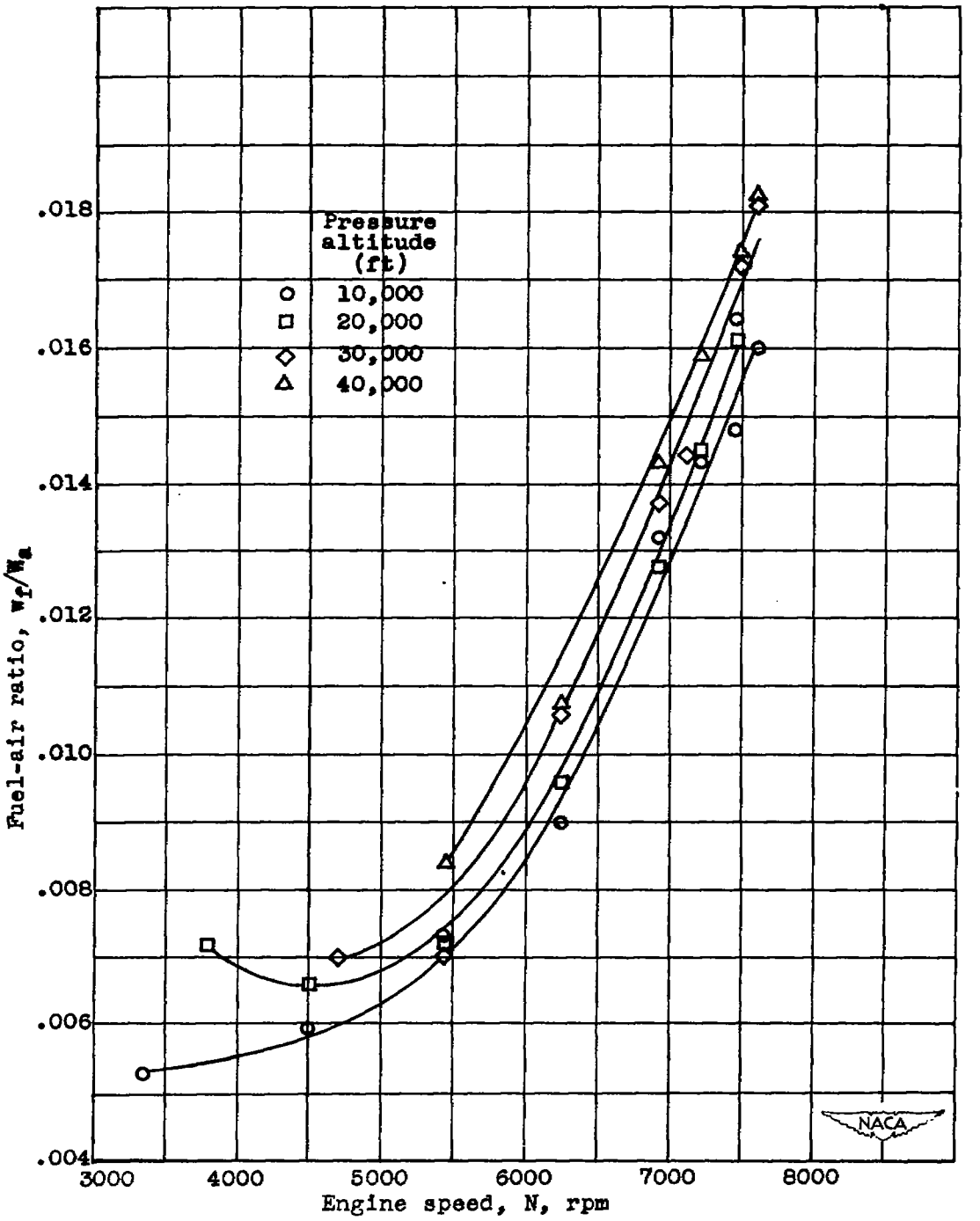

Figure 15.- Effect of engine speed and pressure altitude on fuel-air ratio at a ram pressure ratio of approximately 1.2.

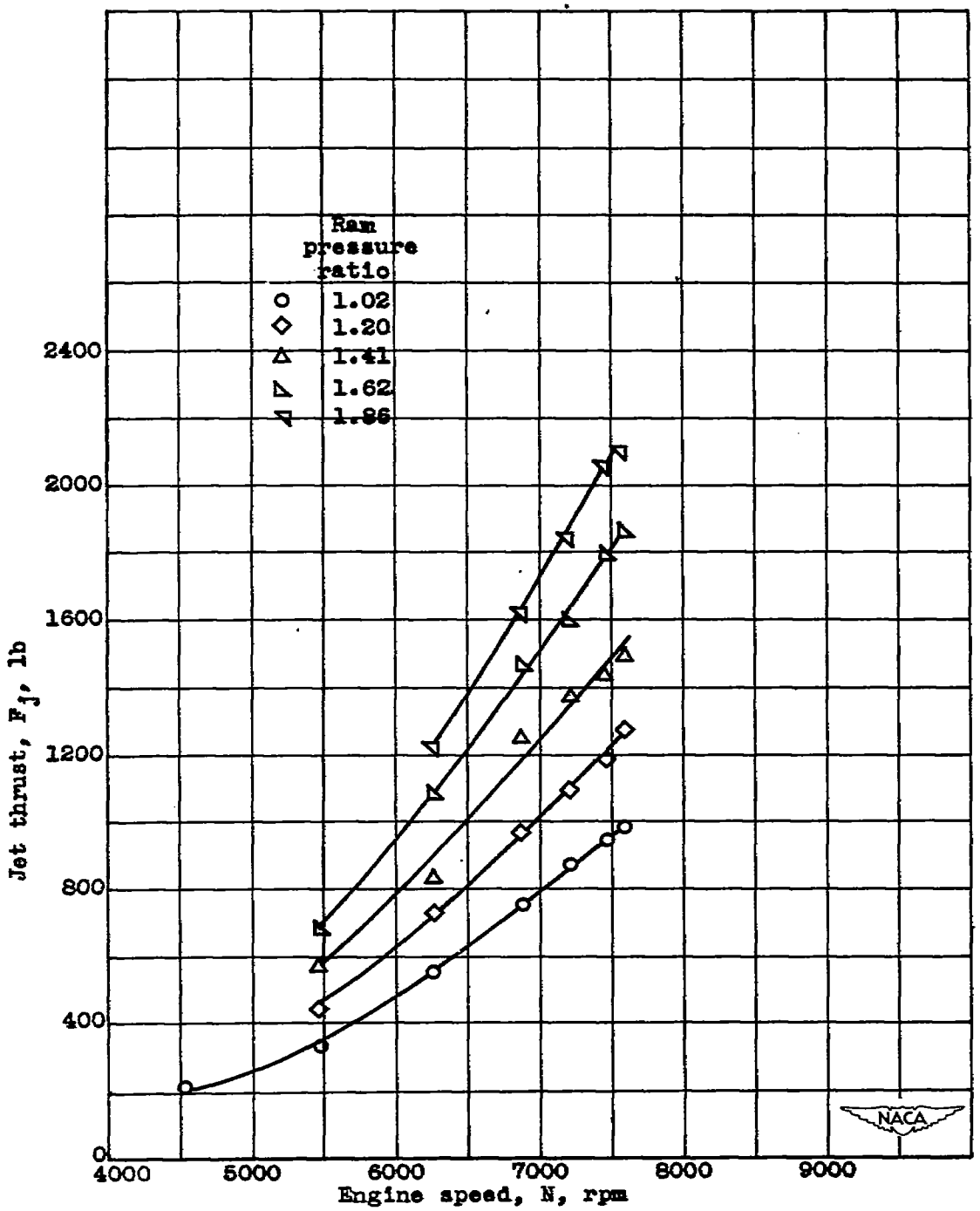

Figure 16.- Effect of engine speed and ram pressure ratio on jet thrust at a pressure altitude of 40,000 feet.

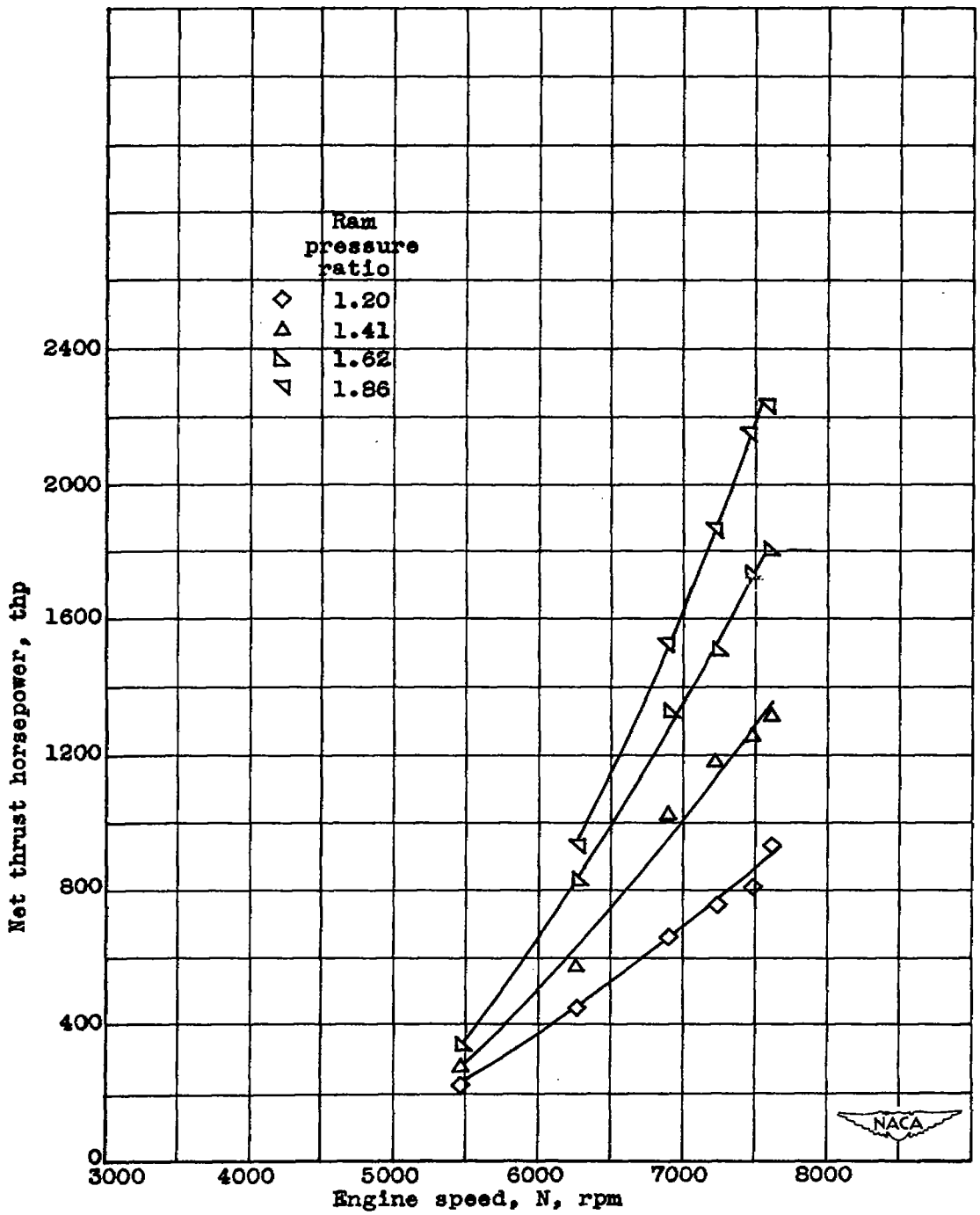

Figure 17.- Effect of engine speed and ram pressure ratio on net thrust horsepower at a pressure altitude of 40,000 feet.

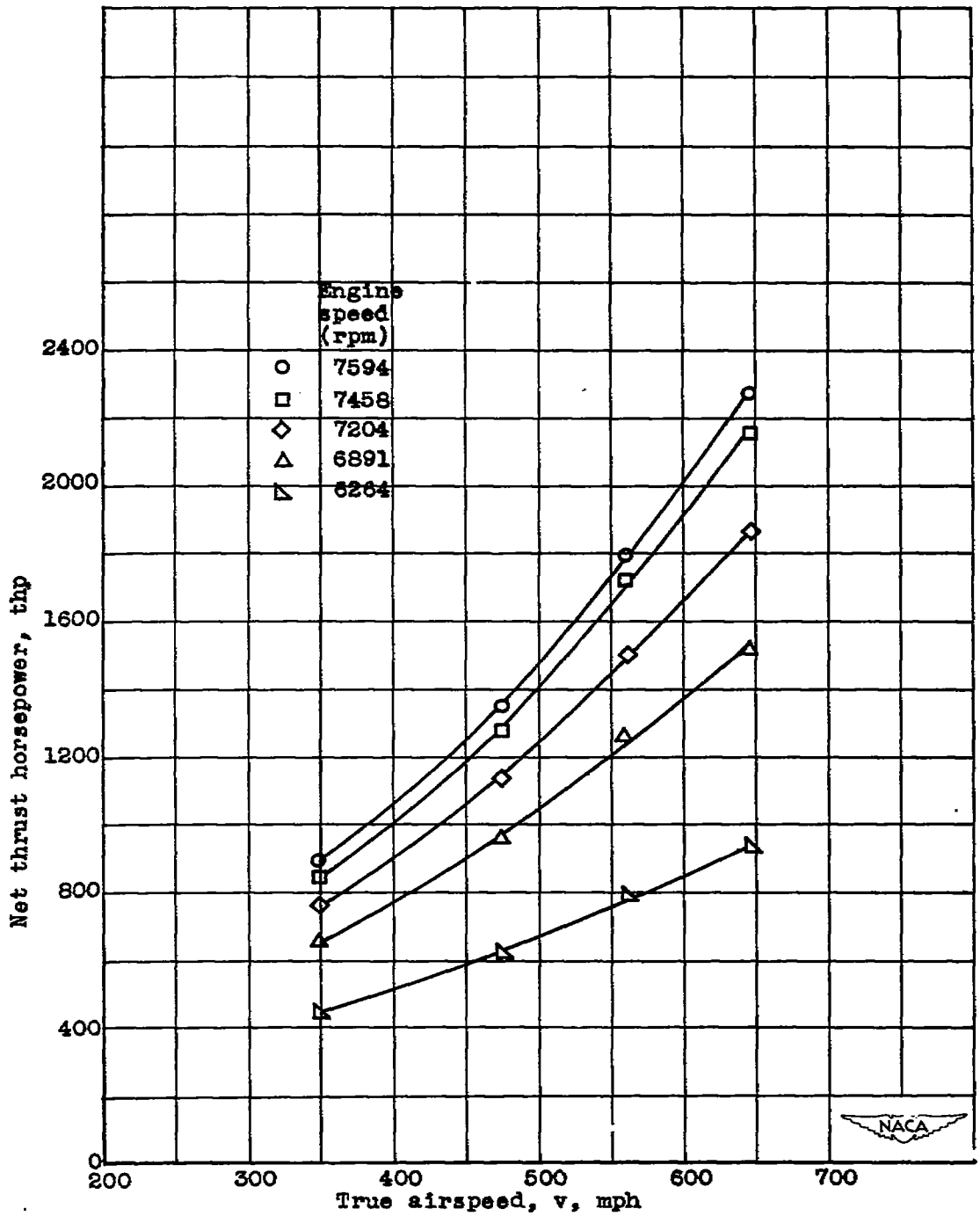

Figure 18.- Variation of net thrust horsepower with true airspeed for several engine speeds at a pressure altitude of 40,000 feet.

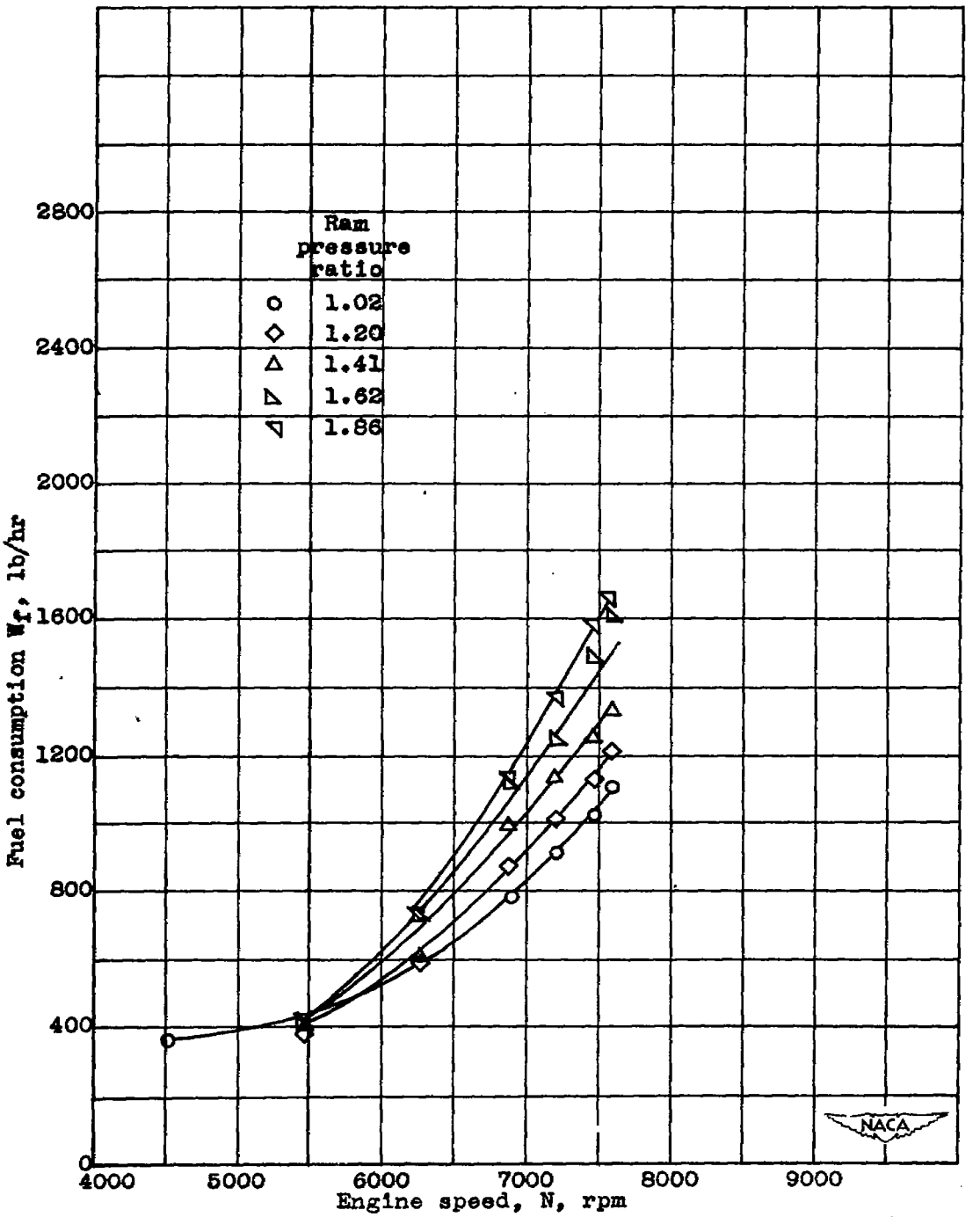

Figure 19.- Effect of engine speed and ram pressure ratio on fuel consumption at a pressure altitude of 40,000 feet.

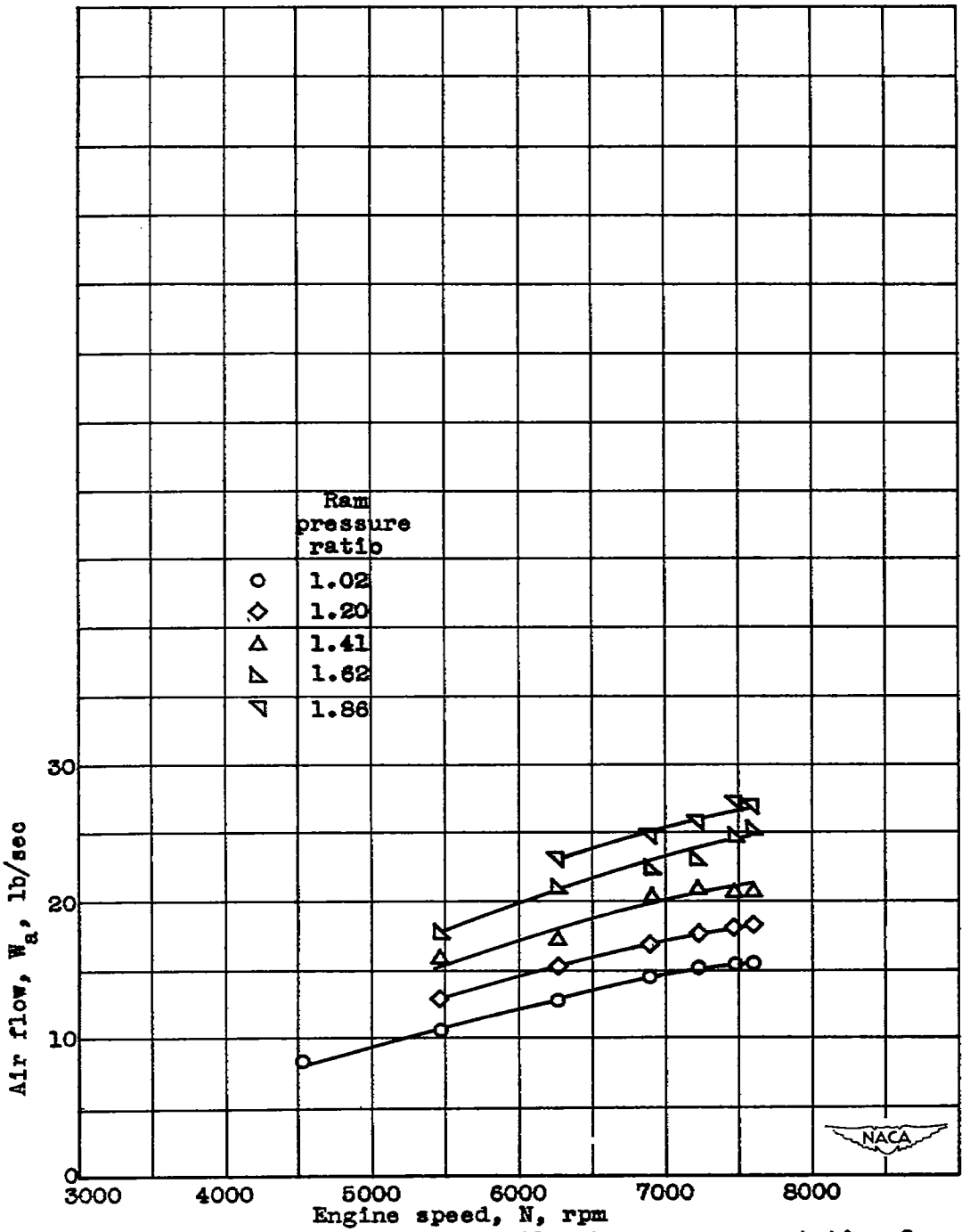

(a) Air flow determined from tail-rake survey at station 8.

Figure 20.- Effect of engine speed and ram pressure ratio on air flow at a pressure altitude of 40,000 feet.

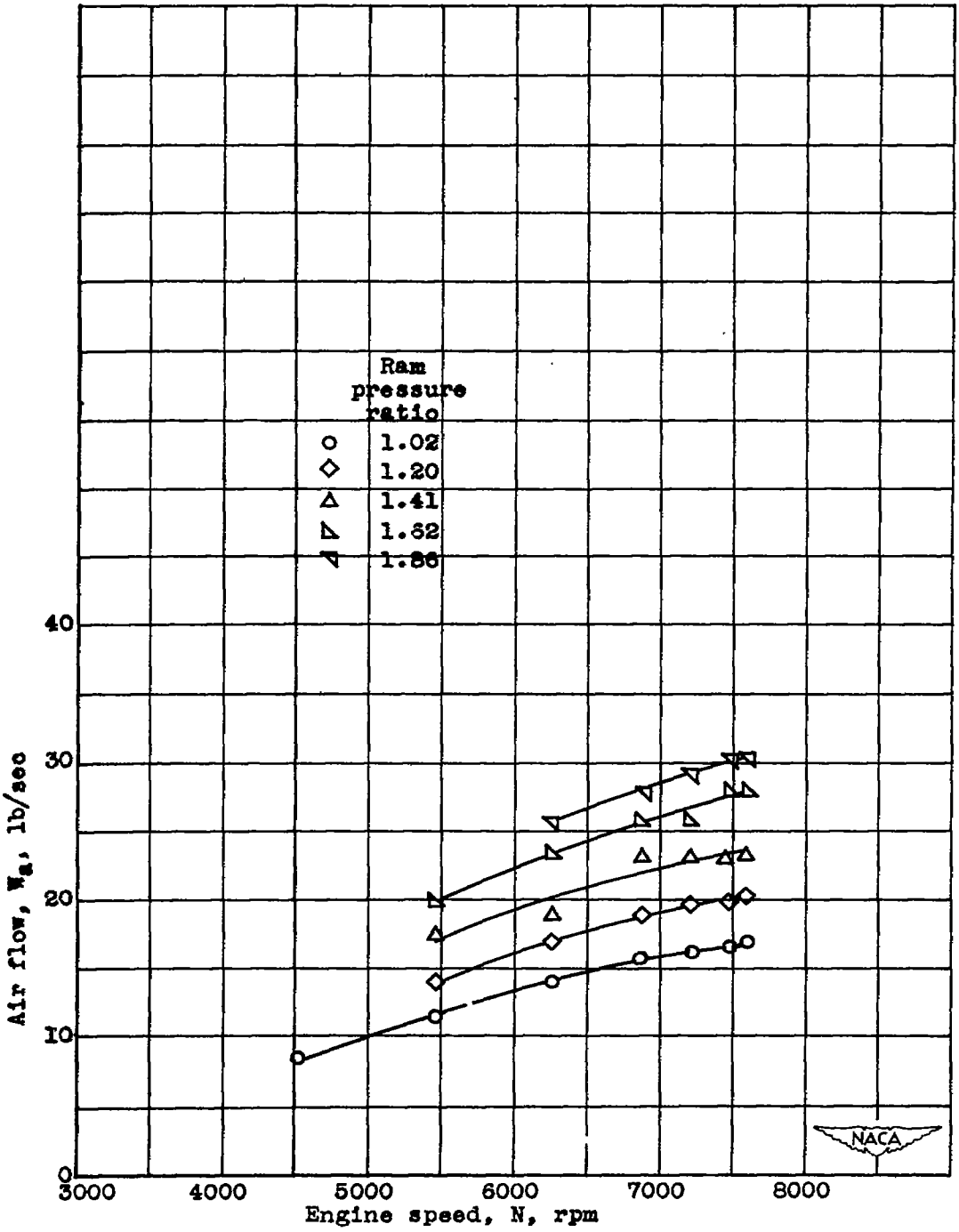

(b) Air flow determined from cowl-inlet survey at station 1.

Figure 20.- Concluded.

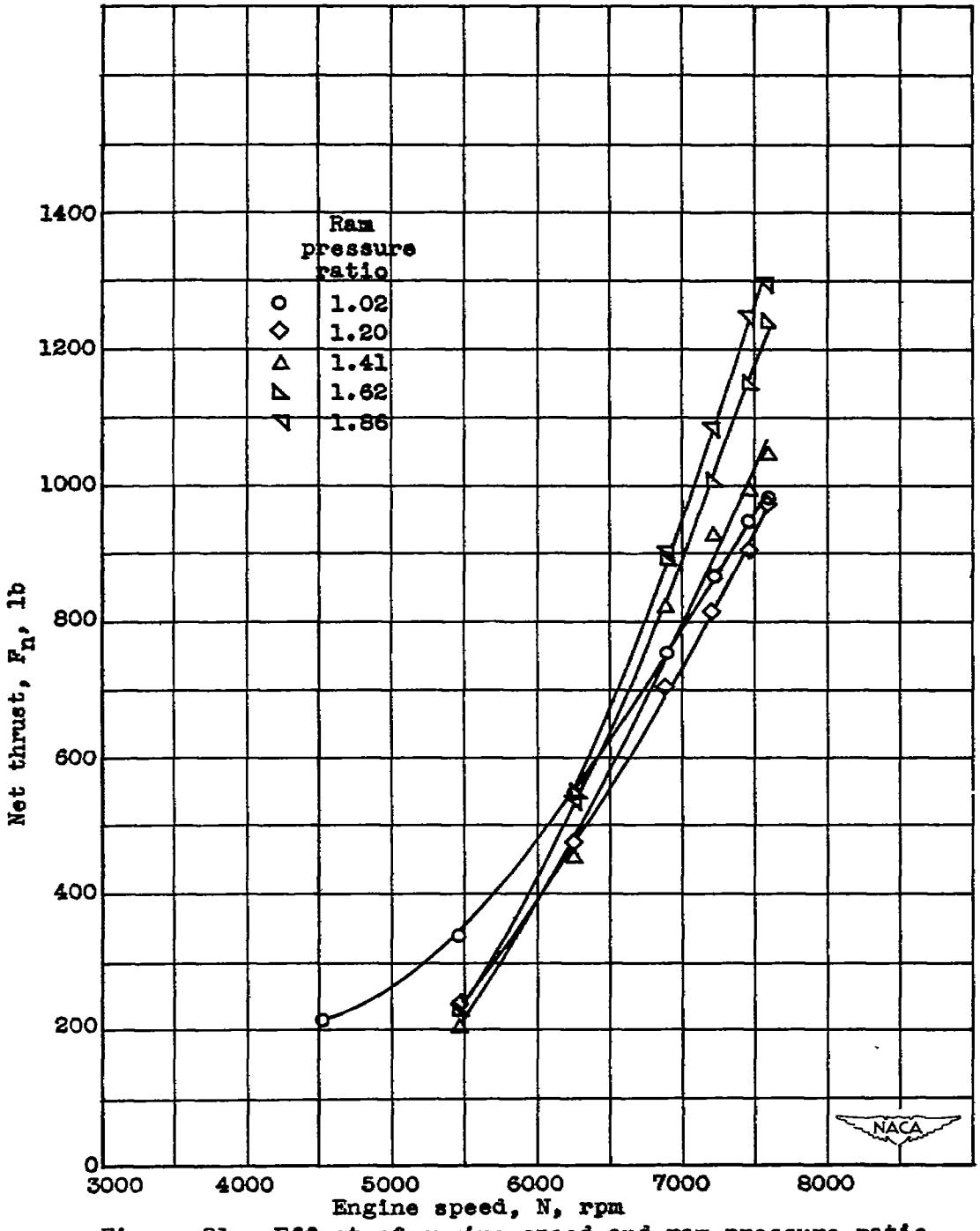

Figure 21.- Effect of engine speed and ram pressure ratio on net thrust at an altitude of 40,000 feet.

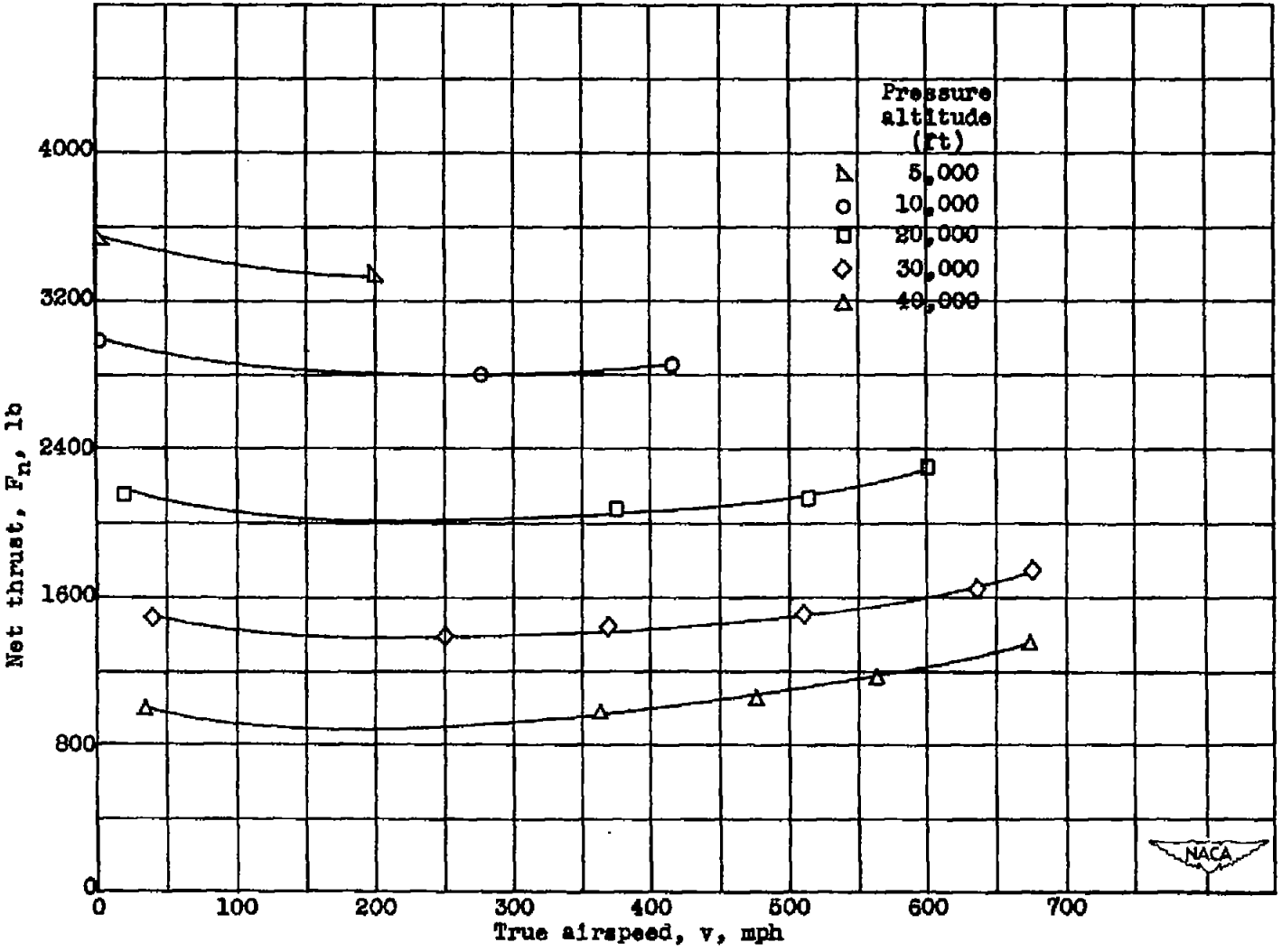

Figure 22.- Variation of net thrust with altitude and true airspeed at an engine speed of 7594 rpm.

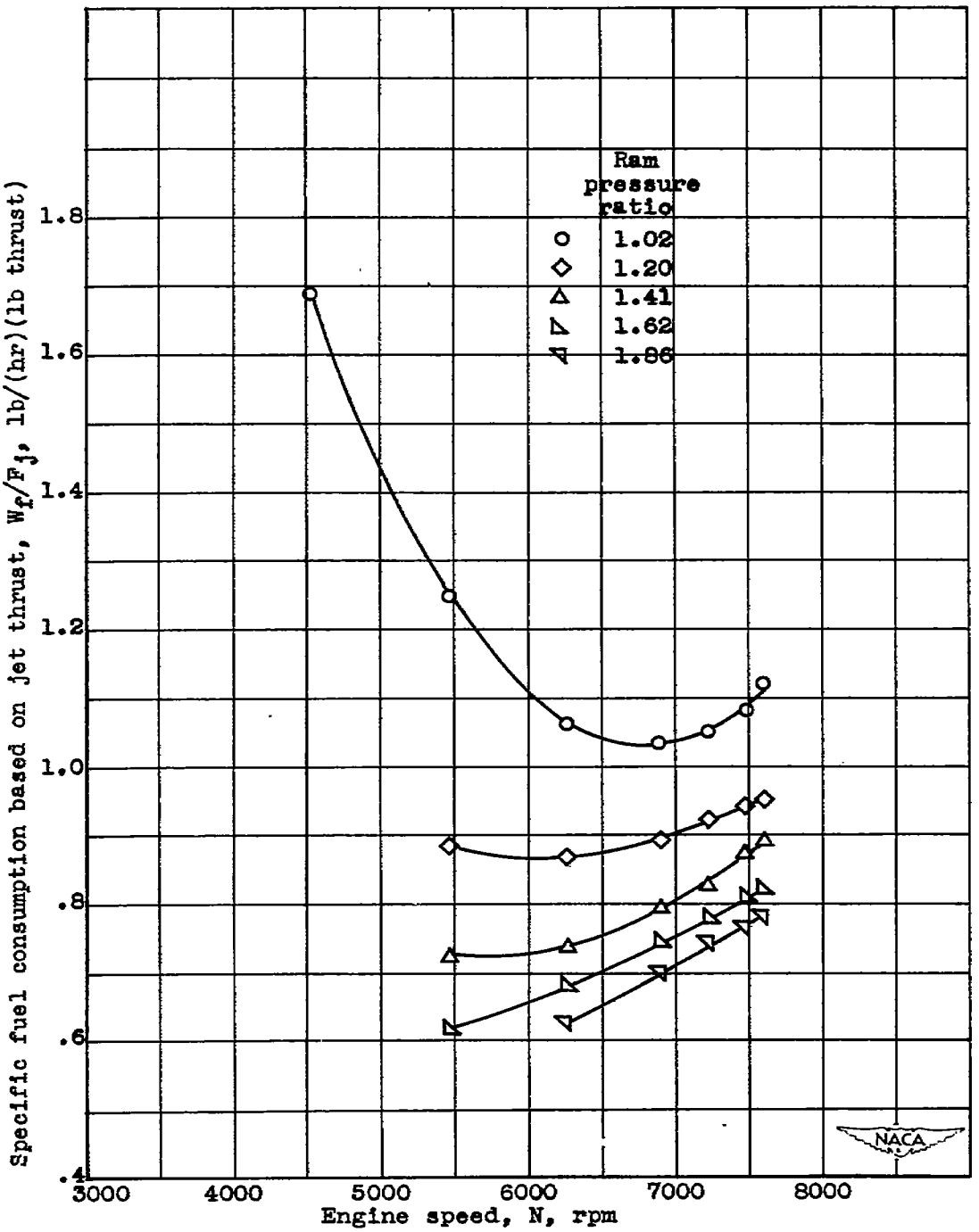

Figure 23.- Effect of engine speed and ram pressure ratio on specific fuel consumption based on jet thrust at a pressure altitude of 40,000 feet.

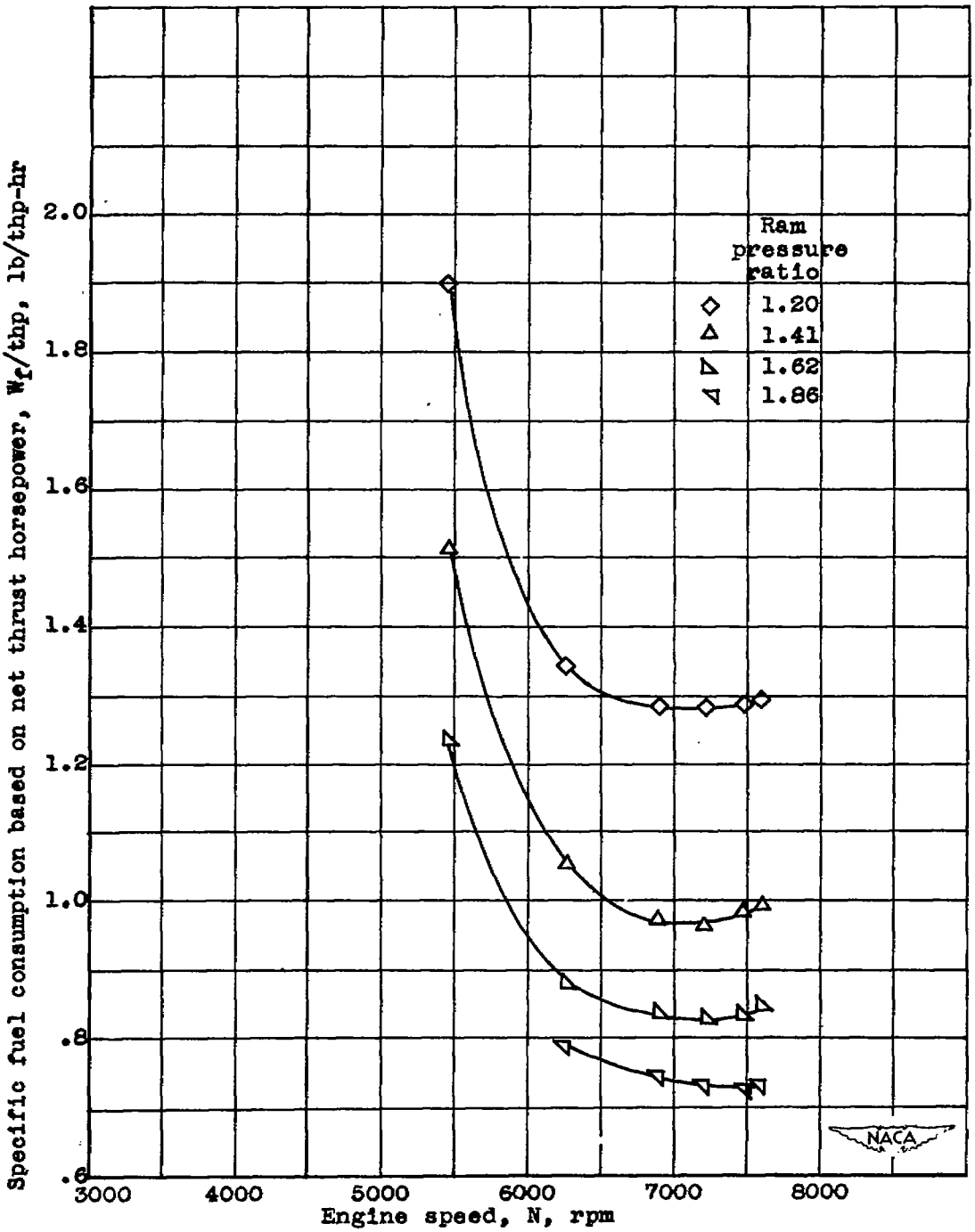

Figure 24.- Effect of engine speed and ram pressure ratio on specific fuel consumption based on net thrust horsepower at a pressure altitude of 40,000 feet.

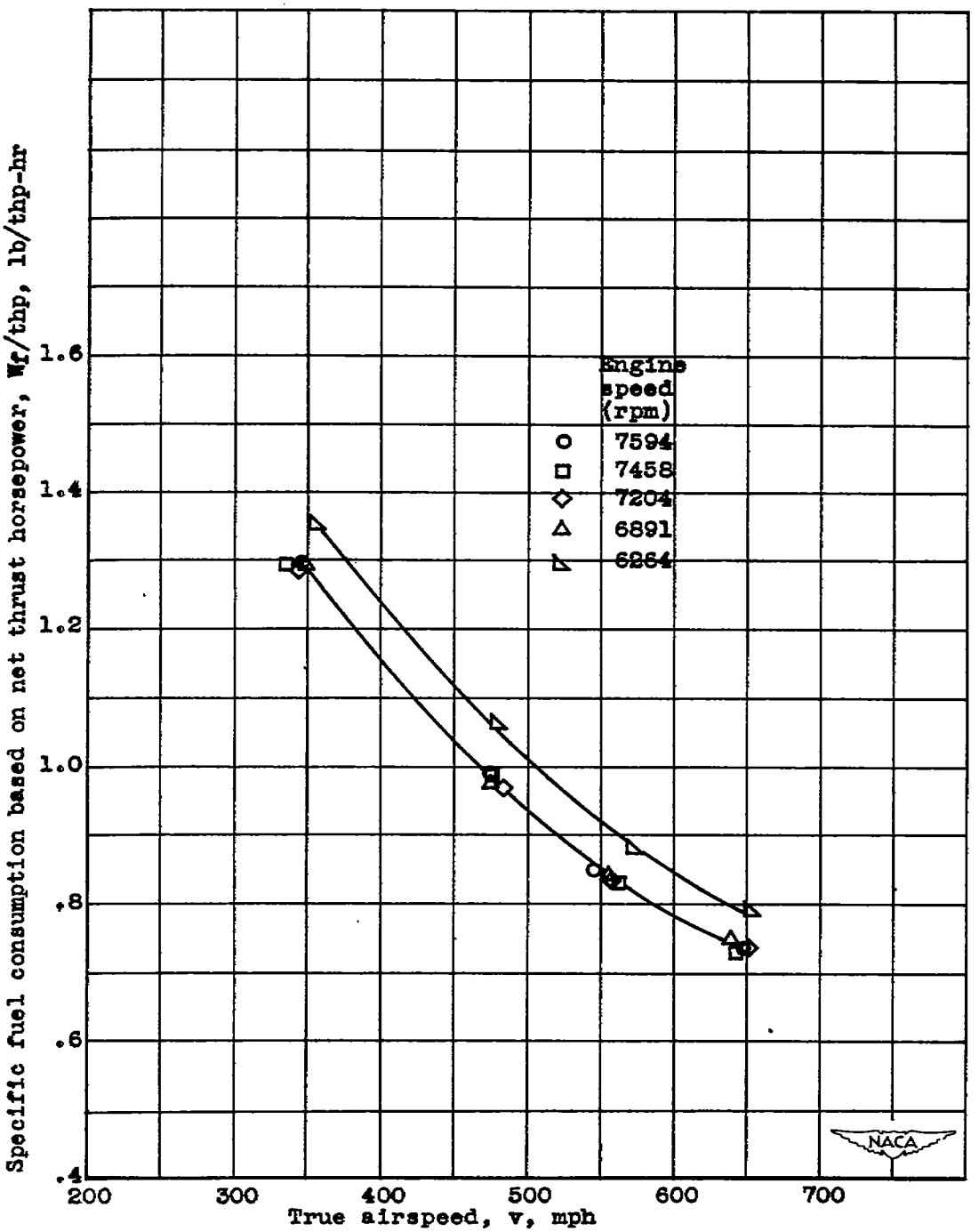

Figure 25.- Variation of specific fuel consumption based on net thrust horsepower with true airspeed for several engine speeds at a pressure altitude of 40,000 feet.

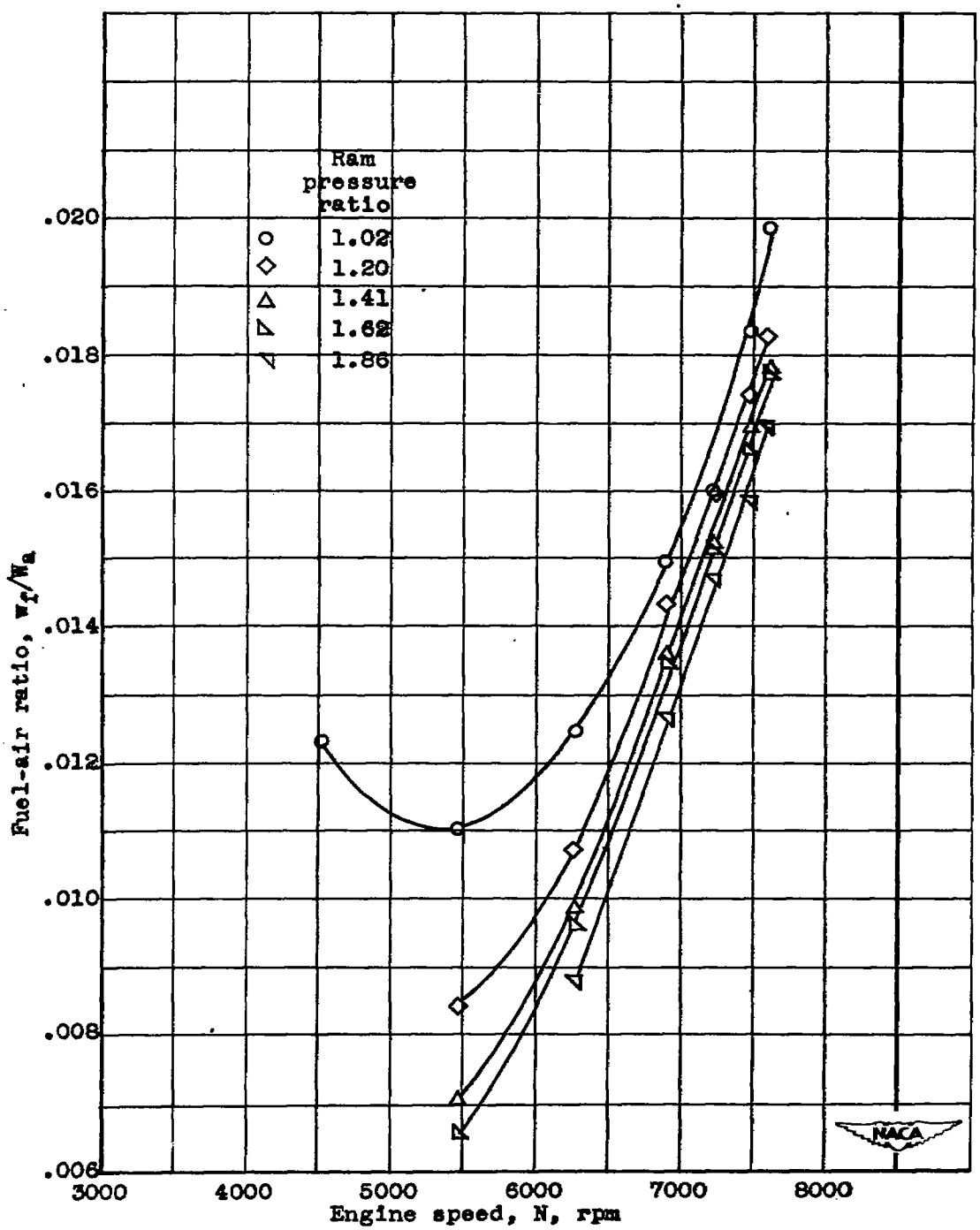

Figure 26.- Effect of engine speed and ram pressure ratio on fuel-air ratio at a pressure altitude of 40,000 feet.

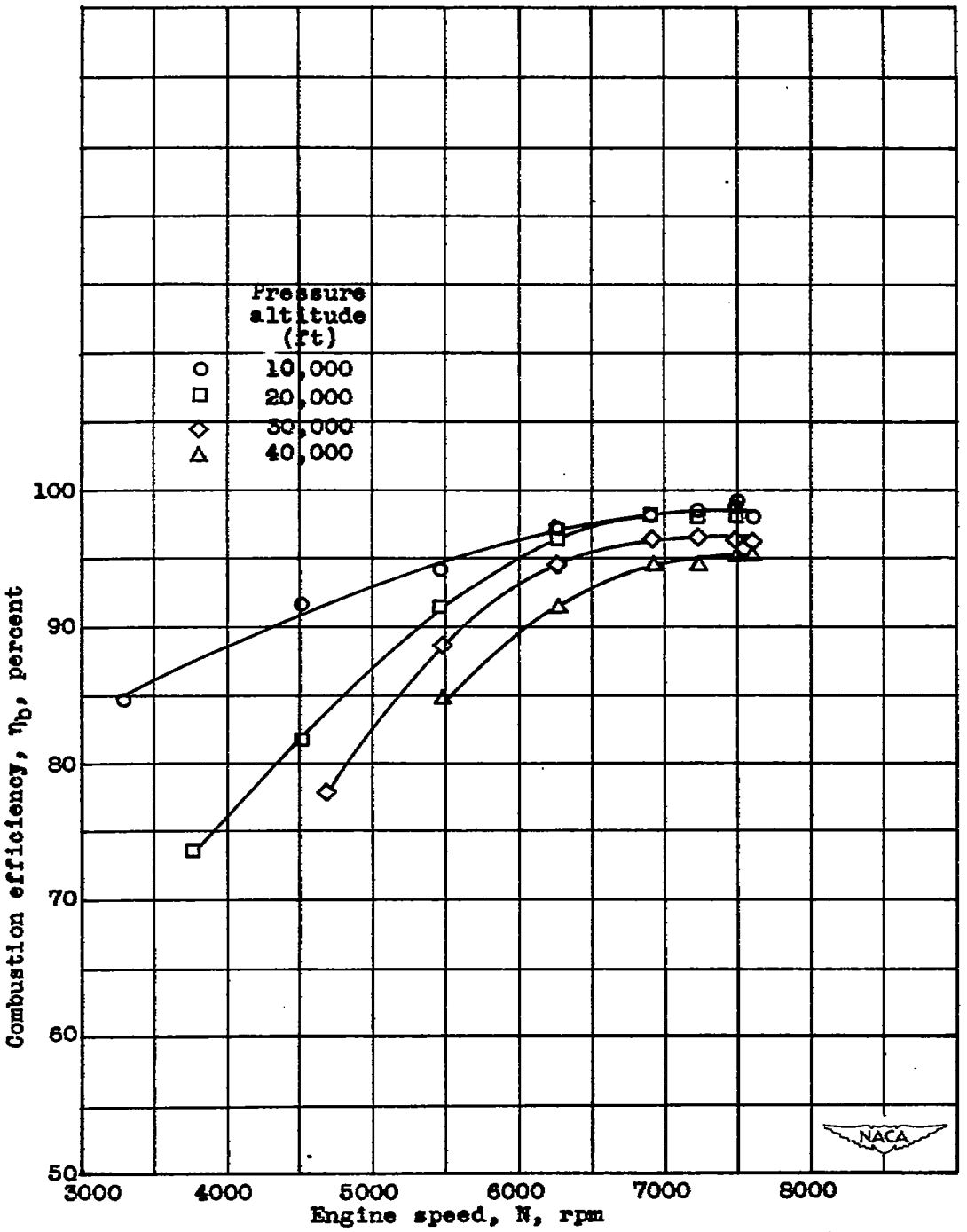

Figure 27.- Effect of engine speed and pressure altitude on combustion efficiency at a ram pressure ratio of approximately 1.2.

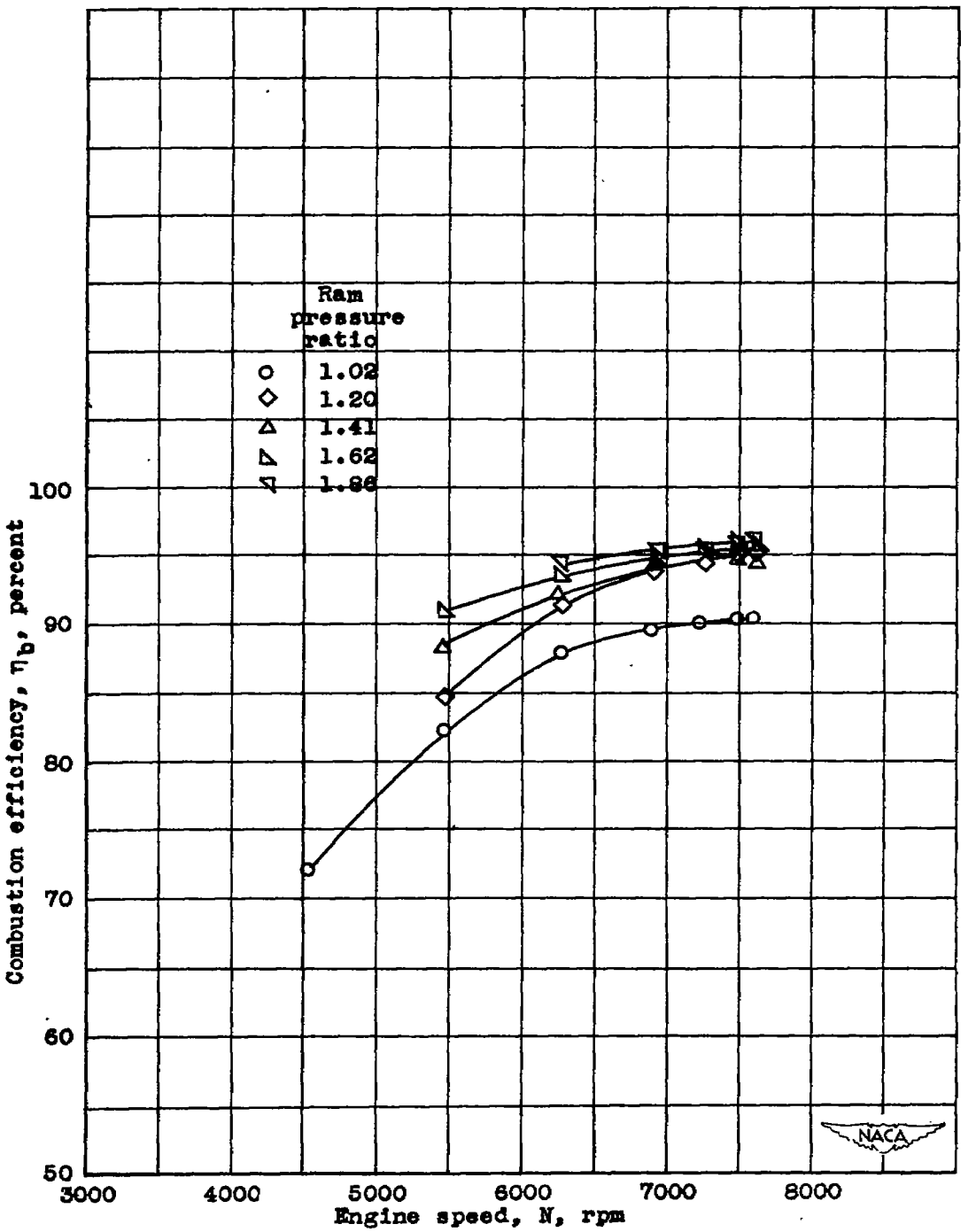

Figure 28.- Effect of engine speed and ram pressure ratio on combustion efficiency at a pressure altitude of 40,000 feet.

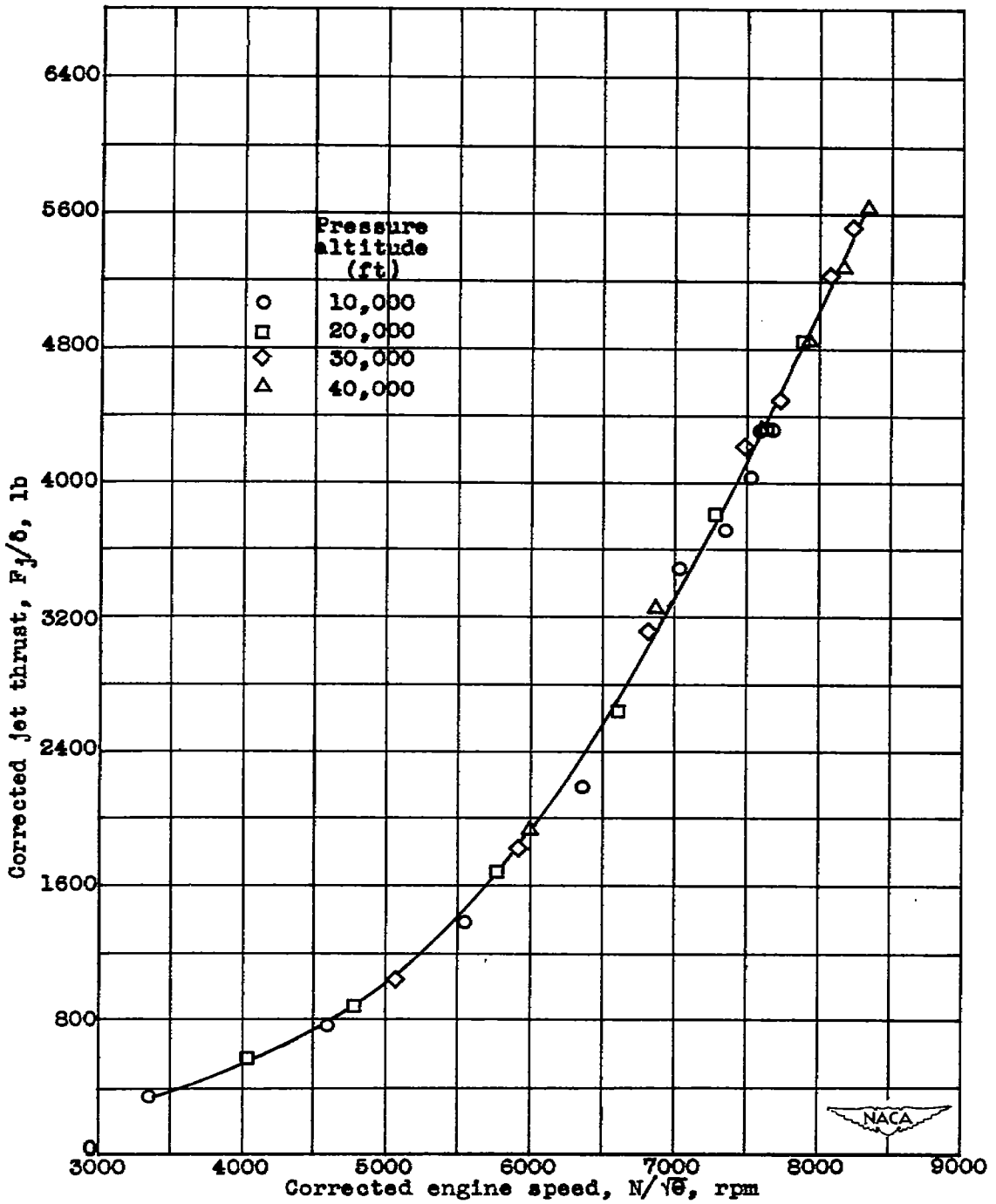

Figure 29. - Effect of corrected engine speed and altitude on corrected jet thrust at a ram pressure ratio of approximately 1.2. Engine speed and jet thrust corrected to NACA standard atmospheric conditions at sea level.

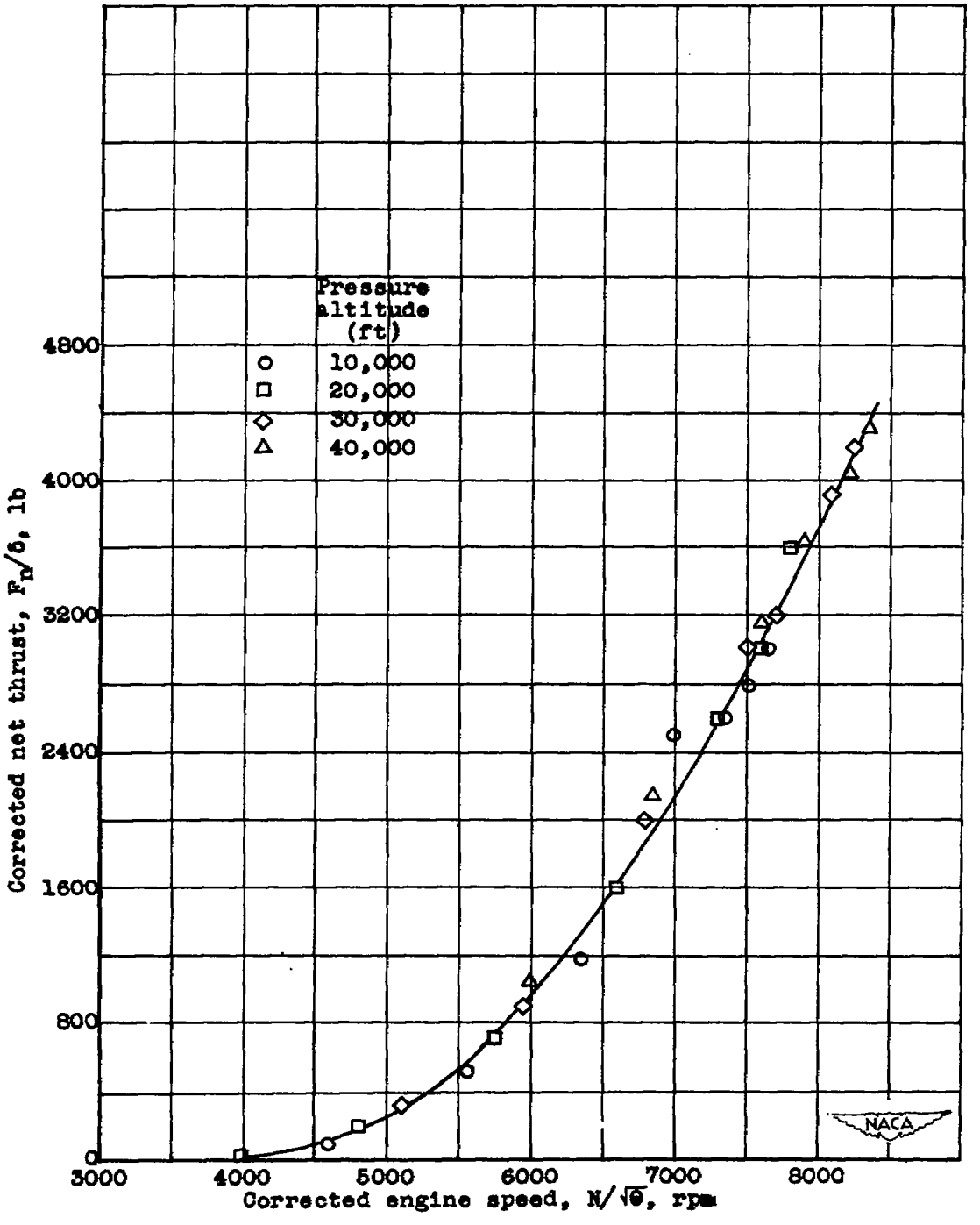

Figure 30. - Effect of corrected engine speed and pressure altitude on corrected net thrust at a ram pressure ratio of approximately 1.2. Engine speed and net thrust corrected to NACA standard atmospheric conditions at sea level.

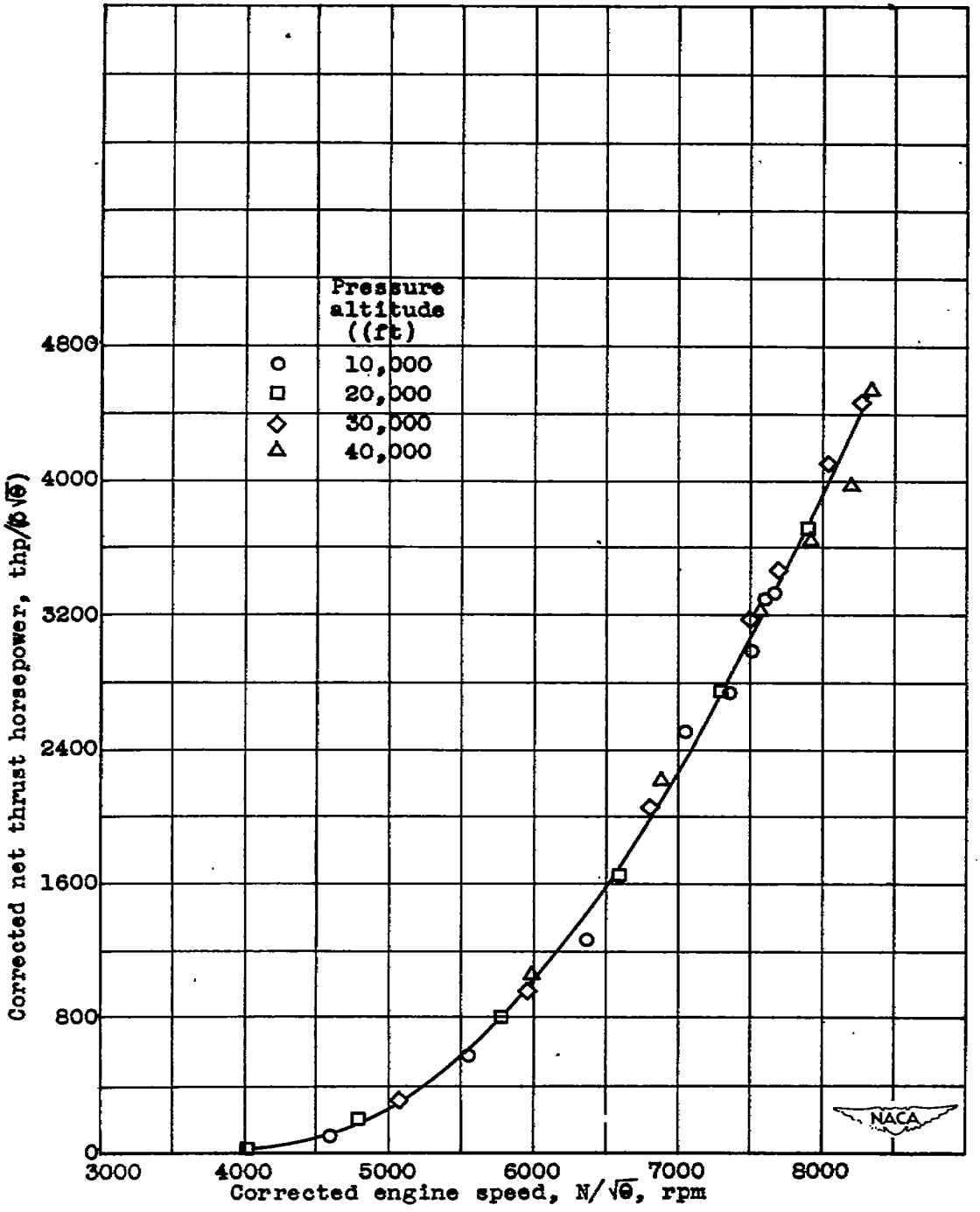

Figure 31. – Effect of corrected engine speed and pressure altitude on corrected net thrust horsepower at a ram pressure ratio of approximately 1.2. Engine speed and net thrust horsepower corrected to NACA standard atmospheric conditions at sea level.

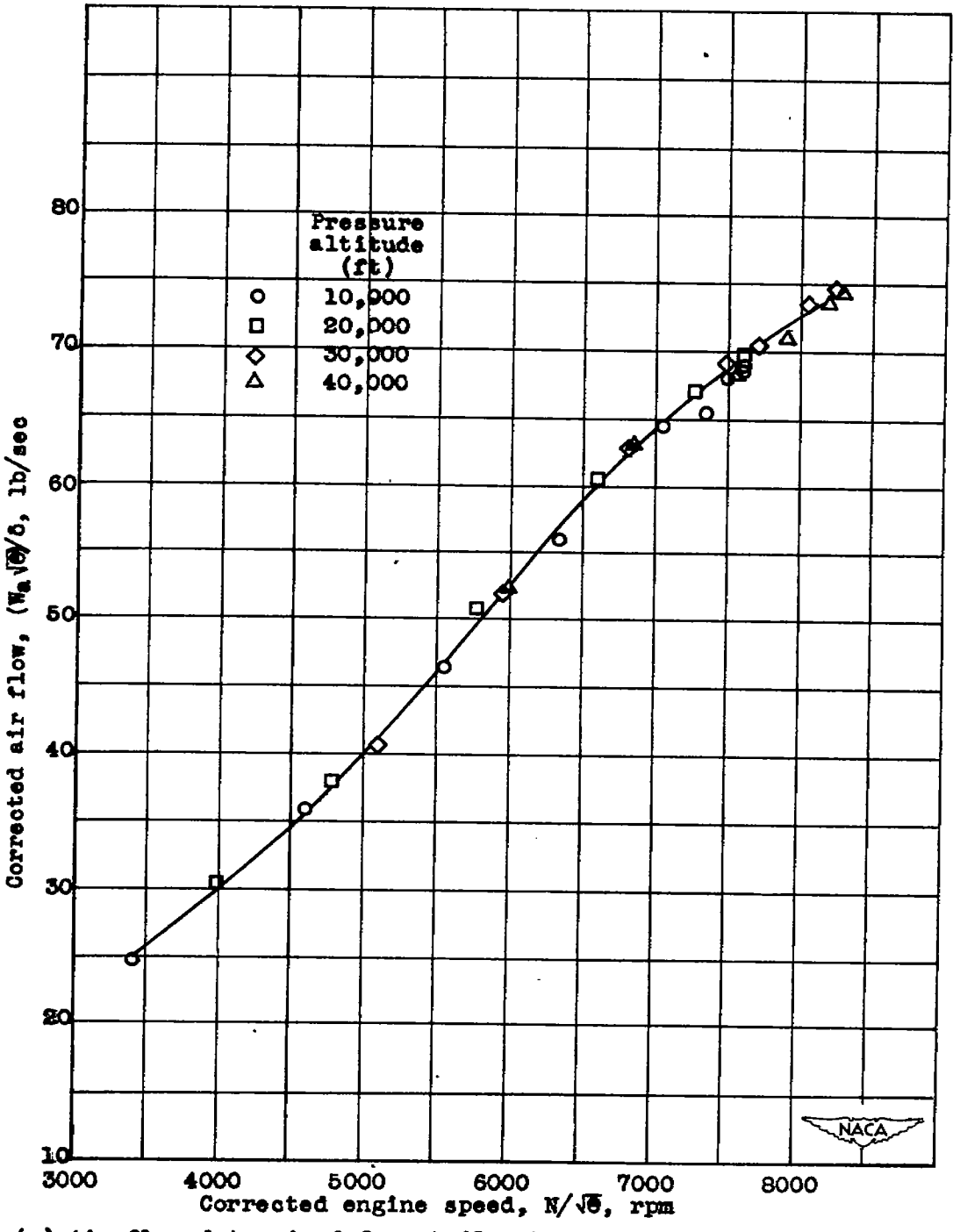

(a) Air flow determined from tail-rake survey at station 8.

Figure 32. - Effect of corrected engine speed and pressure altitude on corrected air flow at a ram pressure ratio of approximately 1.2. Air flow and engine speed corrected to NACA standard atmospheric conditions at sea level.

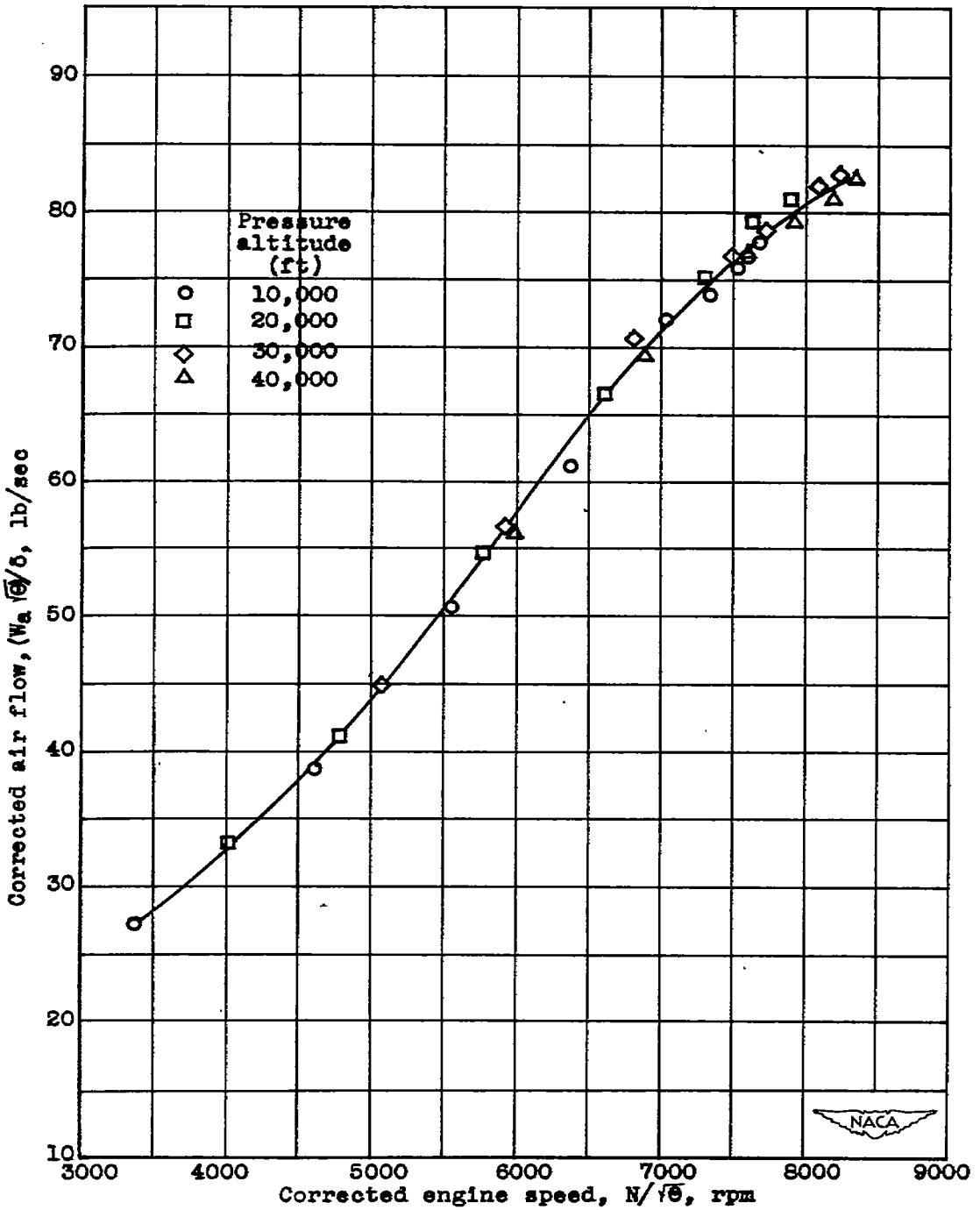

(b) Air flow determined from cowl-inlet survey at station 1.

Figure 32.- Concluded.

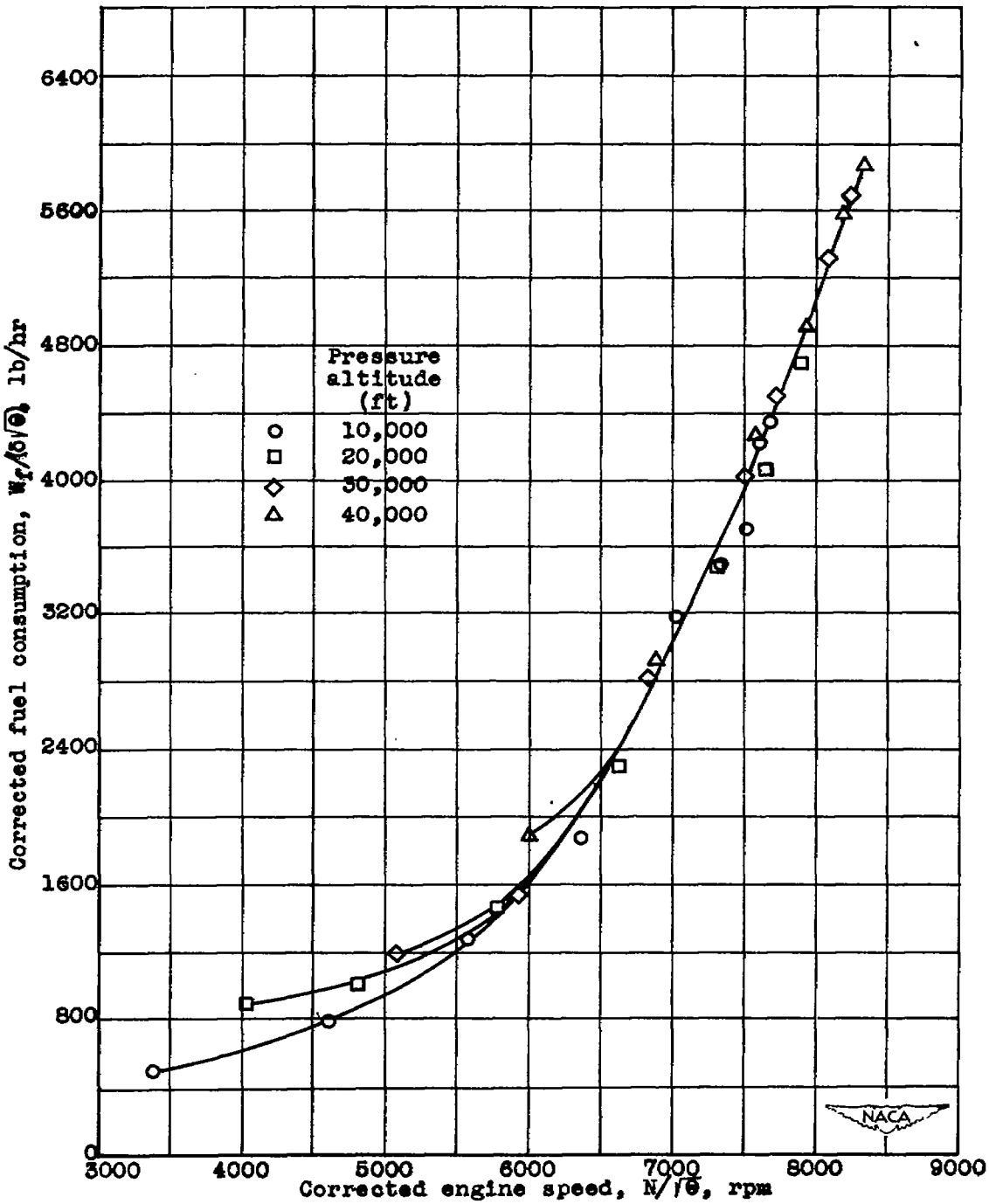

Figure 33. - Effect of corrected engine speed and pressure altitude on corrected fuel consumption at a ram pressure ratio of approximately 1.2. Engine speed and fuel consumption corrected to NACA standard atmospheric conditions at sea level.

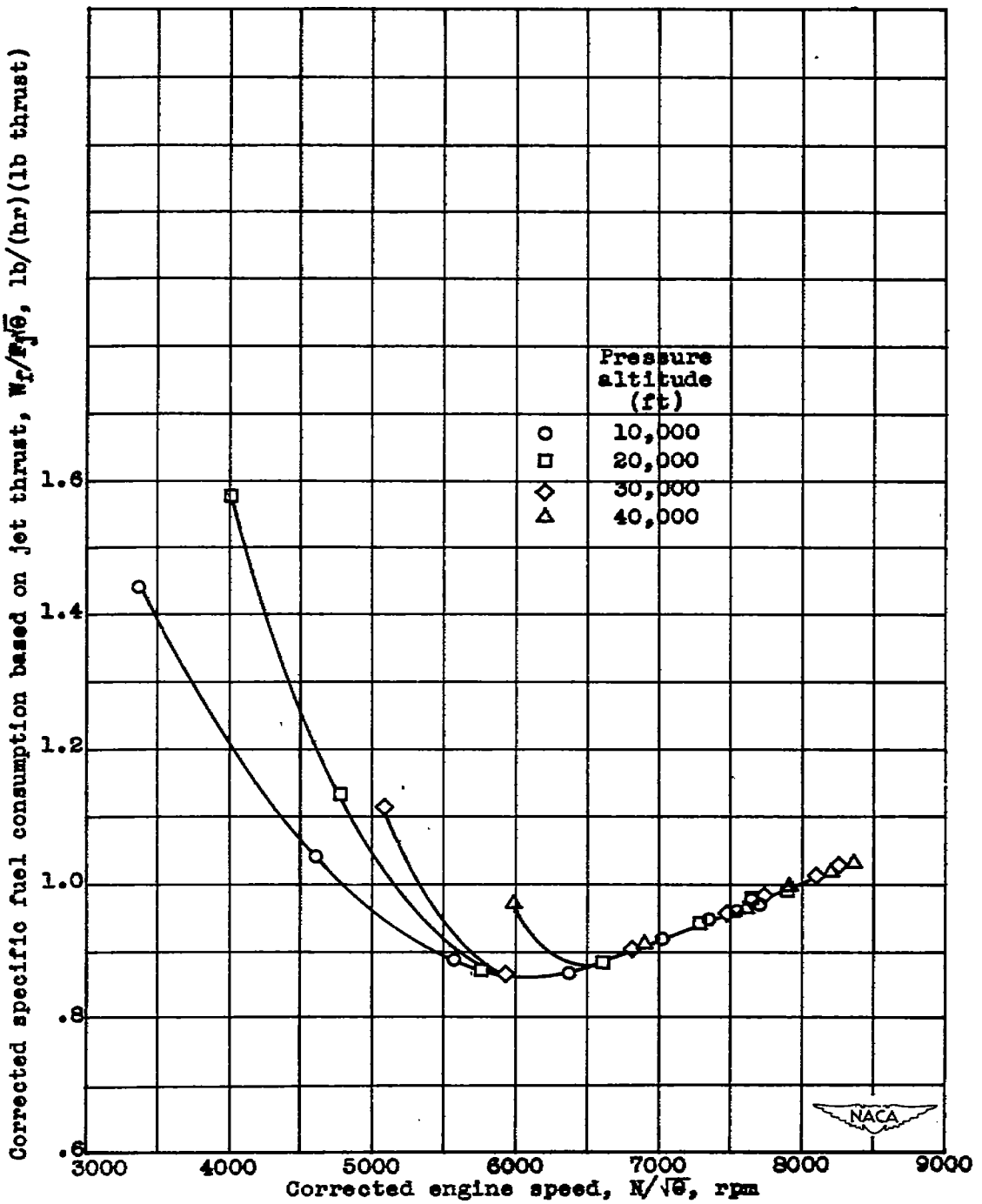

Figure 34. - Effect of corrected engine speed and pressure altitude on corrected specific fuel consumption based on jet thrust at a ram pressure ratio of approximately 1.2. Engine speed and specific fuel consumption corrected to NACA standard atmospheric conditions at sea level.

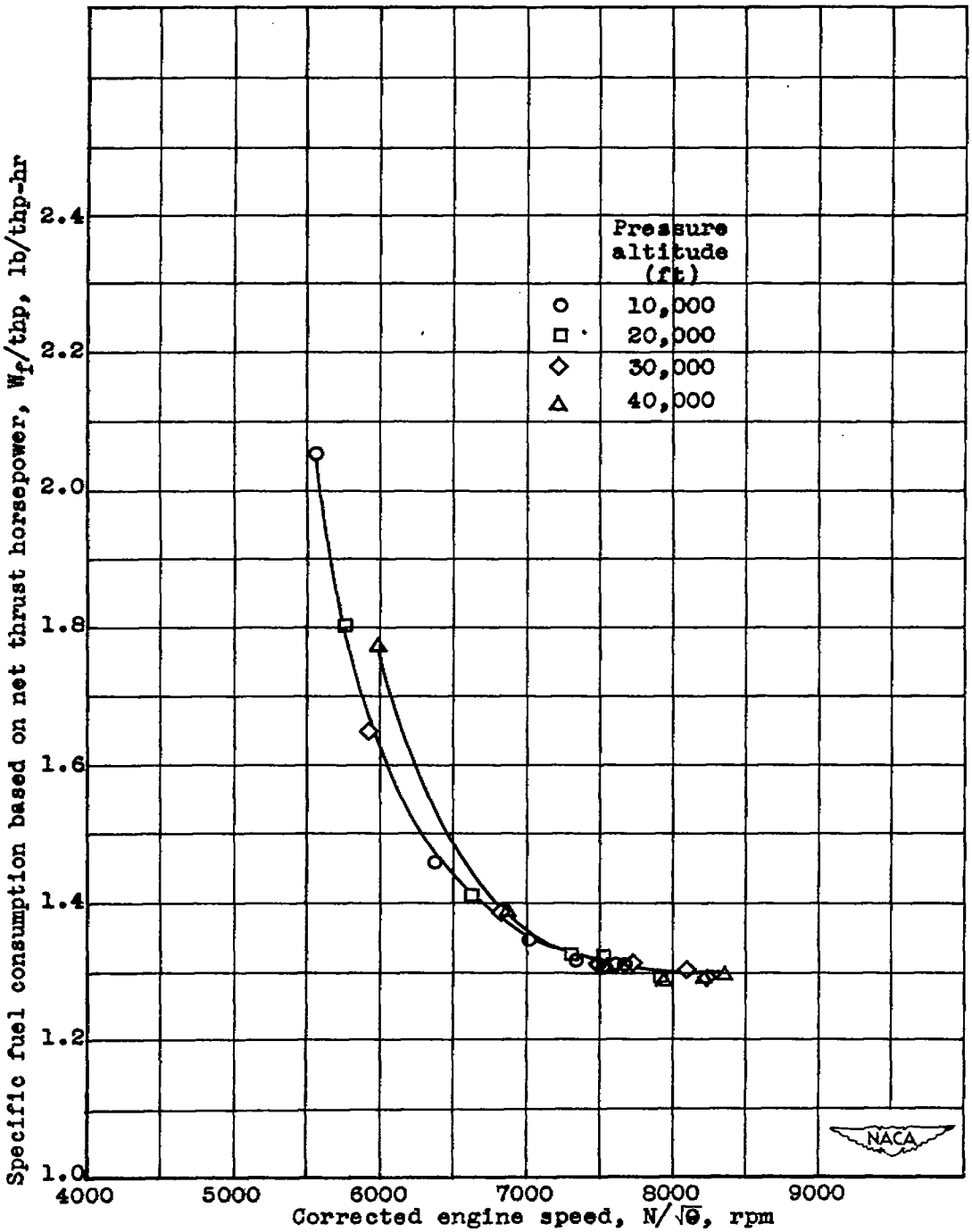

Figure 35. - Effect of corrected engine speed on specific fuel consumption based on net thrust horsepower at a ram pressure ratio of approximately 1.2. Engine speed corrected to NACA standard atmospheric conditions at sea level.

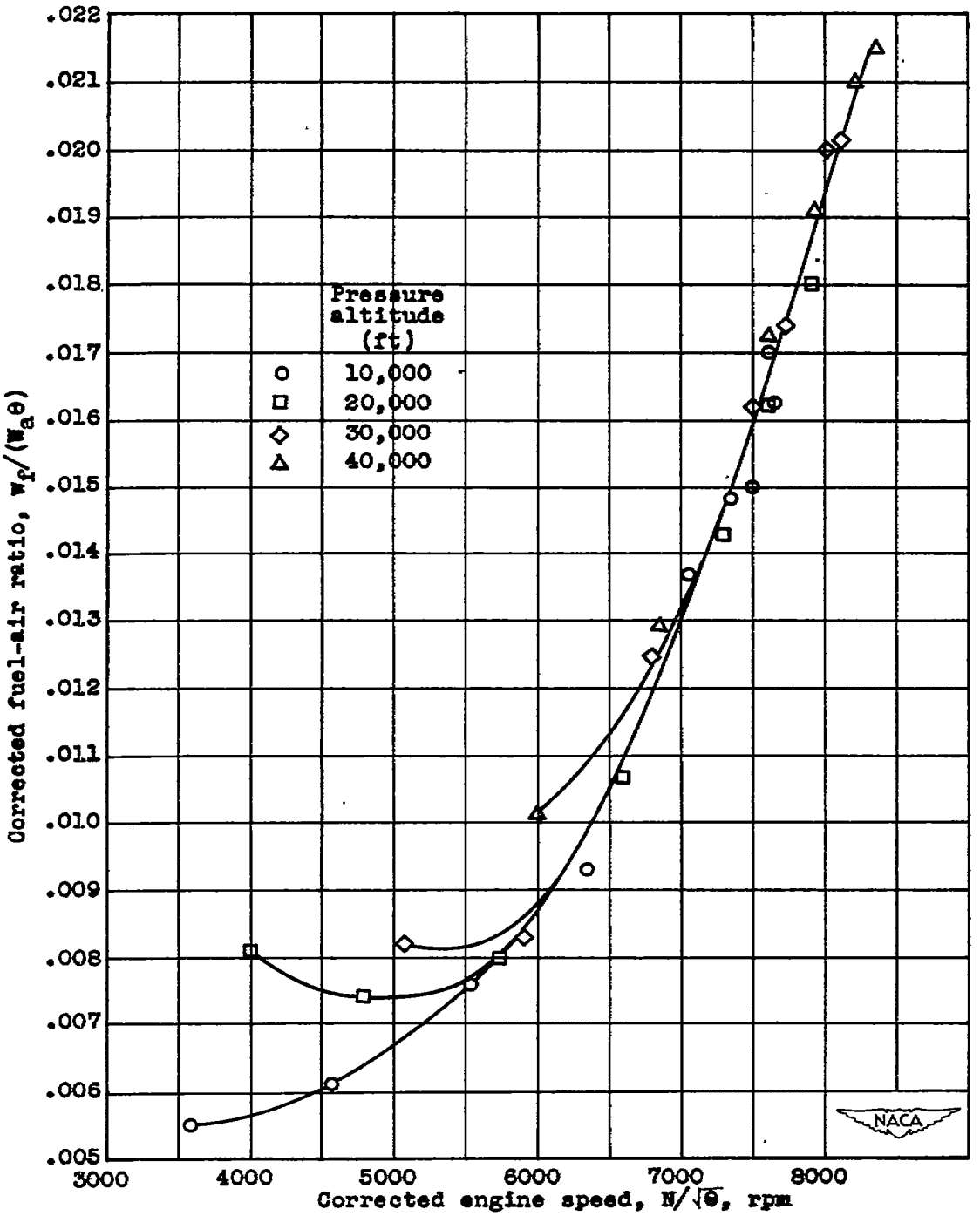

Figure 36. – Effect of corrected engine speed and altitude on corrected fuel–air ratio at a ram pressure ratio of approximately 1.2. Engine speed and fuel–air ratio corrected to NACA standard atmospheric conditions at sea level.

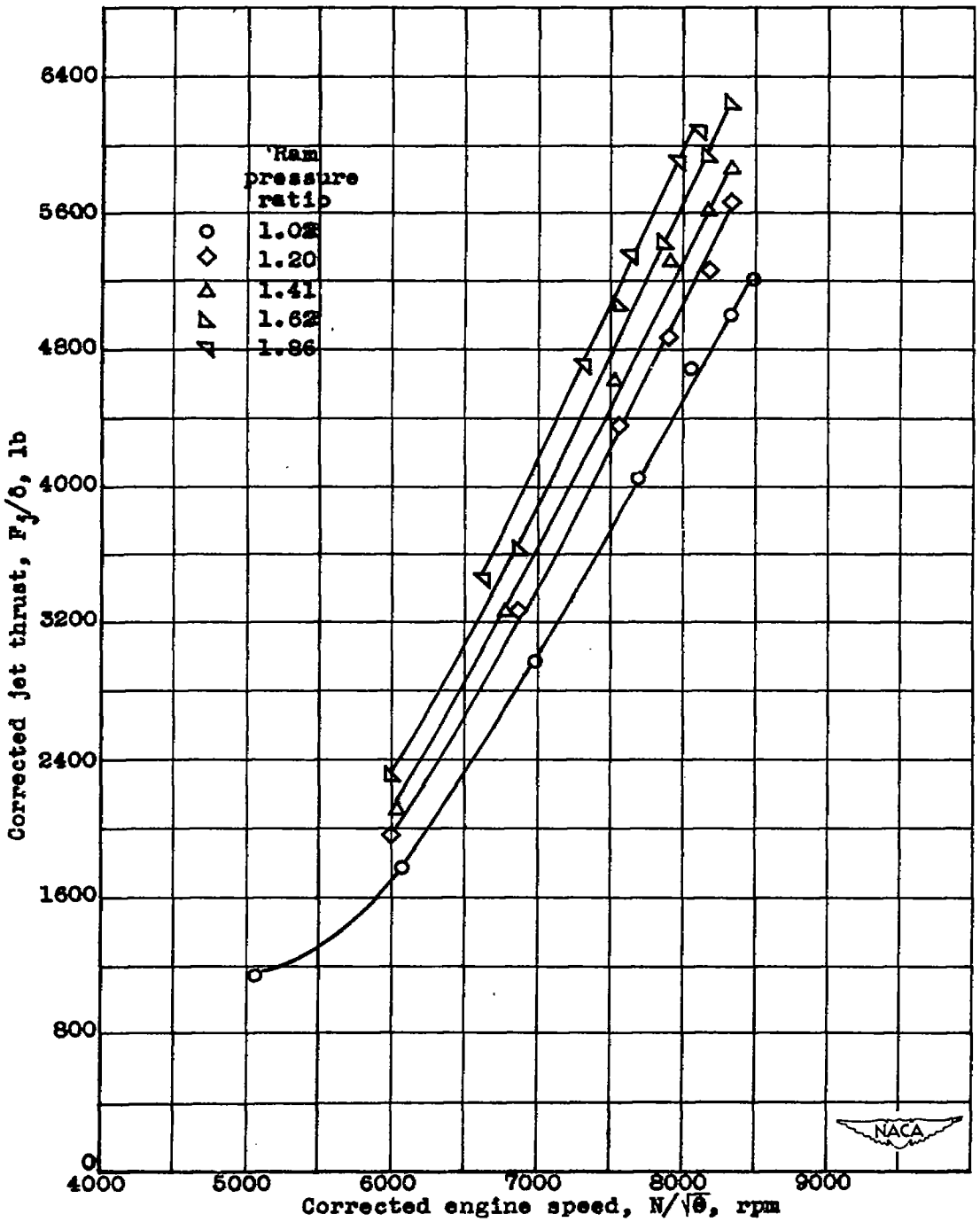

Figure 37. - Effect of corrected engine speed and ram pressure ratio on corrected jet thrust at a pressure altitude of 40,000 feet. Engine speed and jet thrust corrected to NACA standard atmospheric conditions at sea level.

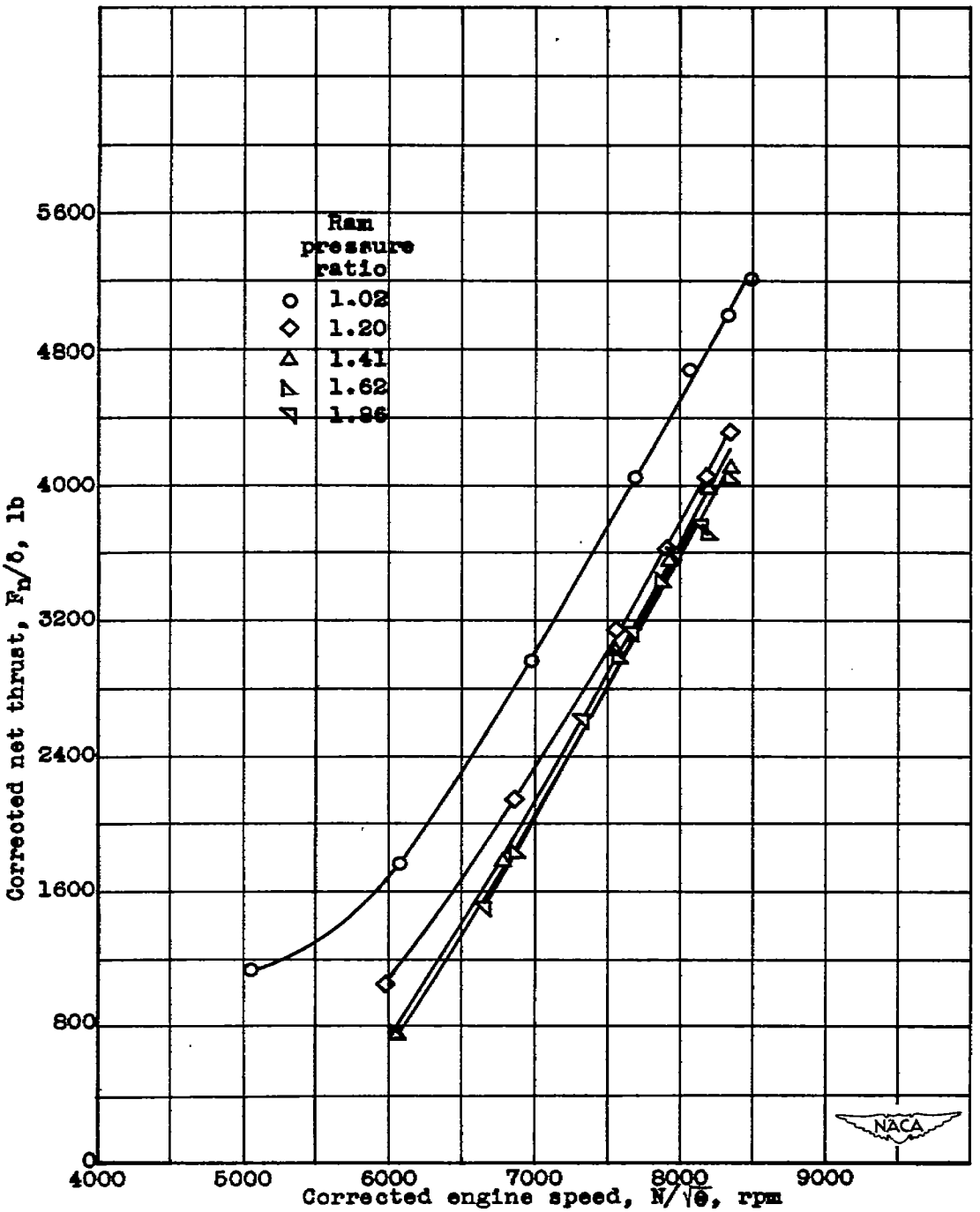

Figure 38. – Effect of corrected engine speed and ram pressure ratio on corrected net thrust at a pressure altitude of 40,000 feet. Engine speed and net thrust corrected to NACA standard atmospheric conditions at sea level.

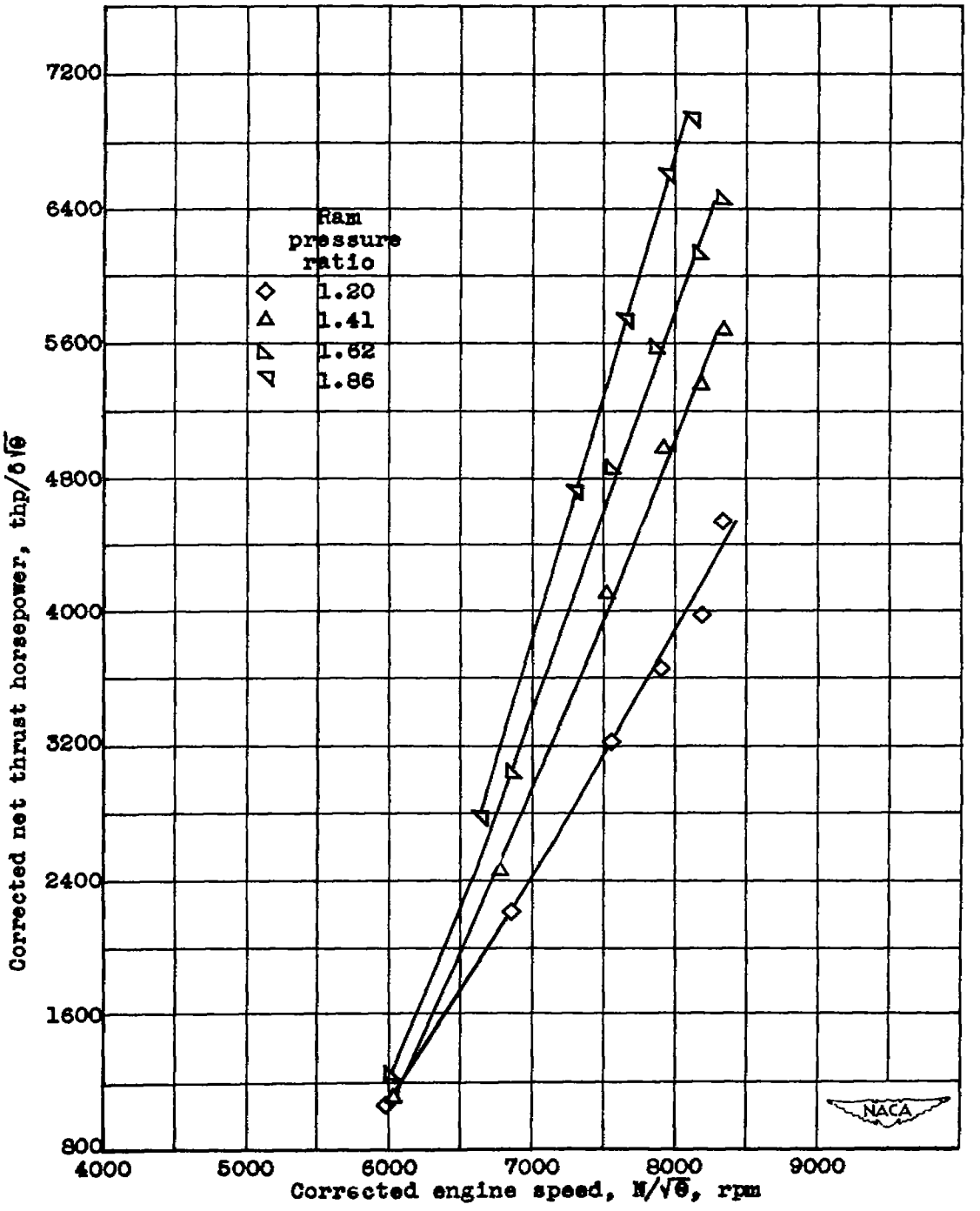

Figure 39. - Effect of corrected engine speed and ram pressure ratio on corrected net thrust horsepower at a pressure altitude of 40,000 feet. Engine speed and net thrust horsepower corrected to NACA standard atmospheric conditions at sea level.

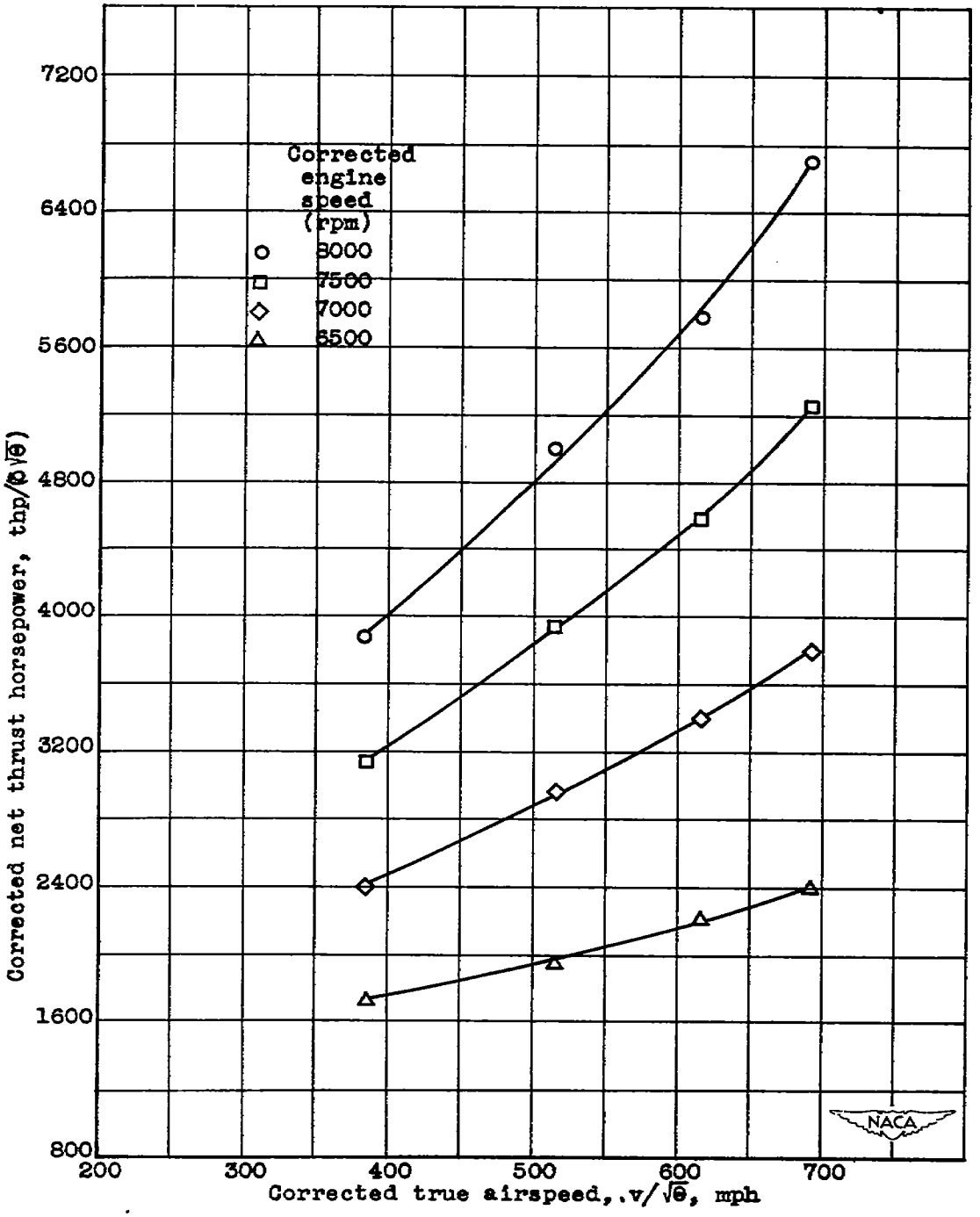

Figure 40. - Variation of corrected net thrust horsepower with corrected true airspeed at various corrected engine speeds and a pressure altitude of 40,000 feet. Net thrust horsepower, engine speed, and true airspeed corrected to NACA standard atmospheric conditions at sea level.

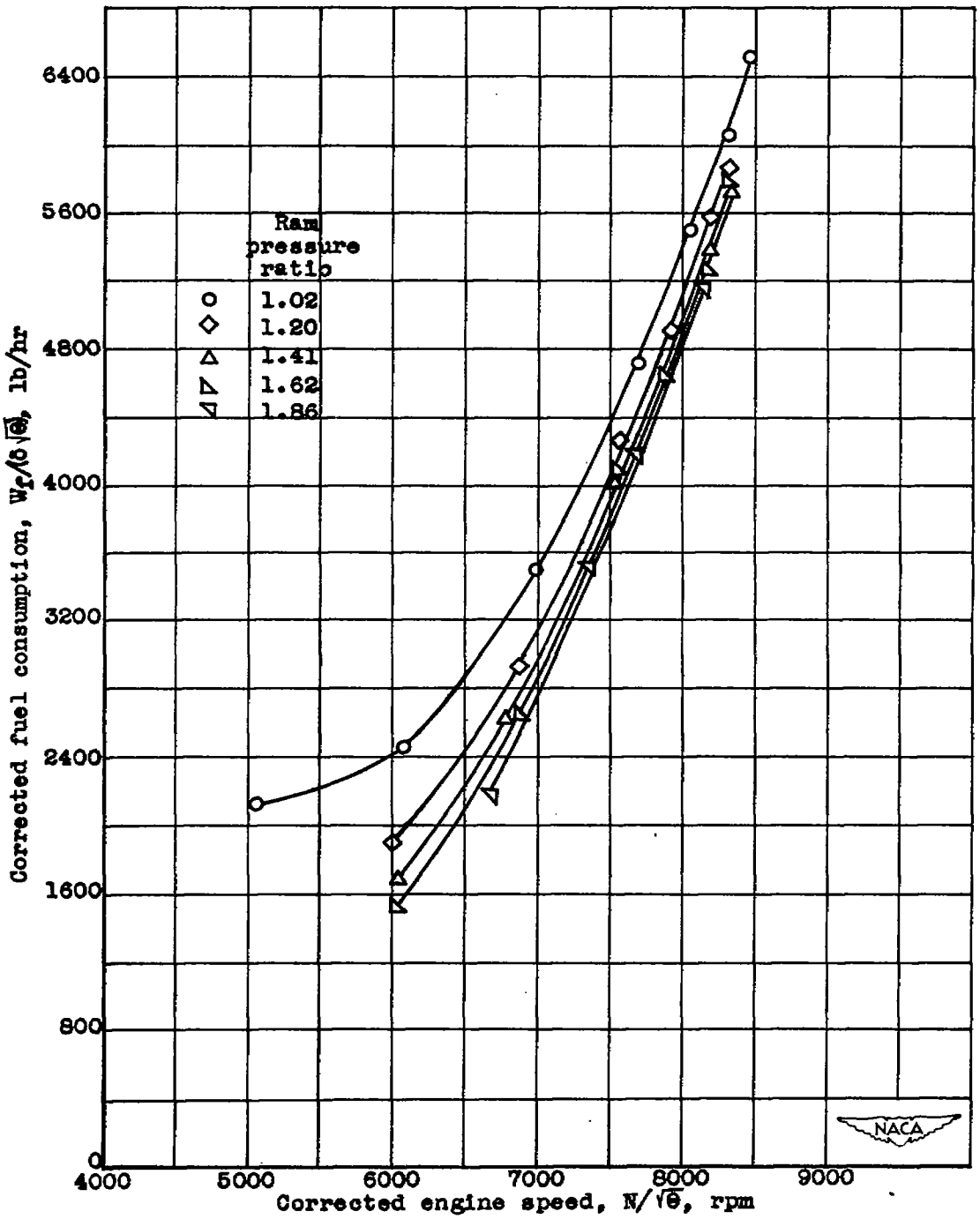

Figure 41. - Effect of corrected engine speed and ram pressure ratio on corrected fuel consumption at a pressure altitude of 40,000 feet. Engine speed and fuel consumption corrected to NACA standard atmospheric conditions at sea level.

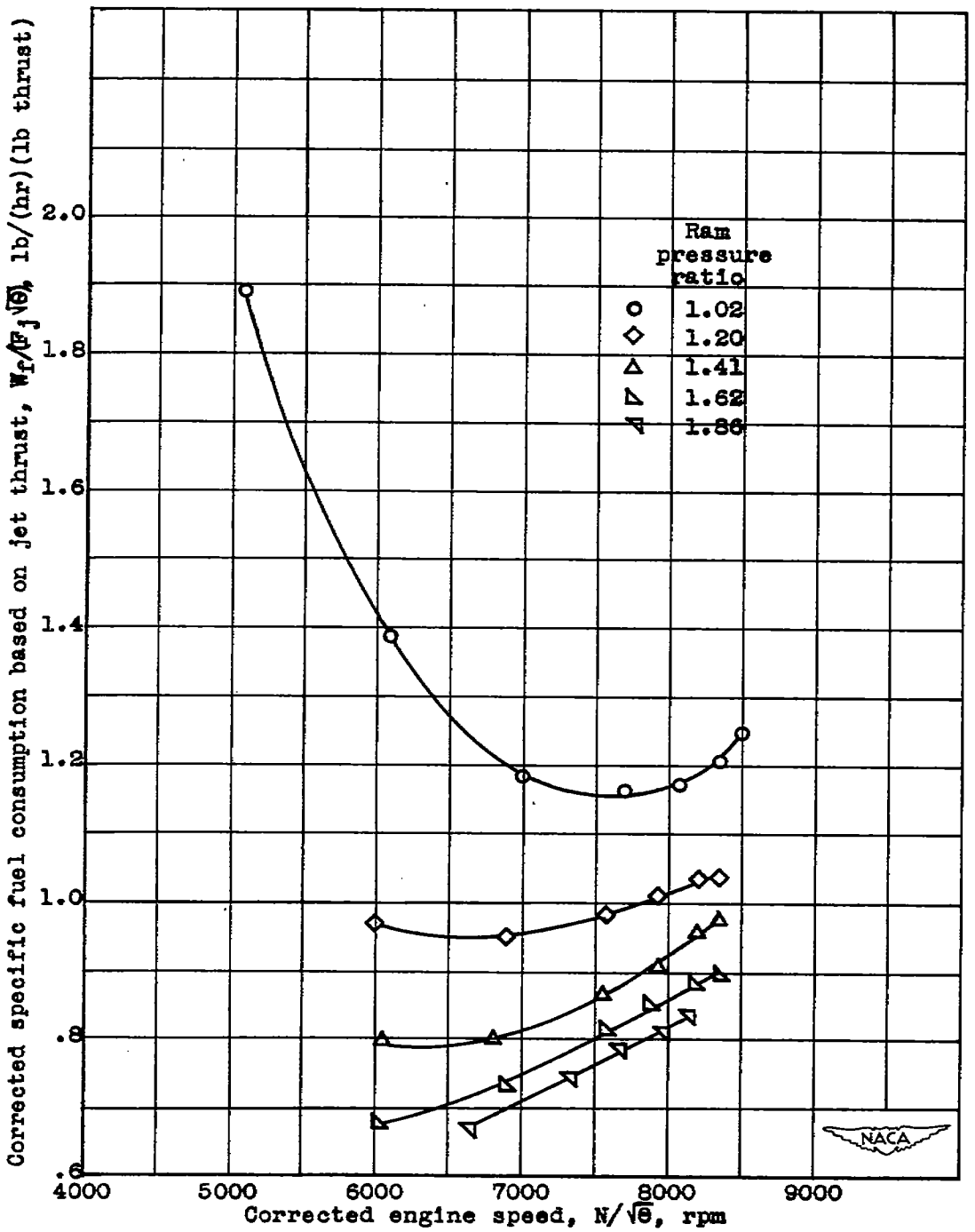

Figure 42. – Effect of corrected engine speed and ram pressure ratio on corrected specific fuel consumption based on jet thrust at a pressure altitude of 40,000 feet. Engine speed and specific fuel consumption corrected to NACA standard atmospheric conditions at sea level.

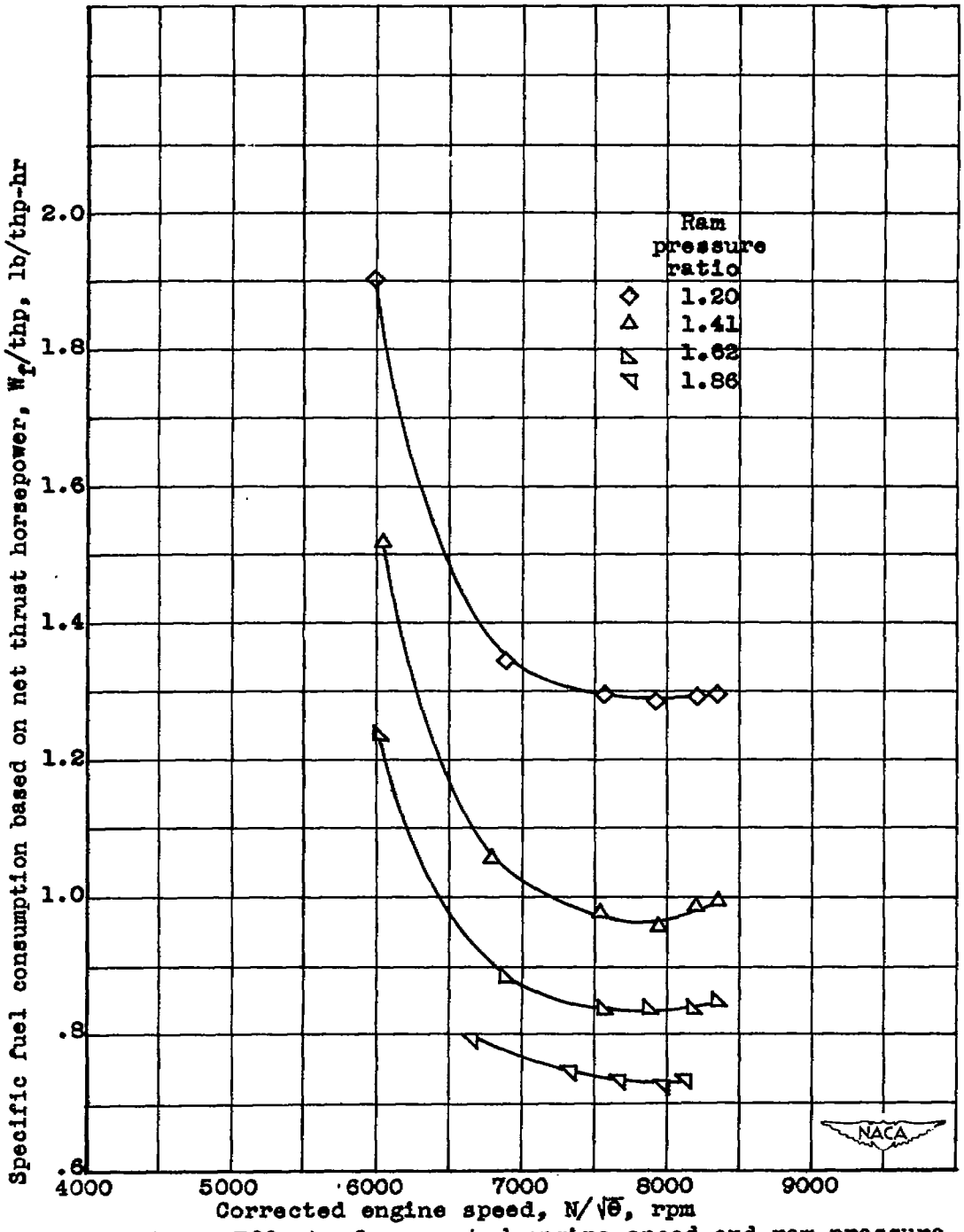

Figure 43. - Effect of corrected engine speed and ram pressure ratio on specific fuel consumption based on net thrust horsepower at a pressure altitude of 40,000 feet. Engine speed corrected to NACA standard atmospheric conditions at sea level.

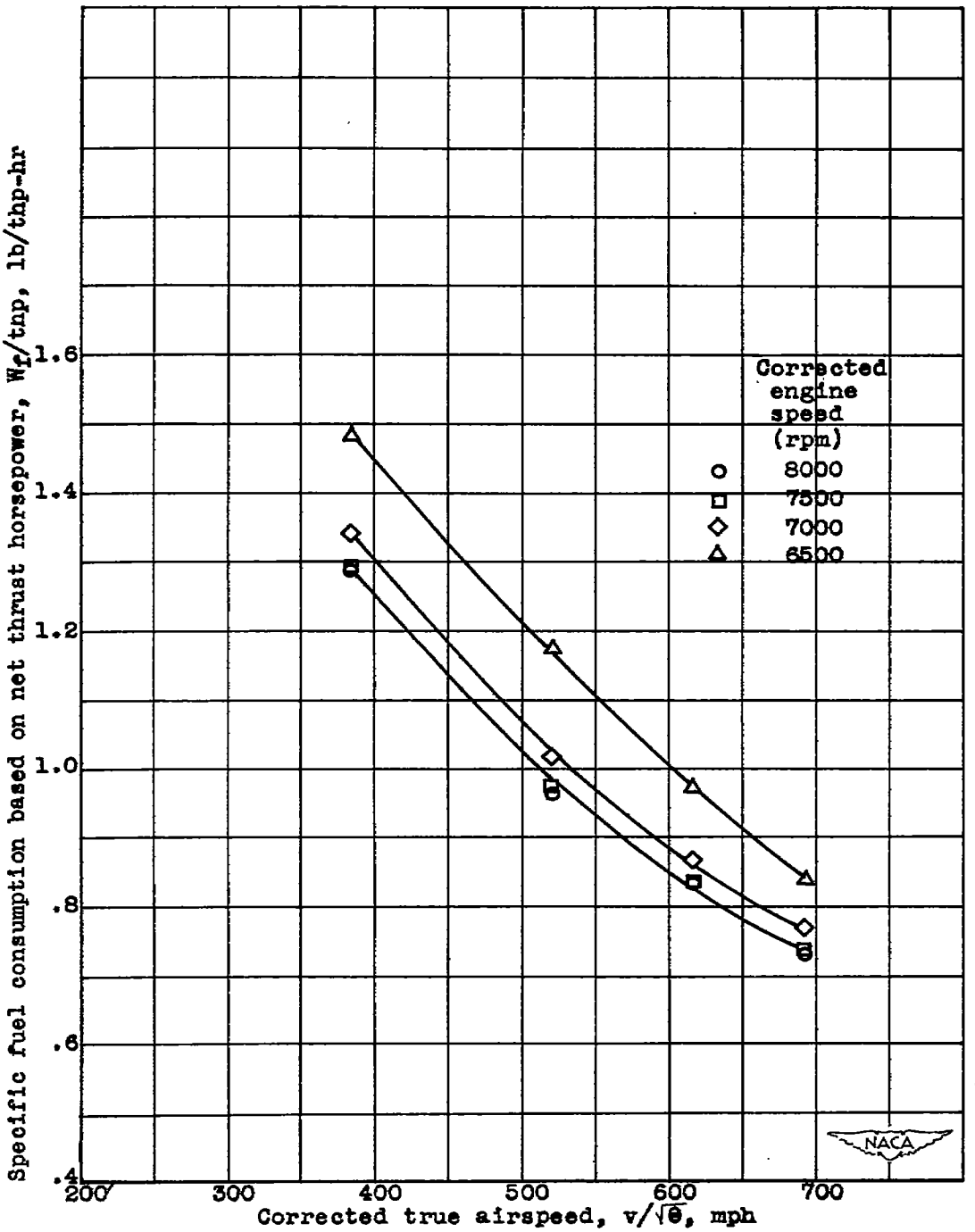

Figure 44. - Variation of specific fuel consumption based on net thrust horsepower with corrected true airspeed at various corrected engine speeds and a pressure altitude of 40,000 feet. True airspeed corrected to NACA standard atmospheric conditions at sea level.

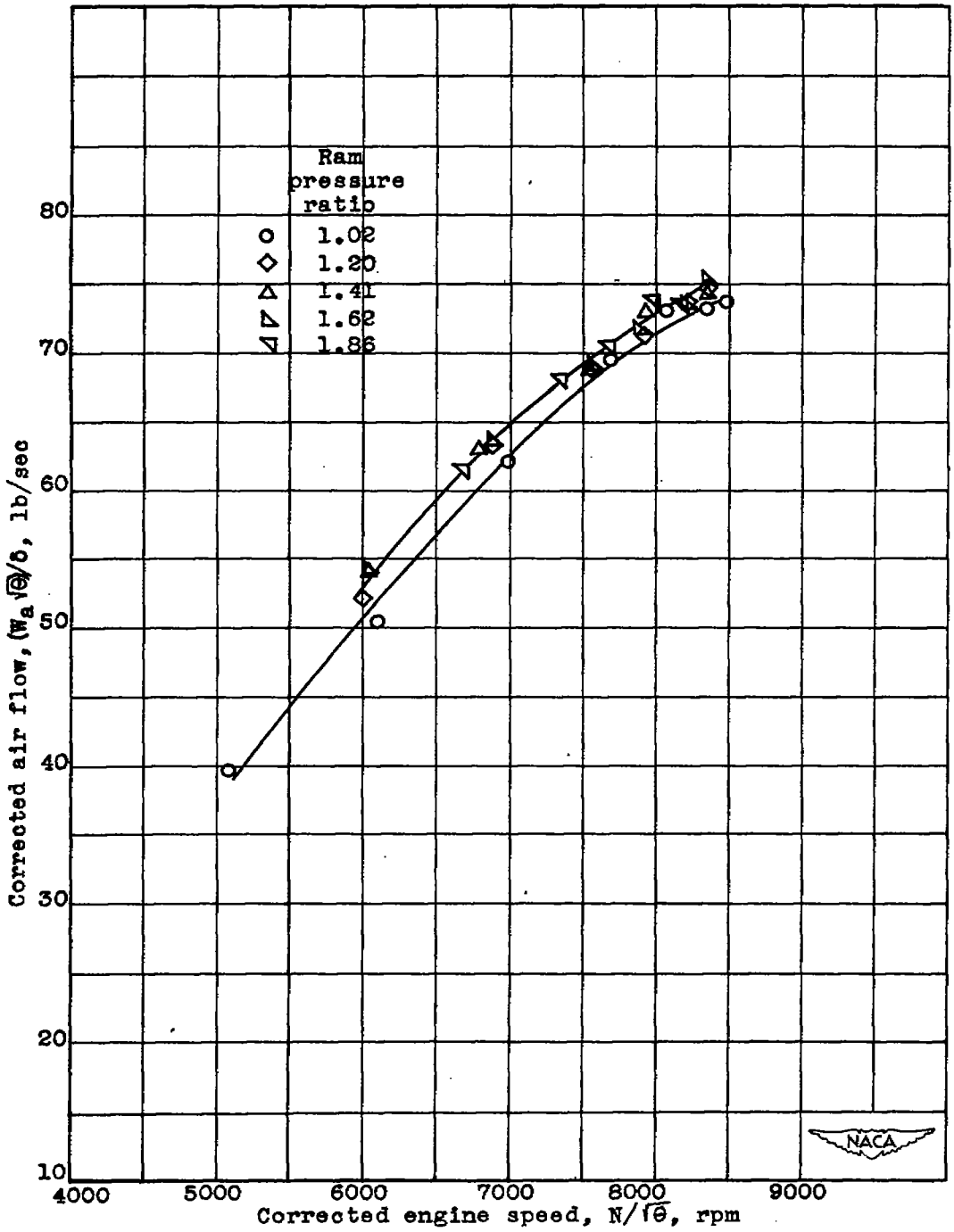

(a) Air flow determined from tail-rake survey at station 8.

Figure 45. - Effect of corrected engine speed and ram pressure ratio on corrected air flow at a pressure altitude of 40,000 feet. Engine speed and air flow corrected to NACA standard atmospheric conditions at sea level.

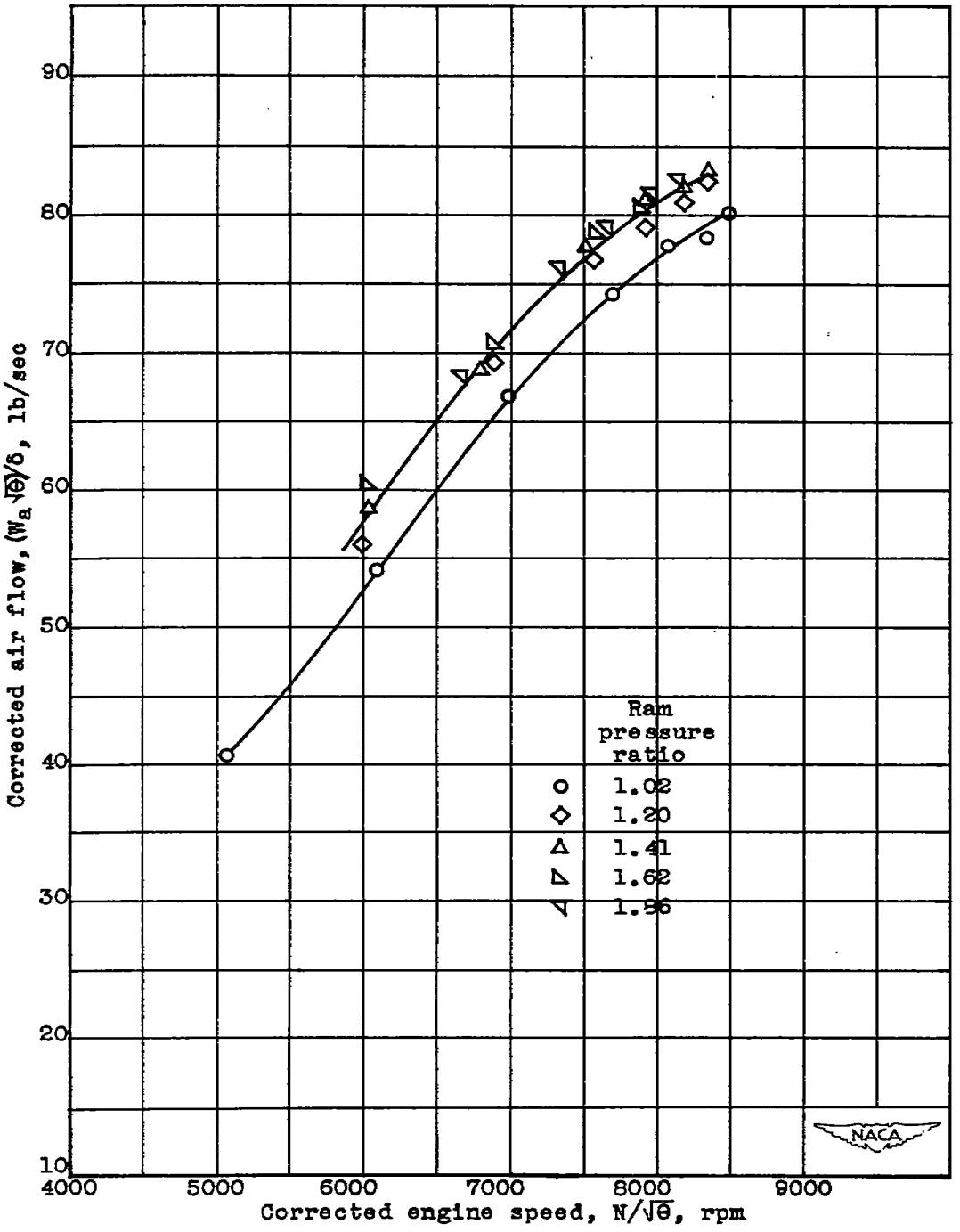

(b) Air flow determined from cowl-inlet survey at station 1.

Figure 45.- Concluded.

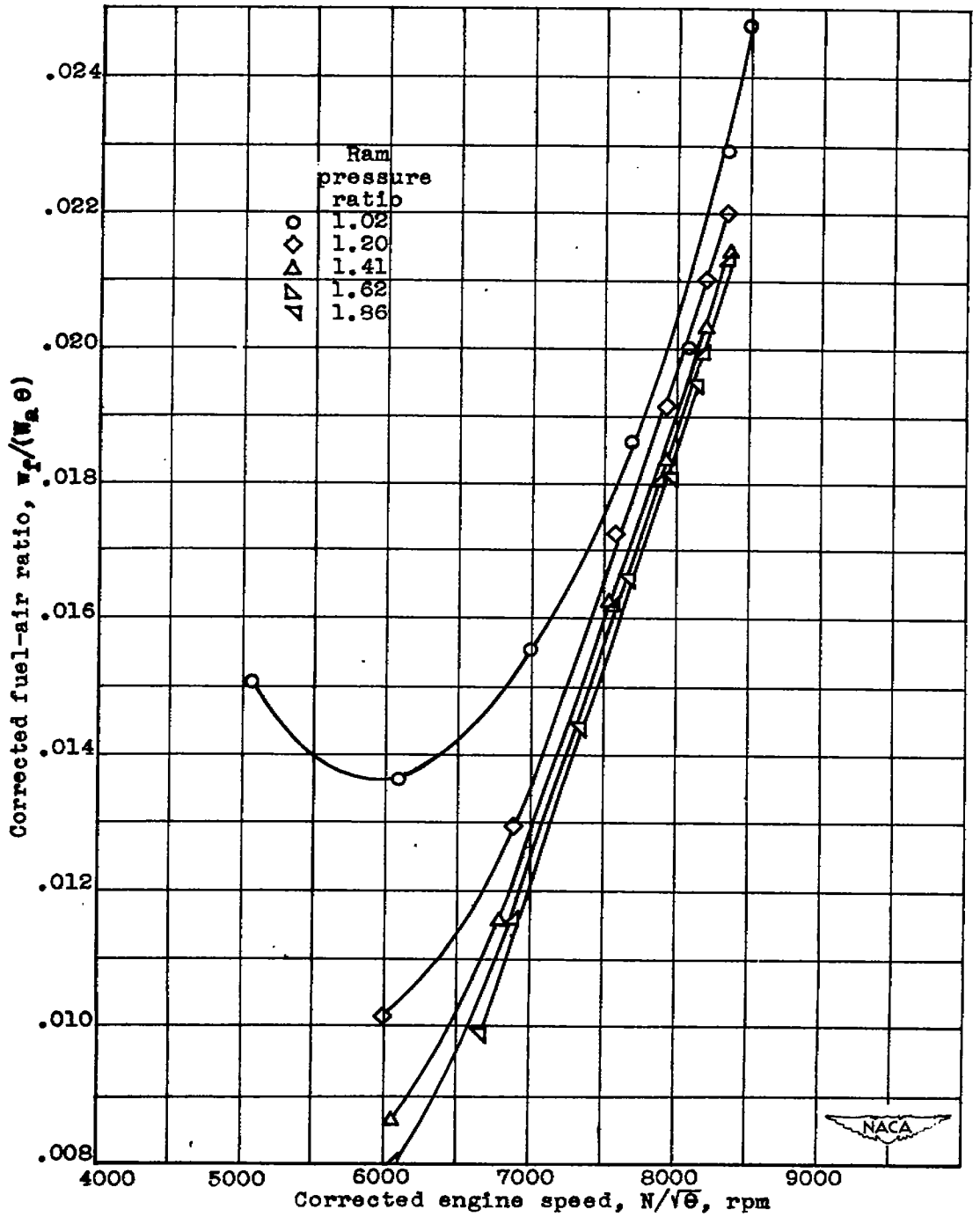

Figure 46. - Effect of corrected engine speed and ram pressure ratio on corrected fuel-air ratio at a pressure altitude of 40,000 feet. Engine speed and fuel-air ratio corrected to NACA standard atmospheric conditions at sea level.

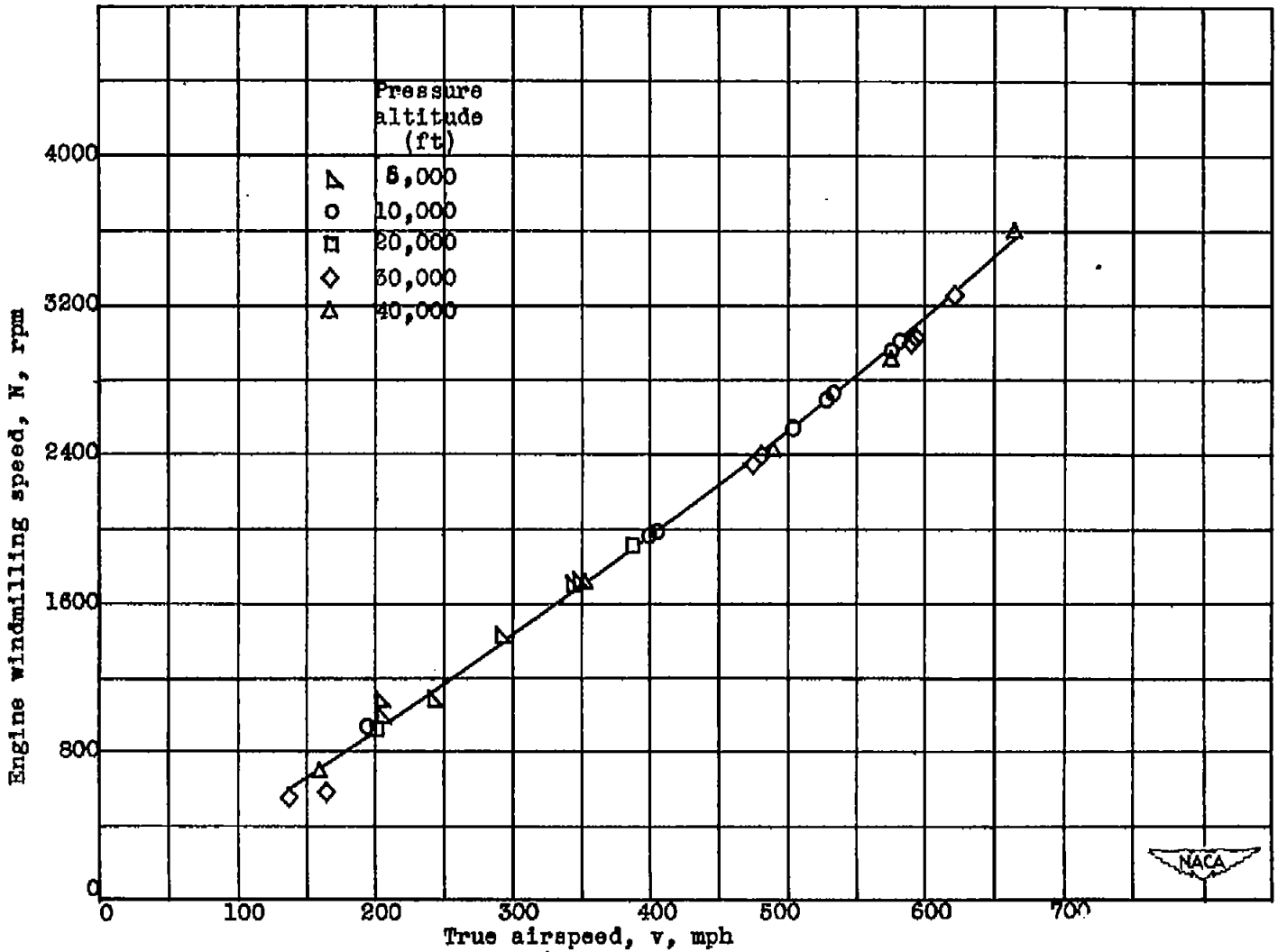

Figure 47.- Variation of engine windmilling speed with true airspeed and pressure altitude.

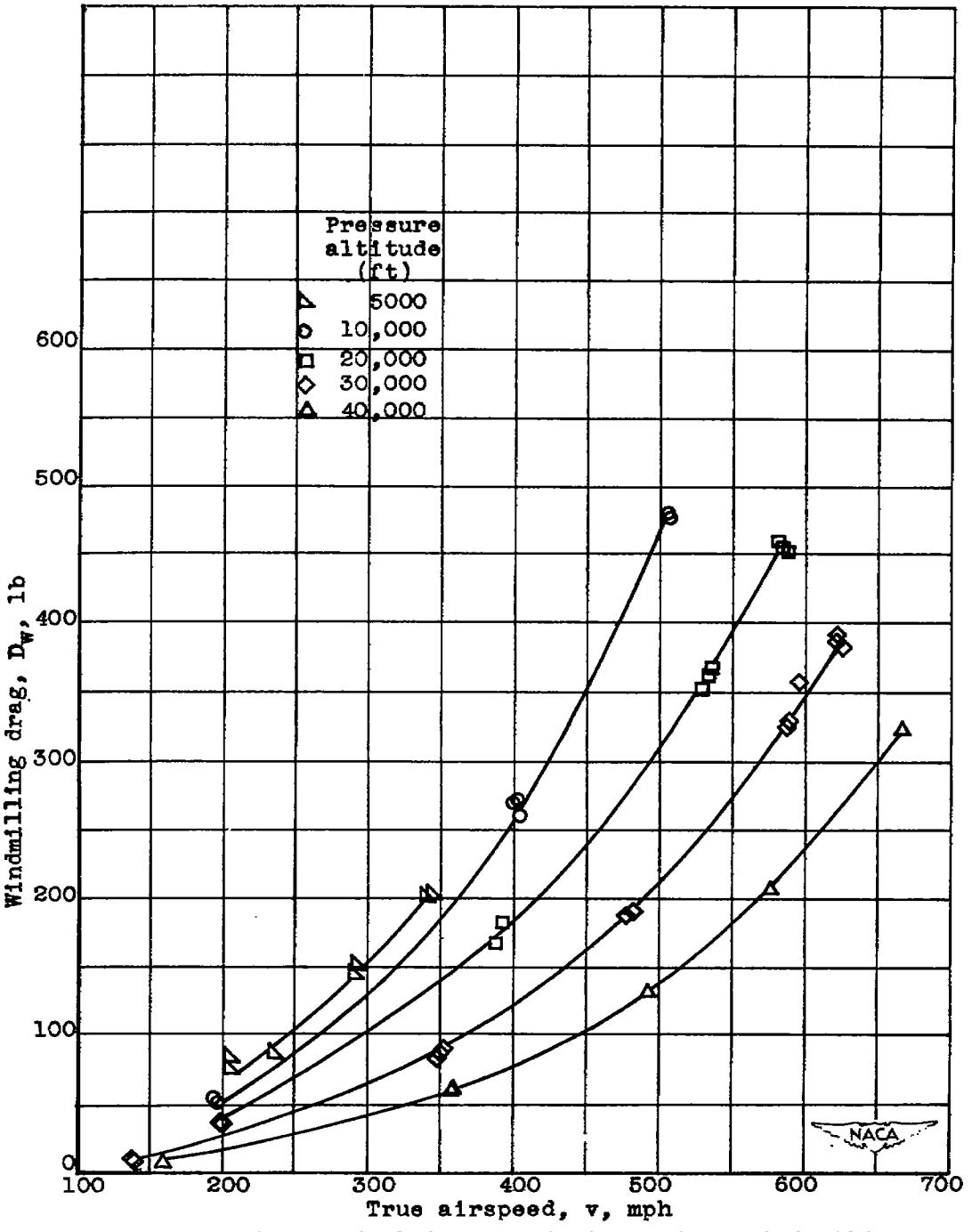

Figure 48.- Effect of altitude and airspeed on windmilling drag.

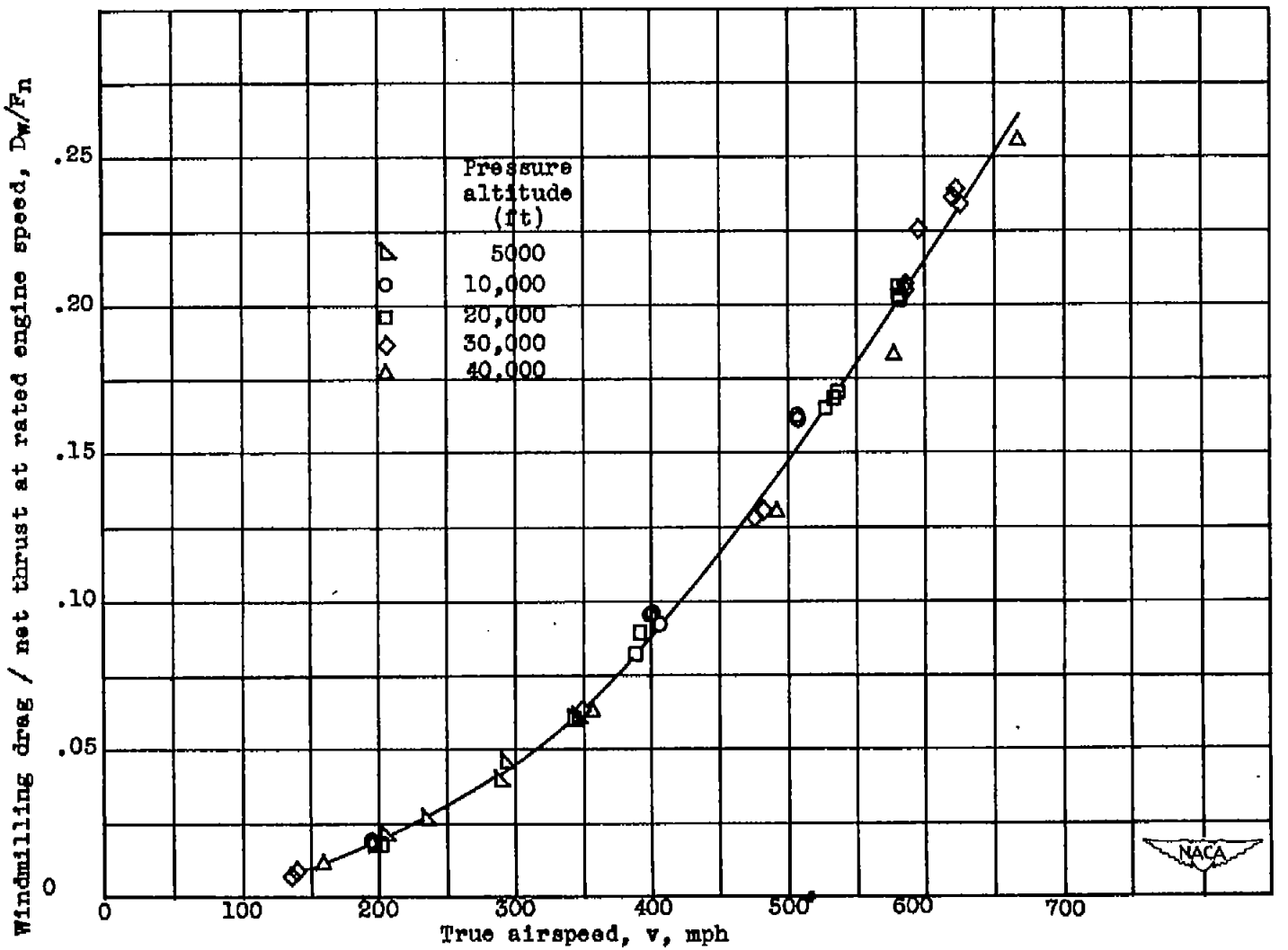

Figure 49.- Effect of altitude and true airspeed on the ratio of windmilling drag to net thrust at rated engine speed.

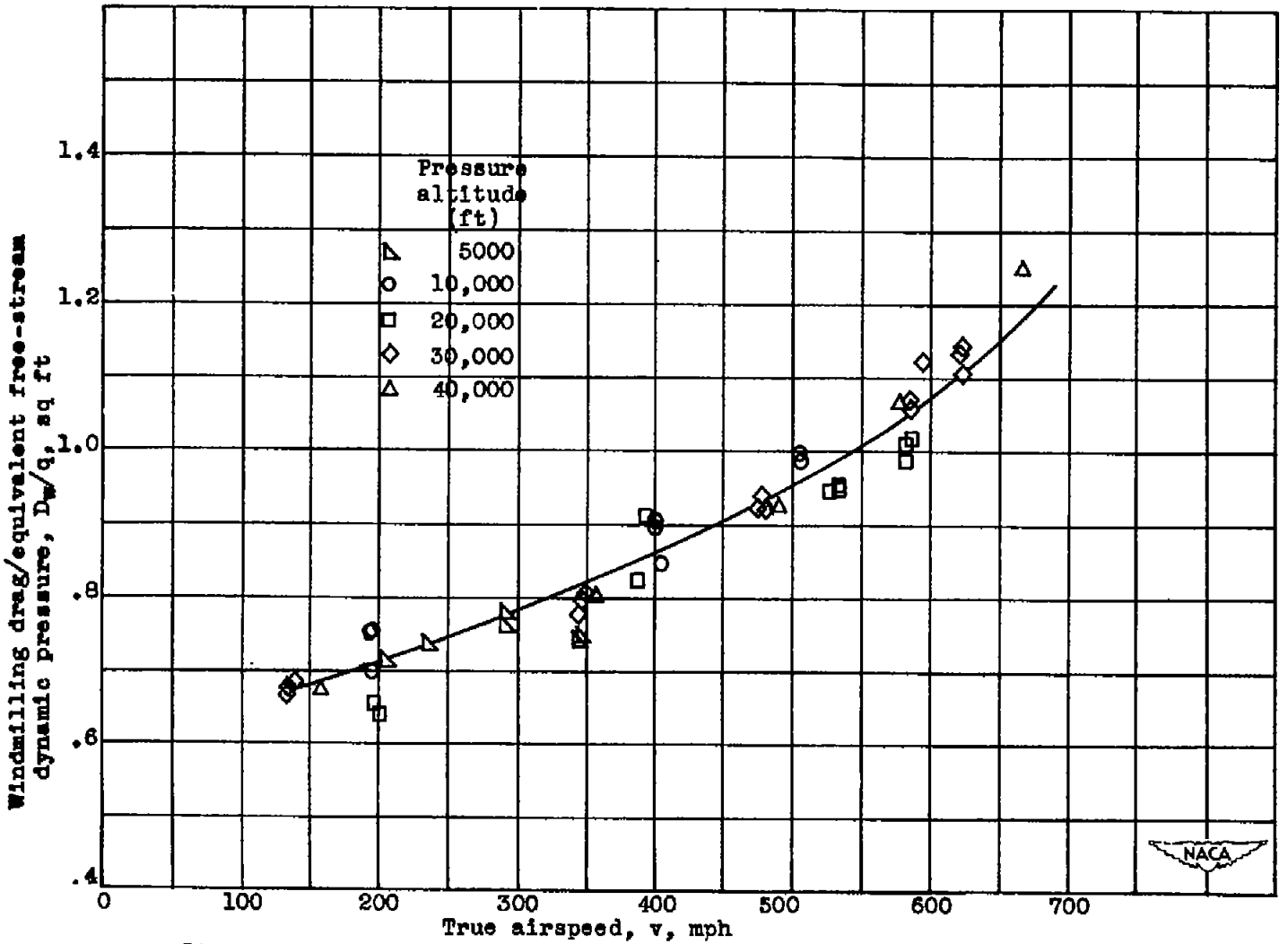

Figure 50.- Effect of altitude and true airspeed on the ratio of windmilling drag to equivalent free-stream dynamic pressure.

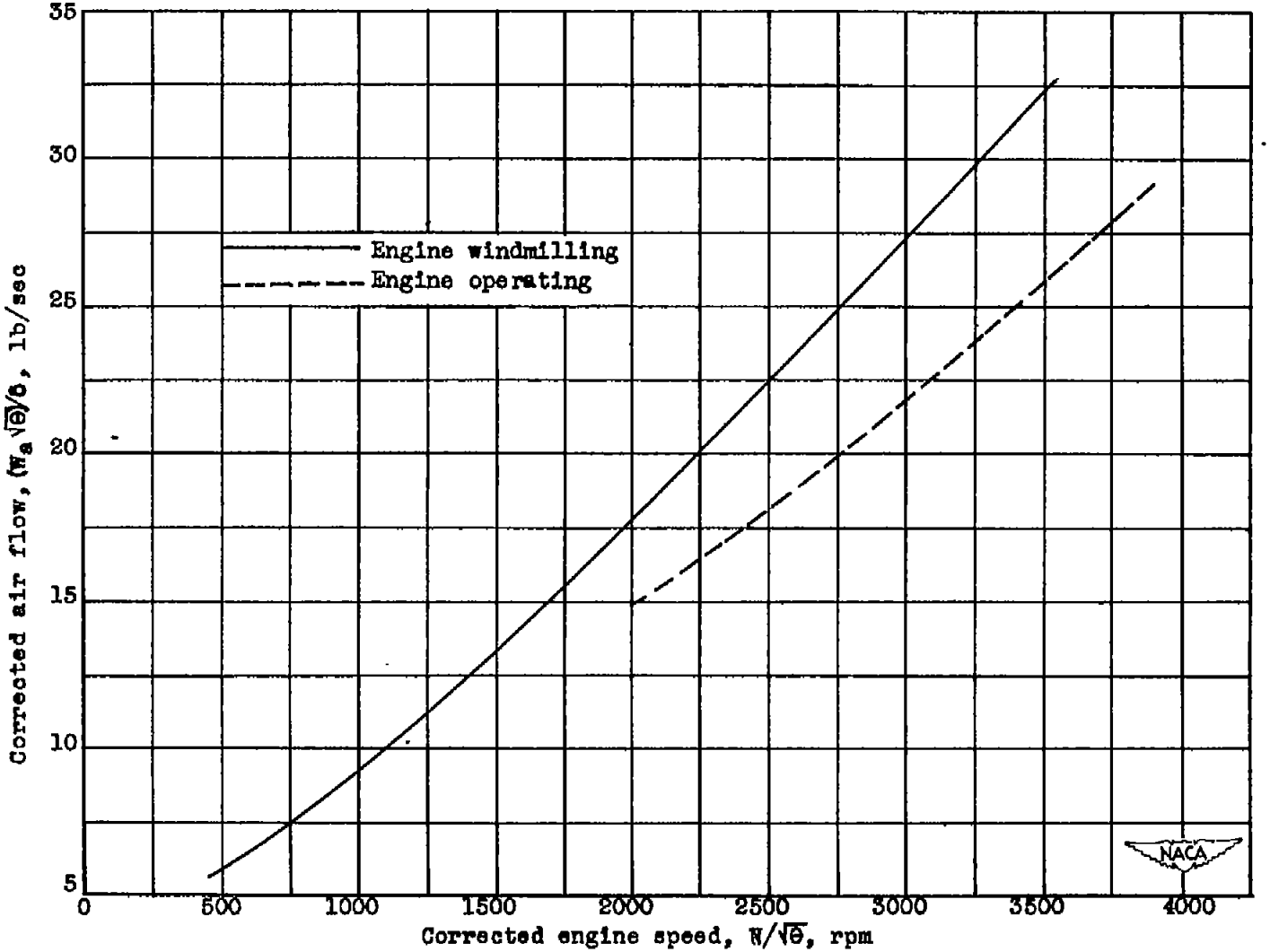

Figure 51. - Comparison of effect of corrected engine speed on corrected air flow with engine windmilling and engine operating. Air flow and engine speed corrected to NACA standard atmospheric conditions at sea level.

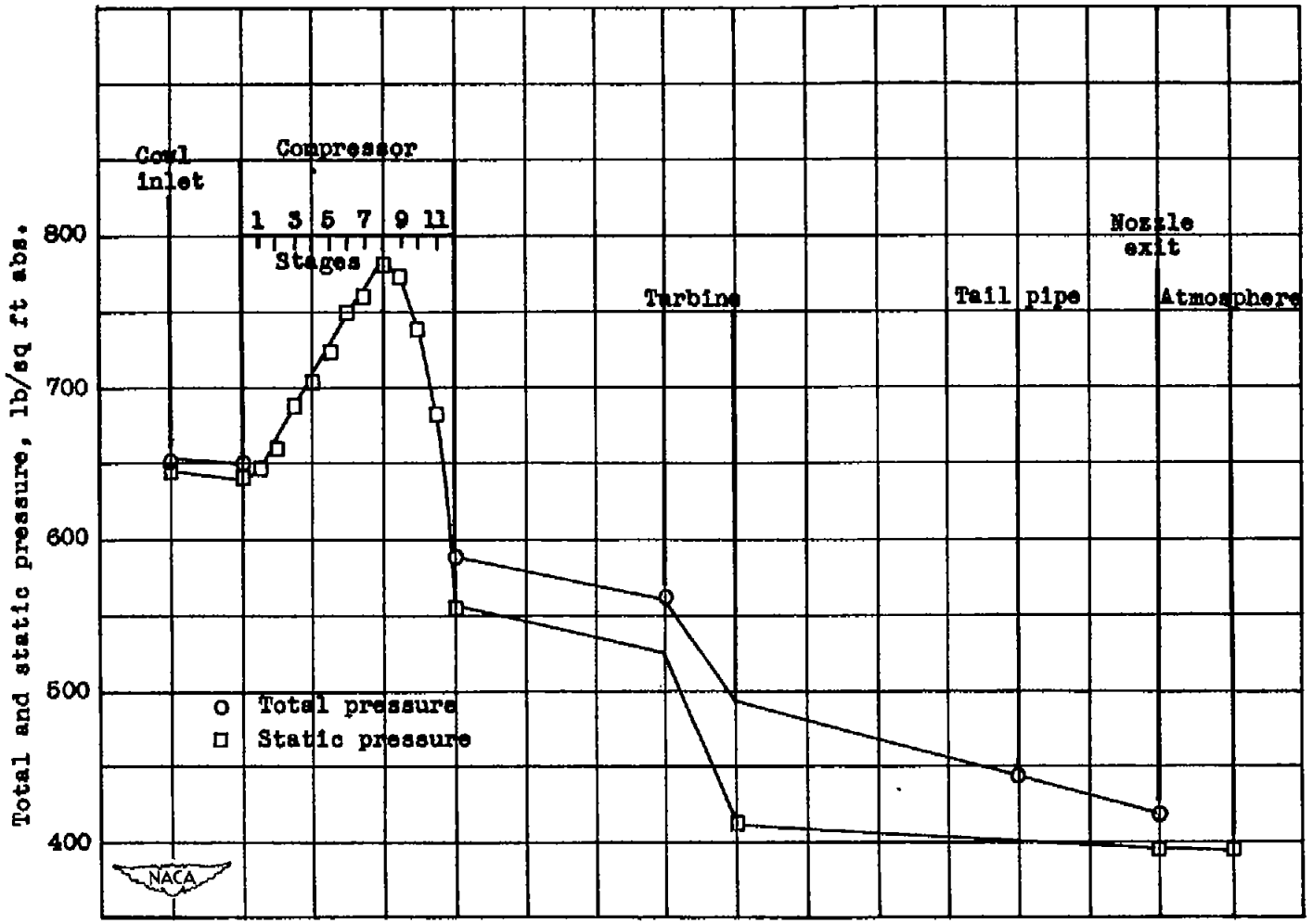

Figure 52. - Total and static pressure survey with engine windmilling. Windmilling speed, 2933 rpm; pressure altitude, 40,000 feet; true airspeed, 575 miles per hour.